Spring Blooms and Seasonal Light Responses in Phytoplankton in the Eastern Bering Sea

Trevor Sloughter

Supervisors:

Dr Neil Banas

Department of Mathematics & Statistics

University of Strathclyde, Glasgow

Dr David McKee

Department of Physics

University of Strathclyde, Glasgow

September 6, 2022

This thesis is the result of the author's original research. It has been composed by the author and has not been previously submitted for examination which has led to the award of a degree.

Abstract

Phytoplankton communities in the Eastern Bering Sea are a prime example of spring blooms in high latitude environments. This project studies the role of changing light responses in regulating spring bloom development.

Seasonality was observed in the light response curves of phytoplankton samples taken in the Eastern Bering Sea shortly before and during the spring bloom. Under-ice samples were found to have lower values of both the maximum nutrient uptake rate v_m and the initial slope α of the photosynthesis-irradiance curve. This trend in α was also noted in a literature review. A trade-off is proposed linking α and maintenance respiration such that below the compensation intensity E_C it becomes advantageous to decrease α. A seasonal NPZD model reflected this trade-off with a seasonal transition from low to high α and μ_0 , at the point where available light is greater than E_C. A parameter analysis found that with this seasonal plasticity the model could accurately reproduce the timing and magnitude of the 2009 spring bloom using parameter combinations within realistic ranges. Without this seasonality, no parameter set could be found that reasonably reproduced the observations. Inter-annual variations applying the model to 2014, 2015, and 2016, when the EBS experienced warmer temperatures and significantly less ice cover. These results were compared with 2009. While changes in physical conditions, primarily ice cover and vertical mixing, are strong drivers of inter-annual differences, their impact on bloom timing was greatly reduced without seasonality in the photoparameters.

Seasonal light response has been experimentally observed in the Eastern Bering Sea and is found to be an important factor for inclusion in numerical models that aim to capture timing of the spring bloom.

Contents

List of Figures

List of Tables

Acknowledgements

I would like to acknowledge my supervisors, Drs Neil Banas and David McKee, for their support during my studies and lengthy writing process. To Dr Juan Bonachela, whose insights and thoughts in the early phases of the project helped it forward. To Prof Ray Sambrotto for not simply lending us his data but being there to discuss the analysis and its implications in detail. To Dr Mike Lomas, who provided useful data and insights.

To everyone in the group, who provided much useful feedback over the years: Dr Laura Hobbs, Dr Sofia Ferreira, Dr Fabian Grosse, Dr Carlos Cáceres, Dr Ricardo González-Gill, Dr Euan McRae, Dr Soizic Garnier, Dr Thai Hoa Nguyen, Dr Melinda Choua, Dr Agnes Ollin, Dr Emma Dolmaire, and Dr Paul Udom. And to colleagues at other institutions: Emma Cairns, Graeme Campbell, Dr Graeme Eddolls, and Dr Robyn Womack; and to my science-interested friends: Brian Eggo, Jenna Shiels, and Brianne Valentic. To my undergraduate and Master's faculty who encouraged me to go this far, including Profs Joachim Vogt, Andrea Koschinsky, Michael Bau, and Agostino Merico. To my parents and my siblings for their support in my education as well as raising me to love science from an early age. Finally, especial thanks to Clara Timo Lücke, Matilda Donaldson, Jessica Vince and Juliane Kube who were invaluable in helping me power through.

Chapter 1

Introduction

1.1 Aims of this Study

The purpose of this project is to explore seasonality of light response within the phytoplankton community of the Eastern Bering Sea and its relevance to, and implications for, numerical models. A case study of high-latitude phytoplankton in seasonal light environments provides insight into how these communities may respond or acclimate to the changing Arctic and sub-Arctic conditions.

In particular, this study focuses on the modelling of spring blooms, examining how seasonality within phytoplankton's light responses impact the timing and magnitude of these. This began with observational data of seasonality in light response curves during the onset of a spring bloom. With a basis in observation and literature, seasonality of light-response could be implemented in a numerical model of the study region.

This project used an NPZD model, a class of ecosystem model named for its budgeting of Nutrients, Phytoplankton, Zooplankton, and Detritus. This NPZD model, with seasonal behaviour in phytoplankton light response, was used to investigate phytoplankton behaviour between cold years (defined by more extensive sea-ice in winter, persisting longer into the year) and warm (defined by higher temperatures and earlier retreat of ice). In total, this project surveys the influence and importance of plasticity in phytoplankton communities' light responses in a region undergoing substantial environmental change. The results suggest a need for more investigation of acclimating

light responses, a reconsideration of heuristics on spring bloom timing, and recognition of seasonality in phytoplankton parameters within numerical models.

1.2 Models & Ecosystems

Nelson Goodman noted "Few terms are used in popular and scientific discourse more promiscuously than 'model' " (Goodman, 1968). While Goodman was discussing the broadest possible sense, encompassing any abstraction whether its in science or art, even within the field of biology the word 'model' has been defined and re-interpreted as anything from a set of axioms that isomorphically map to the real world, to abstractions that mediate between theory and observation (Odenbaugh, 2008).

The focus of this thesis is a question not only of the behaviour of a particular ecosystem, but a question of how to describe and study it. The following chapters will unfold how models are formed based on observation, and the subsequent mismatch between model behaviour and the observed data leads to new hypotheses and thus new models. This process has benefits and risks, however. There are historical examples of models being tinkered with in the light of new evidence to save them when they shouldn't be (Newtonian gravity as one example) and of models being adjusted and added to in a way that reveals new information about reality (the cosmological constant in Einstein's equations, e.g.) (Carroll, 2019). These examples from physics are useful reflection for an ecologist, as they raise the issue of falsifiability while simultaneously demonstrating how successful but incomplete models can drive new discoveries (*ibid.*).

Ecosystems are themselves a type of model, a conceptual description of the arrangements of physical and biological structures and the energy flows between them. Ecosystems can be understood as descriptive tools for field biologists as well as mathematically descriptive structures intended to (successfully or not) have predictive power (Peacock, 2008). On this latter point, there has been some criticism of the description of ecosystems as structured systems following quantifiable laws, on the basis that connecting these back to the real-world is often nebulous or open to interpretation (Sagoff, 2003).

This conceptual groundwork is important for considering how the numerical methods for modelling ecosystems can be developed and used. This thesis is concerned

with an observation of phytoplankton behaviour within an ecosystem (the Eastern Bering Sea). By taking the "models as mediators" approach (Cartwright *et al.*, 1995; Odenbaugh, 2008), we can test hypotheses within the limits of the model's inherent assumptions, and use the results to build on existing frameworks for understanding the EBS and plankton dynamics in seasonal environments generally. What a model can and cannot do within its constraints can rule out some space of hypotheses while pointing toward a more complete picture of the reality that is being modelled (Carroll, 2019).

The method this thesis uses is the NPZD model, so-named for its description of an aquatic ecosystem in terms of interactions between its components: Nutrients, Phytoplankton, Zooplankton, and Detritus. Each of those can be broken into multiple compartments (for example, phytoplankton can be divided into small and large classes, or nutrients could be separated into NO_3 and NH_4, etc). Principally, NPZD models serve to break down plankton ecology into core interactions, where the losses from one component either exit the system or become gains for another component (Gentleman, 2002).

Ultimately, however, all ecosystems on Earth connect in some way to each other. One way of defining an ecosystem is the physical and biological systems and processes that have feedbacks with each other, with external forcing being separate from any feedback (Peacock, 2008). In the case of an NPZD model, we know marine ecosystems are often more complex than the phytoplankton and zooplankton components. Thus in analysing methods for constructing numerical models of marine ecosystems, we first look at a global scale before resolving its components and addressing the limits and advantages of different scales and levels of complexity.

1.2.1 Numerical Ecosystem Models

Even the most complex numerical ecosystem models, spanning the largest domains in space and time, necessarily make assumptions and limit their scope. In the words of some philosophers, they would be said to be not isomorphic with the real world (Odenbaugh, 2008). However the aim of these large models is to try to capture more varied

and generalised behaviour, encompassing processes often excluded from smaller models which lack such broad scope.

MEDUSA is a plankton ecosystem model for the World Ocean. Incorporating two classes of phytoplankton, separating the siliceous diatoms from non-diatoms, and two classes of zooplankton, separated by size between micro- and meso- zooplankton. In addition, MEDUSA tracks the chlorophyll content of all phytoplankton and the silica content of diatoms (Yool *et al.*, 2011, 2013). This level of complexity has a lot of value in a large domain like the world ocean. Though as noted in Yool *et al.* (2011), each additional component is a step toward realism at the cost of error associated with parameterisation. This is a trade-off that has to be considered.

For example, a simplified NPZD model with minimal classes of nutrients, phytoplankton, etc will fail to reproduce ecological changes that fall along the lines of those classes. Yool *et al.* (2011) give the example of increasing ocean stratification and decreasing vertical nutrient supply to the surface. This could have a much stronger negative impact on diatoms than other phytoplankton, since silicic acid is regenerated deeper in the water column than, say, nitrogen or phosphorus. A complex biogeochemical model that makes this differentiation will diverge from a model that ignores silicon or combines it with other nutrients. On the other hand, where there is high uncertainty, attempting to include it can lead to more error. As another example, MEDUSA 2.0 explicitly omitted a process (calcification) from the model on account of the high uncertainty surrounding it (Yool *et al.*, 2013).

Another layer of complexity to consider is dimensionality. The MEDUSA ecosystem model is run within the physical ocean model NEMO, a fully three-dimensional global model (Madec *et al.*, 2019; Yool *et al.*, 2011). The geometric increase in complexity of a 3D model is often a necessary cost in exchange for being able to track organisms and nutrients as they move horizontally between grid cells.

Earlier versions of NEMO could be run with either z or σ coordinates (Madec *et al.*, 2019). The z and σ coordinates are also known as "geopotential" and "terrain-following" coordinates, respectively, and have (Griffies, 2004). Terrain-following coordinates are thus named because the vertical coordinate σ is a dimensionless value

between 0 at the ocean surface and -1 at the bottom. A z-coordinate model will not monotonically map the water column, and ultimately discretises the seafloor based on the vertical grid-size dz. That is, the seafloor is either above or below a grid cell and does not run through it.

Global models do not resolve all the smaller processes that may be the focus of a study. On a smaller scale are regional models which can focus on local phenomenon and resolve them more clearly. BIOMAS (Biology/Ice/Ocean Modeling [*sic*] and Assimilation System) is a pan-Arctic 3D biophysical model incorporating a sea-ice model, an ocean circulation model, and a biological model (Zhang *et al.*, 2010a, 2014, 2015), an extension of the earlier BESTMAS which did not include biological components (Zhang *et al.*, 2010b). Likewise, SINMOD is another pan-Arctic physical-chemical-biological model (Slagstad & McClimans, 2005; Wassmann *et al.*, 2006). While often used for studies of the Barents Sea, SINMOD has portability, and has been applied in other regions such as fjords and seas around New Zealand (Jiang *et al.*, 2015). For its primary purpose, the Arctic seas and in particular the Barents Sea, SINMOD is capable of high resolution of coastal areas, such as Norway's famously complex coastline. BESTMAS and SINMOD have computational advantages over global models in that they can have a higher resolution of their study area since the full domain is smaller.

So far the discussed models have taken an empirical approach, tracking the cycling of nutrients through trophic levels based on ecological processes derived from ecosystem-level observations. There are also models that start with equations of the mechanistic behaviour of phytoplankton. For example, in the paper introducing the mechanistic model Eco3M, Baklouti *et al.* (2006a) lay out the different approaches and the merits and demerits of both. Just as was noted for nutrient selection in MEDUSA, the choice between empirical biogeochemical models and the mechanistic models is often contingent on which is the greater unknown. Some cellular processes are relatively well understood but at there still many uncertainties. A mechanistic approach is inherently more complex, accounting for more processes than need be described at a lower resolution. However as Baklouti *et al.* (2006a) ague, when implemented carefully this approach breaks down parameters that previously needed tuning to observation into

parameters that could be better constrained by the taxa of the individual species, potentially making the model more portable. Though the authors also note the difficulty in such fine measurements of physiological behaviour can lead to high uncertainties in those parameters as well.

Another perspective on constructing phytoplankton ecosystem models is the trait-based approach. An adaptive-trait approach varies model parameters during the run according to trade-off functions and selective advantages. This allows for a model to capture such potential changes as evolutionary adaptation, changes in community structure, or plastic acclimation (Litchman *et al.*, 2013; Merico *et al.*, 2009).

The above examples each have unique approaches to ecosystem modelling but many of their approaches can be applied broadly. Adaptive trait-based models can be NPZD models (Merico *et al.*, 2014), and mechanistic approaches can be applied on any scale. It is the trade-offs that have to be considered. A full mechanistic approach increases the complexity and number of equations quite substantially, and thus may not be suitable in a model already dealing with a large spatial domain and multiple nutrient categories at a high resolution. This is all to say that for a highly specified research question within a well-studied system, the simpler approach is often the best starting point. We must then discuss the details of the basic NPZD model and how it works.

1.2.2 NPZD Models

Precisely how these interactions and exchanges function is highly variable. In the earliest attempts to mathematically describe and model planktonic ecosystems (e.g. Riley & Von Arx, 1949), the lack of computing power limited the complexity of equations. Non-linear rates of nutrient uptake or predation could not be usefully incorporated before the 1970s (Gentleman, 2002), but today can be incorporated throughout the model, greatly expanding the space of possibilities (Gentleman *et al.*, 2003; Heinle & Slawig, 2013b).

The choice of functional forms and parameterisation can have a substantial impact on model behaviour, and the more components and dependencies, the more variation is possible (Gentleman, 2002; Heinle & Slawig, 2013a; Murray & Parslow, 1999). To

quote Tett & Wilson (2000), "marine ecologists have achieved no consensus about a way to model system dynamics". As those authors note, many processes and their parameters have high degrees of uncertainty, and including them would propagate their errors. For example, one reason for the multitude of descriptions of zooplankton grazing behaviour is that different species exhibit different preferences for food sources (Gentleman *et al.*, 2003). More data on the specific zooplankton, and their options for food, being modelled helps constrain the choice. The same is true for phytoplankton. Different taxa may have different strategies and subsequently different behaviours in their photosynthesis and nutrient uptake.

What NPZD models today don't commonly include is acclimation processes (Kerimoglu *et al.*, 2017), such as a specifically seasonal variation in parameterisation of biological functions. One to do so is described in Banas *et al.* (2016), which applies an NPZD model to the Eastern Bering Sea, with the light limitation of phytoplankton switching from one parameterisation in winter to another in spring.

This thesis extends the NPZD model of that study by further exploring the seasonality aspect, both in terms of how seasonal parameterisation affects internal dynamics of the model as well as how it affects the accuracy of the model in reproducing observational data.

1.3 Eastern Bering Sea

As an example of the influence seasonal environments can have on ecosystems, the Eastern Bering Sea (EBS) offers a useful case study due in large part to the seasonal ice cover, which freezes in winter and thaws in spring (Sigler *et al.*, 2014). The region is also an example of the impending changes coming to the Arctic, as ice thins and retreats northward in the EBS as a consequence of rising temperatures (Eisner, 2018, 2019; Stabeno *et al.*, 2017).

The EBS can be divided into three domains: coastal, middle shelf and outer shelf (Kinder & Schumacher, 1981a,b). Observational data described in later chapters were primarily sampled from the mid- and outer shelf zones, where water depths range

from 50 to 200 metres (Coachman, 1986). The onset of spring blooms in the Bering Sea is influenced by many inter-related factors. Sea-ice limits light, but also protects the water column from winter storms and thus strengthens stratification (Hunt, Jr *et al.*, 2002; Mordy *et al.*, 2017). Winter mixing can also redistribute nutrients from deeper layers (Ladd *et al.*, 2018).

Years can be categorised as "warm" or "cold", with cold years experiencing significantly thicker ice cover that extends further south at its maximum and which persists until later in the year. While the years 2007-2013 were cold years (Brown & Arrigo, 2013; Sigler *et al.*, 2014), featuring extensive sea-ice which persisted later into the year, beginning in 2014 the Eastern Bering Sea has been experiencing warm conditions (Duffy-Anderson *et al.*, 2017; Stabeno *et al.*, 2017).

1.3.1 Spring Blooms in the EBS

Phytoplankton seasonality has long been understood to be an essential factor in temperate and high latitude marine ecosystems. In spite of initial dismissal of planktonic organisms in general as uninteresting "philosophical muck" by Johannes Müller in the 1830s (originally "philosophischen Dreck", see Kortum, 2009; Smetacek, 1999), by the early 20th century it was clear that phytoplankton were of fundamental importance for the ecosystem (cf. Gray, 1931, which notes the relationship between ice-melt, diatom growth, and whale migrations). By the mid-century, marine scientists began attempting to understand the driving factors of phytoplankton development and population growth (Sverdrup, 1953). Spring blooms, the rapid increase of phytoplankton biomass in late winter or early spring, are crucial for sustaining the rest of the food web, as phytoplankton feed higher trophic levels (Hunt, Jr *et al.*, 2018; Sigler *et al.*, 2014).

Spring blooms are an annual occurrence in the Bering Sea, though the exact timing can vary by months from late winter to early summer (Hunt, Jr *et al.*, 2002). These blooms are dominated by diatoms (Okazaki *et al.*, 2005; Sambrotto *et al.*, 1986; Takahashi *et al.*, 2002; Taniguchi, 1999). Diatoms are a siliceous group, and the region is not silica limited (Honjo, 1990; Takahashi *et al.*, 2000; Tsunogai *et al.*, 1979). Over the deep basins of the Bering Sea iron may be limiting, but surface waters over the shelf

are iron-replete (Aguilar-Islas *et al.*, 2007).

Higher trophic levels depend greatly on blooms in the EBS. One example is pollock, a species of fish that is also the basis of one of the largest fishing industries in the United States. Their ability to spawn and feed are connected with not just the magnitude of a bloom but its timing as well, via the effects of both on the timing and magnitude of zooplankton growth (Coyle *et al.*, 2011).

One hypothesis about the controls on spring bloom timing is the Oscillating Control Hypothesis (OCH) presented in Hunt, Jr *et al.* (2002). The OCH posits that sea-ice shields the water column from winter storms which would otherwise mix surface water to aphotic depths. This limits the fraction of incoming surface PAR that a phytoplankton cell actually experiences during its mixing in the water column.

Therefore, one would expect that in warm conditions, parts of the EBS without winter ice and where ice melts too early should have a later spring bloom than where ice is persistent, as stratification takes longer to occur and greater day lengths are necessary to give phytoplankton sufficient light. This is concordant with the critical mixing depth hypothesis of Sverdrup (1953), which posits that if the mixed layer extends below a critical depth, phytoplankton do not receive sufficient light for a bloom. This hypothesis has been found to be consistent with blooms in the Pacific (Hunt, Jr *et al.*, 2002; Kikuchi *et al.*, 2020) and Atlantic (Henson *et al.*, 2006; Siegel *et al.*, 2002), though it has its share of caveats (Smetacek & Passow, 1990).

The importance of mixing is agreed on even in papers which question or contradict the OCH. Brown & Arrigo (2013) used satellite data to study spring blooms and found some years that did not accord with the OCH, however, they note that they could not see under-ice blooms, and therefore may not have recorded a start date for the spring bloom until much later than it had begun, after the ice melted. And Ladd *et al.* (2018), in studying coccolithophore blooms in the EBS, suggest a distinction between the middle and outer shelf zones in contrast with the inner shelf; specifically that in the shallow inner shelf, deep mixing can help a bloom begin earlier by bring up nutrients from the deep layers.

1.3.2 Drivers of Seasonal Behaviour of Phytoplankton

Evolutionary adaptations and individual acclimation to changes in temperature, nutrient concentration, turbulence, mixing depth, and light have all been scrutinised (Huisman *et al.*, 2004; Litchman, 2000, and references therein), yet many of the mechanisms behind spring blooms and phytoplankton over-wintering strategies, especially as regards light response, remain not fully understood. For example, the light curves of phytoplankton, measures of photosynthesis versus irradiance, are known to acclimate to changing light conditions (Cullen, 1990; Litchman, 2000; Sambrotto *et al.*, 1986, see also the literature review in Chapter 2). This process is known as photoacclimation, in contrast to photoadaptation, an evolutionary change in the genome of a population (Moore *et al.*, 2006).

Both the plastic response of photoacclimation and the population change of photoadaptation affect how phytoplankton photosynthesise with changes in light. These processes may have significant impacts on timing and magnitude of spring blooms. For example, and as will be discussed in greater detail below, Banas *et al.* (2016) found that in order to reproduce detailed observations of bloom timing and magnitude simultaneously, a model hind-cast of the Eastern Bering Sea required strong seasonal variation in the parameter that defined the light response of phytoplankton.

Responses to changes in light have been studied mostly on very short time scales. Many studies have explored how different phytoplankton respond to fluctuating light, on time scales as short as minutes (Strzepek & Harrison, 2004), hours (Ban *et al.*, 2006; Fujiki & Taguchi, 2002), or days (Claustre *et al.*, 2002; Cosper, 1982; Marra, 1978; Nicklisch, 1998). Typically, within these studies of short-term variation and acclimation the response observed has been to increase photosynthetic efficiency as light diminishes, though there are exceptions (Ban *et al.*, 2006; Sakshaug & Slagstad, 1991).

In contrast, Sambrotto *et al.* (1986) observed a rapid, nearly ten-fold increase in photosynthetic efficiency in the Southeastern Bering Sea during the onset of one spring bloom: the opposite of what simple photoacclimation would be expected to produce during a period of increasing light. Those results provided the motivation for imposing

seasonality in the photosynthetic efficiency of the model in Banas *et al.* (2016), denoted by the variable α.

Seasonal change in photosynthetic efficiency necessarily reflects the net effect of a complex array of variable physiological processes. Changes in pigment concentration have a non-linear effect on efficiency. After a threshold is reached, excess pigments self-shade, creating what is known as the "package effect", reducing efficiency (Brunelle *et al.*, 2012). Additionally, pigments require maintenance, and thus bear a metabolic cost in the form of maintenance respiration. Many cells have been shown to increase intra-cellular pigments as light decreases (Dubinsky & Stambler, 2009), but such trends can be the opposite after a period spent in zero light, after which pigments decrease again (Gibson, 1985). Peters & Thomas (1996) found that marine Antarctic diatoms preserved and maintained their photosynthetic apparati in winter and could resume assimilating carbon immediately upon the return of light after at least three months of darkness. In contrast, Peters (1996) observed decreased photosynthetic potential in temperate species, at higher temperatures, during long periods of darkness. This complexity, and variety of strategies, shows it is therefore difficult to create a unified theory of seasonality in photoresponse.

This study builds on the above with more recent data from the Eastern Bering Sea, discussed in Chapter 3, which show lower values for both the maximum nutrient uptake rate v_m and α (the initial slope of the photosynthesis-irradiance curve) in under-ice over-wintering samples compared with open-water samples in optimal spring bloom conditions.

All the aforementioned adaptations and acclimation strategies connect photosynthetic efficiency with metabolism and respiration, with literature establishing models of respiration that depend on parameters of light response governing the efficiency of photosynthesis. These "photoparameters" are defined in the next section.

While theories of respiration can provide explanations for why seasonality occurs, the relevance and importance of seasonality is demonstrated in numerical models. In this project, NPZD models are used to experiment with the above ideas, in Chapters 4 & 5 . To understand how light responses can be measured and modelled, it is necessary

to first define the principal terms, such as the photoparameters, and discuss their meaning both in mathematical and biological terms.

1.4 Photoparameters and Models of Light-Limited Photosynthesis

The relationship between photosynthesis (P) and light availability (E) is often expressed in the form of photosynthesis-irradiance (P-E) curves. The irradiance E is usually expressed in terms of photosynthetically active radiation (PAR), the fraction of incoming light which chlorophyll can absorb and use for photosynthesis. The form of P-E curves is initially linear or nearly linear at low irradiance, approaching some maximum rate of photosynthesis, denoted P_m or P_{max}, before the curve flattens (cf. Jassby & Platt, 1976; Platt *et al.*, 1980). When measurements are made at high light levels, P-E curves can also show the process of photoinhibition, when increased light causes a decrease in photosynthesis (Neale & Richerson, 1987; Powles, 1984).

Multiple mathematical models of this relationship exist, though no single expression can be thought of as universal. Owing to the complex nature of photosynthesis, its many external dependencies and wide array of different internal components, Steeman Nielsen & Hansen (1959) speculated it was unlikely any equation would be able to describe the P-E relation in an "unequivocal" way. Nonetheless, two of the most prominent formulations are the Platt model (Platt *et al.*, 1980, 1982):

$$P = P_m \left(1 - \mathrm{e}^{-\alpha E/P_m}\right) \mathrm{e}^{-\beta E/P_m} \tag{1.1}$$

and the Smith model (Smith, 1936):

$$P = \frac{\alpha E}{\sqrt{\alpha^2 E^2 + P_m^2}} \tag{1.2}$$

These models are defined by four photoparameters: P_m, α, E_k, and in the case of the Platt model: β.

P_m, sometimes written P_{max}, is the maximum rate of photosynthesis, typically

expressed in units of carbon per time (e.g. mg C h^{-1}). Biomass specific photosynthesis, normalised to amount of chlorophyll, is commonly denoted P_m^B.

β is the photoinhibition parameter of the Platt Model, and controls the extent to which photosynthesis decreases at supra-optimal irradiance.

α is the initial slope of the P-E curve. Because of the quasi-linear nature of this relationship at low irradiance, α is related to P_m via the parameter E_k, the saturating light intensity:

$$\alpha = P_m / E_k \tag{1.3}$$

E_k is the irradiance at which photosynthesis saturates. Irradiance can be measured in W/m^2 or in μE/m^2/s, where μE is a micro-Einstein, a micromole of photons. The conversion between these units depends on the wavelengths being measured, as watts are a unit of power and micro-Einsteins a count of the photons, however for PAR, being in the 400-700 nm band, this conversion can be approximated as 1 W $m^{-2} \approx 4.57$ μE m^{-2} s^{-1} (Thimijan & Heins, 1983). Any changes between units in the rest of this thesis use this approximation.

Specific growth rates of cells, often denoted with μ, measure the amount of uptake of a nutrient relative to the internal concentration, and thus has units of 1/time. Difference must be noted between the carbon-specific growth rate of a cell and photosynthesis. Converting photosynthesis rates into growth rates requires assumptions about carbon fixation and cell division that are not constant even within a single cell. Some amount of carbon goes into storage compounds and not into growth or maintenance (Falkowski & Raven, 2007). Hence it is important to distinguish which value is being measured or discussed in any context. But specific growth rates can still be modelled with a formulation similar to the Platt Model of photosynthesis (Falkowski & Raven, 2007; Li *et al.*, 2015)

$$\mu = \mu_0 \left(1 - \mathrm{e}^{-\alpha E / \mu_0}\right) \tag{1.4}$$

The result of the above equation is that, in this context, α can also represent a

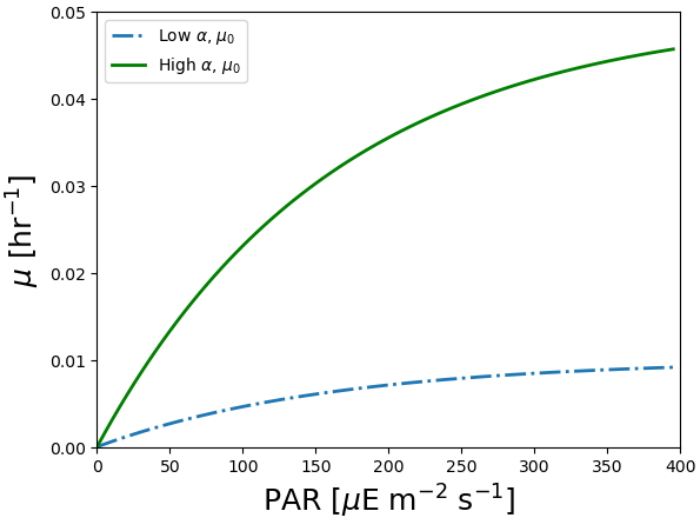

Figure 1.1: Example μ-E curves using Equation 1.4, where α and μ_0 vary with a fixed E_k. Carbon-specific growth values used were $\mu_{0,high} = 0.05$ and $\mu_{0,low} = 0.01$ hr^{-1}. Initial slopes were $\alpha_{high} = 3.1 \cdot 10^{-4}$ and $\alpha_{low} = 0.62 \cdot 10^{-4}$ hr $^{-1}$ (μE m^{-2} s^{-1})$^{-1}$. The high μ_0 value came from that use in the model of Banas *et al.* (2016). The high α value came from data presented in Chapter 3.

relationship between specific growth and saturation intensity:

$$\alpha = \mu_0 / E_k \tag{1.5}$$

It is common for carbon-specific growth to be labelled μ_C (Falkowski & Raven, 2007), while the uptake rate for a nutrient such as nitrogen would be denoted with V or v, although μ has also been used for nitrogen uptake (Li *et al.*, 2015). Hence it is important to clarify. In this thesis, v will primarily be used to refer to nitrogen uptake unless otherwise specified, and μ will be used for carbon-specific growth. Specific nitrogen uptake will be converted into carbon-specific growth rates in such cases where a constant C:N is assumed (as will be expanded on in Chapter 4).

Figure 1.1 shows two examples of hypothetical curves of carbon-specific growth, using the above model of the same form as the Platt Model of photosynthesis. Both curves in the figure use the same E_k, but differ in α and μ_0. By virtue of having the same saturation intensity E_k, the curve with the smaller photoparameters not only

has a lower maximum specific growth rate, but requires much higher irradiances to approach it.

As α describes a quasi-linear relationship, a ratio of photosynthesis (or specific growth) to irradiance, it can be thought of as a measure of photosynthetic efficiency. In this sense, α can also be defined as the product of the chlorophyll-specific absorption cross-section $\bar{a}^*$, and the maximum quantum yield ϕ_{max}:

$$\alpha = \bar{a}^* \phi_{\max} \tag{1.6}$$

The chlorophyll-specific absorption cross-section is a measure of the amount of incoming PAR that can physically be absorbed by chlorophyll. An increased area of chlorophyll increases $\bar{a}^*$, however after a threshold is reached, excess pigments overlap and self-shade, creating what is known as the "package effect", reducing the absorption cross-section (Brunelle *et al.*, 2012).

Maximum quantum yield (MQY, denoted ϕ_{max}) is the maximum number of moles of O_2 evolved from the minimum number of photons absorbed (Nickelsen, 2015; Nickelsen & Govindjee, 2011). In this sense, it is the maximum efficiency of oxygen production from photon absorption.

In another sense, maximum quantum yield can be defined by the structure of the photosystems. In photosynthetic reactions, the first protein complex is Photosystem II (PSII), which captures photons and begins electron transport (Falkowski & Raven, 2007). The area over which the light harvesting proteins can absorb photons is the absorption cross section. MQY can be expressed as the ratio of the absorption cross sections of PSII to that of the the Photosynthetic Unit (PSU).

$$\phi_{max} = \frac{\sigma_{\mathrm{PSII}}}{\sigma_{\mathrm{PSU}}} \tag{1.7}$$

The photosynthetic unit is not, strictly speaking, a physical structure or chemical, but a representation of the whole system of processes from absorption of a photon to production of O_2. The "size" of the PSU can be represented as the ratio of chlorophyll to evolved oxygen (Chl/O_2) (Falkowski & Raven, 2007). The PSU accounts for the

antennae and reaction centres of a photosystem, as well as the chlorophyll which carries electrons between them. Thus, α can be derived from the fundamental biochemistry of a given cell as in Equation 1.6, or from the other photoparameters as in Equation 1.5.

Important to note is that the above models, the Platt model and the specific growth equation, so far do not account for any losses due to respiration. They are descriptions of gross rates (of μ or P), and not net. Net growth rate is determined by subtracting specific respiration R (in units of 1/time) from the gross specific growth rate. When respiration losses are greater than gains from growth, net growth becomes negative (which can be thought of, in a model, as representing mortality).

$$\mu_{net} = \mu_0 \left(1 - \mathrm{e}^{-\alpha E/\mu_0}\right) \mathrm{e}^{-\beta E/\mu_0} - R \tag{1.8}$$

In the case of the Platt model of photosynthesis, or any model of P or μ solely as a function of light, when respiration is accounted for then below an irradiance E_C respiration dominates and the net carbon uptake rate is negative. This is known as the compensation intensity, or compensation irradiance or point. This limit is thus named because it is the irradiance at which carbon losses due to respiration balance any gains, so the net for photosynthesis or specific growth is zero (Falkowski & Raven, 2007; Geider & Osborne, 1989).

1.5 Outline

The following chapters will sequentially build on the above to create an overview of phytoplankton seasonality in the EBS across multiple perspectives.

Chapter 2 presents a literature review which demonstrates that a difference can be seen between photoacclimation strategies on short time scales (less than 30 days) and those on the scales of months or more. While a decrease in α during winter months is a counter-intuitive response, it will be shown that this is established in prior literature of high latitude phytoplankton.

Chapter 3 examines observational data from the EBS that sampled sites which were still ice-covered and those which were already in peak bloom conditions. These data,

from the cold year of 2009, show the same seasonal trend in α as seen in the literature review. This chapter also proposes a trade-off mechanism as an explanation for this behaviour, linking α to maintenance respiration costs.

In Chapter 4, the seasonal pattern observed in the data was then used as the basis for seasonal photoparameters in an NPZD model of the EBS. This model was tuned using observational data from 2009, a cold year, and compared with a model that lacked seasonal light response.

In Chapter 5 the NPZD model, with its seasonal photoparameters, was applied to the warm year of 2015. These runs were used to study the interplay between ice, light, and mixing as influences on the spring bloom.

Finally, Chapter 6, the Conclusion, we summarise the case for including seasonality in models of phytoplankton. From the observational evidence of this process to its effectiveness in the model experiments, we conclude future modelling approaches in highly seasonal environments like the EBS ought to consider photoacclimation, and we present perspectives that may inform these future studies as well as the prospective data that may harmonise theory with observation.

Chapter 2

Literature Review

As stated in Chapter 1, prior research already implied the seasonality of photoparameters in phytoplankton of the East Bering Sea. Two in particular were the initial impetus for the investigation this thesis is about. In Sambrotto *et al.* (1986), photoparameters were measured in winter and spring and detected a lower α in the over-wintering samples. In Banas *et al.* (2016), an NPZD model of the spring blooms in the EBS necessitated the use of seasonal α, lower in winter than in spring, to produce a model output that matched observational data.

A literature review was conducted to establish whether these results could be generalised or be otherwise indicative of a pattern. The literature on short term acclimation (from minutes to days) in marine phytoplankton is vast, dating back at least as far as the 1930s (Steemann Nielsen, 1937), despite the difficulties in making measurements at the time. Attention to the role of light in photoacclimation and seasonal ecology increased significantly from the 1950s, laying the groundwork for today's studies (Steeman Nielsen & Hansen, 1959; Sverdrup, 1953).

The primary focus of this study is high latitude, marine phytoplankton experiencing prolonged periods of darkness on the time scale of months, and as such the literature on short-term acclimation was sampled primarily to demonstrate the high variability of results. Many strategies exist for coping with short-term changes in irradiance, and these cannot always be said to be viable for longer periods.

For long term acclimation, studies where samples of high-latitude phytoplankton

which had 30 days or more to acclimate to light were specifically sought out. Decades of research into photoacclimation and photoadaptation have used a variety of methods and measured many different parameters. The papers surveyed here reflect the diversity of study methodology and phytoplankton strategy.

Tables 2.1 and 2.2 present a summary of some of the literature on adaptations of α in response to decreases in light over time scales less than 30 days (Table 2.1) and longer than a month (Table 2.2, designated as 'seasonal'.), along with the impact of photoacclimation on chlorophyll-specific absorption $\bar{a}^*$ (see Equation 1.6). Table 2.1 is not meant to be comprehensive, only illustrative of the large variance in observed relationships between irradiance and light response, and irradiance and photochemistry.

2.1 Short Term Photoacclimation

In many cases for short-term acclimation, cells increase the initial slope of the P-E curve α (Ikeya *et al.*, 2000) and potentially even maximum growth rate μ_0 as well Sakshaug & Slagstad (1991). This strategy reflects the need to do more with the decreasing amount of light available, if it is possible. Changes in α are not consistently uni-directional. Ban *et al.* (2006) experimented with lab cultures of *Chaetoceros gracilis*, and found that samples grown at 20 μE m^{-2} s^{-1}had higher values of α than those grown at 350 μE m^{-2} s^{-1}. However, the samples growing under 3 μE m^{-2} s^{-1}had lower values of α than the 20 μE m^{-2} s^{-1}samples. However, the maximum relative Electron Transfer Rate (rETR) positively correlated with irradiance.

From another perspective, we see a complex picture in the biochemistry as well. In Fujiki & Taguchi (2002) and Obata & Taguchi (2009), both studying photoacclimation on a time scale of hours, $\bar{a}^*$ increased at high irradiance, which Obata & Taguchi attribute to the package effect. In Sakshaug & Slagstad (1991), while $\bar{a}^*$ decreased in the samples that had undergone photoacclimation over a period of days, α^B and P_m stayed approximately the same, and yet ϕ_{max} had increased at the lower irradiance.

While increased efficiency when light is scarce (as in Ban *et al.*, 2006) may appear to be the logical response, as the next section demonstrates this is not necessarily the case when the scarcity persists for long periods on the order of months. Furthermore,

this literature review and Chapter 3 will explore whether such a strategy would even be viable for such a timescale.

2.2 Seasonal Photoacclimation

As noted, in the Eastern Bering Sea, Sambrotto *et al.* (1986) found different values of α for pre-bloom and spring bloom samples taken in May 1981, with $\alpha_{summer} = 0.16$ (W m^{-2})$^{-1}$ day^{-1} and $\alpha_{winter} = 0.01$ (W m^{-2})$^{-1}$ day^{-1}. In the units used below, this corresponds to 3.0×10^{-2} (μE m^{-2} s^{-1})$^{-1}$ hr^{-1} (summer) and 1.9×10^{-3} (μE m^{-2} s^{-1})$^{-1}$ hr^{-1} (winter).

Previous literature demonstrates how the photoparameters cannot be taken as constants. For example, a meta-analysis by Smith Jr. & Donaldson (2015) of observations in the Ross Sea found that the photoparameters were sensitive to changes in irradiance. Moreover, prior studies have shown not only seasonal variability of photoparameters such as α and $\bar{a}^*$ (likely the direct result of seasonality in irradiance, as will be discussed below), but also variability in photoacclimation strategies (see Table 2.2).

As an overview of some of the variability: Two papers reporting α observations for marine phytoplankton over a seasonal time scale (Platt & Jassby, 1976; van Hilst & Smith, Jr, 2002) found lower values of both α and P_m associated with a lower light regime. However another paper found the reverse trend for freshwater diatoms in a permanently ice-covered Antarctic lake (Morgan-Kiss *et al.*, 2016). Sambrotto *et al.* (1986) compared light response between samples from Subsurface Chlorophyll Maxima (SCMs) and the overlying lower chlorophyll, higher light layers, and found larger α in the SCM. Palmer *et al.* (2011) found higher α and P_m in open water samples than in under-ice conditions in Franklin Bay, particularly for large cells, but no significant difference in Darnley Bay. Palmer *et al.* (2013) also found no significant difference between open water and under ice in the Chukchi and Beaufort Seas. Rochet *et al.* (1986) found high variation in observed α from April to May, such that while the final measurement was lower than the maximum in mi April, the trend in the data was weak. Variation in $\bar{a}^*$ on a seasonal time scale was reported in Matsuoka *et al.* (2011), which found a decline in $\bar{a}^*$ going from spring to summer and then a rise again into autumn.

And Matsuoka *et al.* (2009) found a slight increase between October and November. Brunelle *et al.* (2012) found a decrease from summer to autumn in the Amundsen Gulf at all depths. In summation, field observations of phytoplankton communities that are expected to have been acclimated to seasonal light changes have shown considerable variability in the response of photoparameters.

Long term lab studies using cultures taken from field samples (Wulff *et al.*, 2008), and experiments on lab cultures (Wu *et al.*, 2008) also showed lowered α in lower light conditions. Though van Hilst & Smith, Jr (2002) found lower α in lower light in their field measurements, samples cultured in the lab and tested later with an acclimation period of 13 days had the reverse trend: higher α in lower light. Four studies looked at the response to decreasing light or total darkness (Matsuoka *et al.*, 2009; Morgan-Kiss *et al.*, 2016; Wu *et al.*, 2008; Wulff *et al.*, 2008), while three examined the response to an increase in light (Brunelle *et al.*, 2012; Matsuoka *et al.*, 2011; Rochet *et al.*, 1986; van Hilst & Smith, Jr, 2002).

The diverse observations on the interaction of phytoplankton light response with the seasonal physical oceanographic changes in temperate and polar regions is strong motivation for revisiting the interpretation of these parameters that are important to marine productivity. Here, this study builds on these field observations with an expanded, more recent data set from the ice edge environment of the Eastern Bering Sea (EBS) along with a model representation of this phenomenon for a more mechanistic perspective.

Source	Location	Taxonomy	Timescale	$\Delta\alpha$	P_m / μ_0	E_k	Notes
Short-Term Acclimations							
Steeman Nielsen & Hansen (1959)	Arctic, Davis Strait	Community	Depth profile	$\sim$	+	+	Measuring net photosynthesis
Platt *et al.* (1982)	65-80°N Baffin Bay	Community	Depth profile	+	$\sim^B$	$\sim$	Late summer comparison of different depths of mixed layer.
van Hilst & Smith, Jr (2002)	Ross Sea	Community	Depth, 50% vs 1% light level	$-^B$	$-^B$	+	Uncertainty for E_k ad P_m values overlapped
Ikeya *et al.* (2000)	44°N, Brackish Lagoon	*Chaetoceros* sp.	Hrs	$-^B$	$\sim$	+	
Fujiki & Taguchi (2002)	Lab Culture	*Chaetoceros gracilis*	Hrs				Increase in $\bar{a}^*$ and photopigments at higher light
Obata & Taguchi (2009)	44°C Saroma-Ko Lagoon	Diatom dominated thing-ice algae	Hrs			$\sim$	Increase in $\bar{a}^*$ at higher light
Sakshaug & Slagstad (1991)	$\sim$ 80°N, Barents Sea	*T. nordenskioeldii* & *C. furcellatus*	Days	$\sim^B$	$+^B$	+	Decrease in ϕ_{max} at higher light, but increase in a^*.
Ban *et al.* (2006)	Lab culture	*Chaetoceros gracilis*	Days	–		+	α was lowest at max irradiance, 350, but peaked at 20 before decreasing again at 3μE m^{-2} s^{-1}. ETR correlated with light
		P. tricornutum		–		+	ETR correlated with irradiance
van Hilst & Smith, Jr (2002)	Ross Sea	*Phaeocystis antarctica*	13 dys	$+^B$	$+^B$	+	
		Pseudonitzschia sp.	13 dys	–/+	$+^B$	+	α highest at middle irradiance, lowest at lowest irradiance

Table 2.1: Directional change of PE parameters acclimating to changes in light on short time scales (less than 30 days). A plus (+) indicates a higher value for the parameter was measured at the higher light level(s), a minus (–) indicates the reverse, and a $\sim$ indicates no significant difference. "B" indicates the study reported values of α^B, i.e. α normalised to biomass.

Seasonal Acclimations							
Source	**Location**	**Taxonomy**	**Timescale**	$\Delta\alpha$	μ_0	E_k	**Notes**
Platt & Jassby (1976)	Costal Nova Scotia		Years: July '73 – March '75	$+^B$	$+^B$		
Sambrotto *et al.* (1986)	EBS	Diatom dominated (in spring)	Spring bloom transition	$+$	$+$		
This study	EBS	Centric diatom dominated (during bloom)	Under-ice vs. open-water; spring-bloom transition	$+$	$+$	$\sim$	
Rochet *et al.* (1986)	$\sim$ 55°30'S Hudson Bay	Diatom dominated (in May)	Months (March to May)	$\sim^B$	$-$		
van Hilst & Smith, Jr (2002)	76°30'S, Ross Sea	*Phaeocystis* dominated	Months (spring to summer)	$+^B$	$+^B$	$-$	
Wu *et al.* (2008)	Lab culture	*Microcystis aeruginosa* and *Scenedesmus quadricauda*	30 dys	$+$		$+$	ETR decreased at higher light
Wulff *et al.* (2008)	62°15'S	Diatoms, benthic (5-7 m depth)	64 dys	$+$		$+$	ETR increased at higher light
Palmer *et al.* (2011)	Darnley Bay Franklin Bay	Subsurface Chl Maximum	Open water vs. under-ice	$\sim$ $+^B$	 $+^B$		
Palmer *et al.* (2013)	Chuckchi & Beaufort Seas	Community	Open water vs. under-ice	$\sim$	$\sim$	$\sim$	
Morgan-Kiss *et al.* (2016)	77°S, permanently ice-covered lake	Diatoms	31 Dys (Feb to March)	$-^B$	$+^B$	$+$	

Table 2.2: Directional change of PE parameters acclimating to changes in light on long time scales (more than 30 days). A plus (+) indicates a higher value for the parameter was measured at the higher light level(s), a minus (–) indicates the reverse, and a $\sim$ indicates no significant difference. "B" indicates the study reported values of α^B, i.e. α normalised to biomass.

2.3 Taxonomy of Photoacclimation Strategies

While it is appealing, and even tempting, to look for a simple hypothesis linking taxonomy with the strategy of winter reduction in photosynthetic efficiency, none was apparent from this literature review. Further, a question remains whether the variation in PE parameters for a whole community represent intra-cellular photoacclimation, or a shift in community composition.

Matsuoka *et al.* (2011) propose changes in community composition from larger to smaller cells as the driving factor behind decreases in $\bar{a}^*$, as the package effect decreases with cell size. Decreases in α may be replicable as the result of decreased $\bar{a}^*$ in regions where spring blooms are dominated by diatoms with larger cell sizes than winter communities, such as the EBS in the next chapter as well as Sambrotto *et al.* (1986, 2015), the Ross Sea in van Hilst & Smith, Jr (2002), or the Amundsen Gulf in Palmer *et al.* (2011, 2013).

As for whether specific taxa have common strategies of photoacclimation, Jochem (1999) distinguishes two types of long-term dark response in global phytoplankton: those which decrease metabolic activity (Type I) and those which do not (Type II). Type II populations require a period of replenishing when re-illumination begins before cells can divide again. The same study found three subjects (*Brachiomonas submarina*, *Pavlova lutheri*, *Chrysochromulina hirta*) to be Type I and three more (*Prymnesium parvum*, *Bacteriastrum* sp. and an unidentified pennate) to be Type II.

Peters & Thomas (1996) reported that several marine polar diatoms maintain their photosynthetic apparati in winter, as indicated by rapid growth responses upon re-illumination and measures of Chl-a. (It should be noted the darkness in that study lasted only to a maximum of 12 days). Still, Peters & Thomas (1996), Jochem (1999), and Dubinsky & Stambler (2009) all cite literature attesting to other diatom species which decrease metabolism over winter, suggesting a blanket strategy based on taxonomy may not be possible to formulate.

Chapter 3

A Trade-off Model of Seasonal Light Response in Eastern Bering Sea Phytoplankton

This chapter will present observational data collected in the EBS (Eastern Bering Sea) and the photoparameters derived from it. As hypothesised after the literature review presented in the previous chapter, these photoparameters exhibited different light responses at different irradiances, having undergone photoacclimation.

Photoacclimation was observed in both the maximum carbon- and nitrogen- specific growth rates, and the initial slope of the P-E curve. For consistency, v will be used for uptake rates in general, and μ will always indicate carbon processes. As before, the initial slope is denoted with α. These photoparameters had lower values in the samples from sites taken to represent over-wintering phytoplankton. It was thus inferred that this represented seasonal photoacclimation. The seeming disadvantage of lowering α in winter, at low irradiance, is indicative of a trade-off. A model of maintenance respiration as a function of α will be laid out to explain this counter-intuitive behaviour. The premise for this model is that for extremely low irradiances that persist for a long period of time, phytoplankton find an advantage in reduces the energetic costs inherent in high values of α.

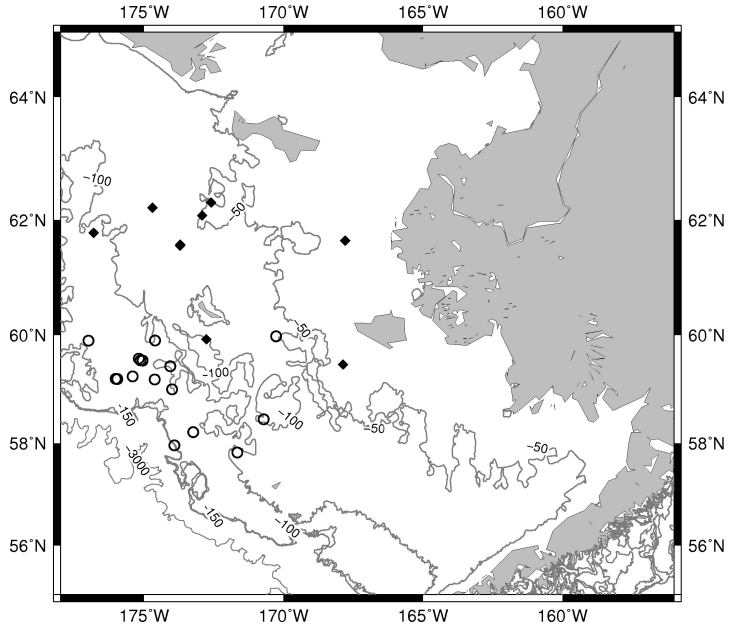

Figure 3.1: Location of the sample sites in the Eastern Bering Sea. Open circles represent open water sampling sites, and closed diamonds represent sites that were at least partially ice-covered at the time of sampling.

3.1 Observational Data of Photoparameters

Data were collected in the Eastern Bering Sea in spring 2007, 2008 and 2009 as part of the BEST-BSIERP field campaign on the USCG Healy (Sambrotto *et al.*, 2015). The sample sites were in the mid- and outer shelf, with water depths ranging from 50 to 200 metres (Coachman, 1986). Figure 3.1 shows the sampling locations, labelled according to ice-cover at the time of sampling. The region experiences seasonal ice cover. Samples were collected before and after ice retreat during each cruise. Each vertical profile covered depths from the surface down to a light level of 1% of the surface value. A four-day-average light level $E_{above\,ice}$ was calculated from the daily averages of incident light on the deck of the ship on the day of sampling and for the three days prior.

Uptake rates of NO_3 and inorganic C were measured in the same incubation bottle using a dual-label approach with a combination of the stable isotope tracers $^{15}NO_3$ and $H^{13}CO_3$ (Sambrotto, 2001; Sambrotto *et al.*, 2008). Samples were taken from

the euphotic zone (100, 55, 30, 17, 9, 5 and 1.5% of maximum submarine light) and collected in 2.2-L PET bottles. The original light levels were simulated with layers of black screen and the bottles were incubated for 24 hours in on-deck incubators cooled with surface seawater pumped from the ship's sea chest. Complete details of sampling and measurement procedures can be found in Sambrotto *et al.* (2015).

The photoparameters are denoted with v for uptake rates in general, mu_0 for carbon-specific growth, α as the initial slope, E_k the saturation intensity, and β as the photoinhibition coefficient. These were derived by fitting the carbon uptake data with the Platt Model as defined in Equation 1.1. Here, μ_0 is the maximum specific carbon uptake rate (derived from the uptake rates in Sambrotto *et al.*, 2015), E_k is the saturation light intensity, and β is the photoinhibition parameter. The parameter α, the initial slope of the PE curve, often referred to as photosynthetic efficiency, is defined in this formulation as in Equation 1.5. Though β was fit with the other parameters, it only impacts the Platt Model at higher light levels than were relevant to the present study. Therefore, in the theoretical discussions below regarding the Platt model and photoacclimation, the β component of the equations is ignored for the sake of clarity. A more realistic version would include photoinhibition, but the overall trends would be the same.

Measured values of v , α, and E_k are shown in Figure 3.2 as a function of the light at the water surface surface, E_{surf}. As mentioned, a three-day average irradiance was measured from the deck of the ship and taken as the above-ice light level. Under ice light values had to be corrected for attenuation by the sea ice. This attenuation is highly dependent on factors which were not measured, including ice thickness, density of ice algae, and snow thickness (Kauko *et al.*, 2017). The value of E_{surf} below the ice was estimated as a linear function of the deckboard-measured light and percent ice cover C, as without more data a more complicated model of attenuation could not be justified. The linear form used here was fit such that in areas with complete ice cover, it was assumed that no light reached the water surface:

$$E_{surf} = E_{above\,ice}\left(1 - \frac{C}{100}\right) \tag{3.1}$$

The assumption of there being no transmittance at maximum ice cover is reflective of observations and studies showing that ice and snow cover in winter can dramatically decrease transmittance (Assmy *et al.*, 2017; Kauko *et al.*, 2017). The possibility and implications of this approach under-estimating light transmittance is discussed in the results below.

Figure 3.2 shows observed values of the three relevant PE parameters v_m, α, and E_k plotted against PAR at the water surface (E_{surf} as defined in Equation 3.1). In Figure 3.2, middle row, two clusters appear in the data for α. Open water samples have a mean $\alpha = (3.1 \pm 1.3) \times 10^{-4}$ (μE m^{-2} s^{-1})$^{-1}$hr^{-1}. In under ice samples, values of α are generally lower than in open water populations, with a mean of $\alpha = (1.3 \pm 2.0) \times 10^{-4}$ (μE m^{-2} s^{-1})$^{-1}$hr^{-1}. One outlier stands out in the α values for under ice samples shown in Figure 3.2, at $E_{surf} = 43.2$ μE m^{-2} s^{-1}. Given the complex wind-driven transport of sea ice in the area, it is possible that this or other samples taken from locations identified as ice-covered may have previously been in open water, such that their phytoplankton could have already acclimated to open-water conditions and higher light levels. This is only a speculation regarding this particular outlier, but it should be noted that without it, the under-ice values of α have a mean of $(0.65 \pm 0.4) \times 10^{-4}$ (μE m^{-2} s^{-1})$^{-1}$hr^{-1}.

A one-tailed Mann-Whitney U test was conducted to establish the significance of the observed difference. Including the outlier in the under-ice data, $U_{under\,ice} = 17$ and $U_{open\,water} = 111$, indicating that the under-ice values are significantly lower than open water ($p < 0.01$). The same pattern is found even when normalised to chlorophyll, that is $\alpha^B = \alpha \frac{C}{Chl}$. Here, a one-tailed Mann-Whitney U test also shows statistical significance for the hypothesis that $\alpha^B_{under\,ice}$ is less than $\alpha^B_{open\,water}$ ($p < 0.05$).

A similar but less dramatic pattern appears in the data for v_m. The mean for under-ice values was 0.014 ± 0.016 hr^{-1}, while open water samples, $v_{m,\text{avg}} = 0.026 \pm 0.015$ hr^{-1}. The difference is also significant ($p < 0.05$) by a one-tailed Mann-Whitney U test where, including the outlier, $U_{under\,ice} = 31$. Values of E_k do not appear to differ significantly between under-ice and open-water conditions. For under-ice samples, $E_k = 120 \pm 60$ μE m^{-2} s^{-1}. Open-water samples had $E_k = 100 \pm 80$ μE m^{-2} s^{-1}.

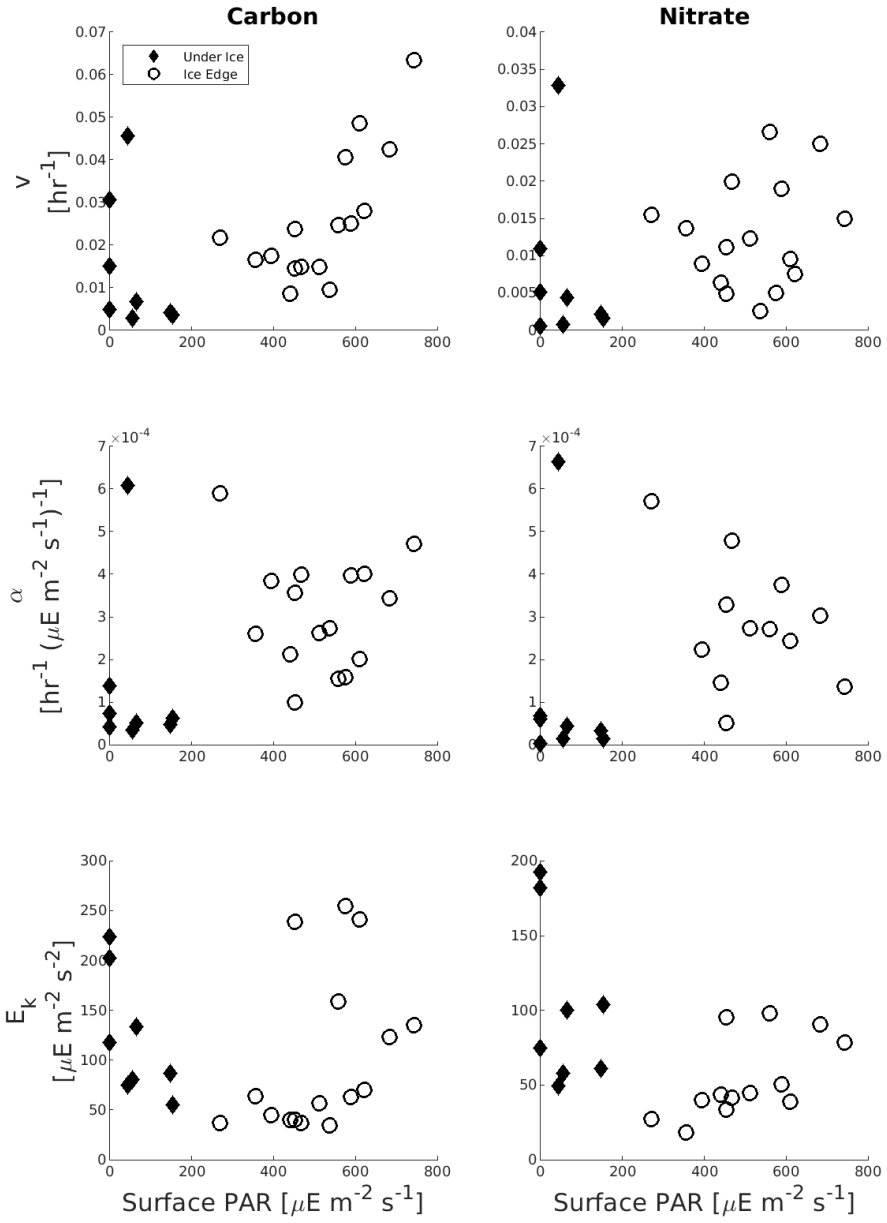

Figure 3.2: Photoparameters plotted against surface PAR. Open circles are data from open-water sampling sites, closed diamonds are data from sites that were at least partially ice-covered at the time of sampling.

3.2 Growth Model with Respiration

As noted by Platt & Jassby (1976), the commonly used form of the Platt curve represents gross rates, not net. In terms of μ (see also Cullen, 1990), the gross specific growth rate μ_{gross} is the sum of net growth rate μ_{net} and dark respiration R_D, such that

$$\mu_{net} = \mu_{gross} - R_D \tag{3.2}$$

where $R_D > 0$. Thus, Cullen (1990) rewrote the model to explicitly include respiration by

$$\mu_{net} = \mu_0 \left(1 - \mathrm{e}^{-\alpha E/\mu_0}\right) - R_D \tag{3.3}$$

It has also been show that dark respiration is a linear function of growth rate μ:

$$R_D = r\mu_{gross} + R_M \tag{3.4}$$

where $r > 0$ is a species-specific slope, and R_M is maintenance respiration which occurs even when there is no growth (Baklouti *et al.*, 2006a; Falkowski & Raven, 2007; Geider *et al.*, 1986). Combining Equations 3.4 and 3.3 and solving for μ_{net} gives

$$\mu_{net} = (1 - r)\,\mu_0 \left(1 - \mathrm{e}^{-\alpha E/\mu_0}\right) - R_M \tag{3.5}$$

Although the actual complexity of photochemistry does not behave so simplistically, it is often assumed that r is constant and therefore Equation 3.4 is linear (Geider, 1992; Geider & Osborne, 1989; Geider *et al.*, 1986). This would make $(1 - r)$ also constant, and thus replace $(1 - r)\mu_0$ with a new μ_0 representing the maximum growth rate for the new growth altogether.

Maintenance respiration can be expressed as a product of α and the compensation intensity E_C, i.e. the light level at which respiration and gross growth rates balance and net growth is zero (Langdon, 1988; Siegel *et al.*, 2002). Langdon related R_M to α_P, the initial slope of the photosynthesis-irradiance curve, rather than the slope of the the

growth-irradiance curve (which is the α used here), such that:

$$R_M = \alpha_P E_C \tag{3.6}$$

As with μ, α can be approximately estimated by multiplying α_P with the carbon to chlorophyll ratio. We can thus say, assuming an approximately constant C:Chla ratio, that

$$R_M \propto \alpha E_C \tag{3.7}$$

Not also that this is the logical consequence of the linearisation of the models for small E, because at low irradiance $\mu \approx \alpha E$, and the compensation irradiance is where $\mu(E_C) = R_M$ (cf. Siegel *et al.*, 2002). This relation expresses the idea that an increase in α necessitates an increase in photosynthetic machinery and thus a higher energy cost to maintain, which has been shown empirically to approximately follow the linear relation shown above. Inserting this formulation into equation 3.5 gives:

$$\mu = \mu_0 \left(1 - \mathrm{e}^{-\alpha E/\mu_0}\right) - \alpha E_C \tag{3.8}$$

Based on EBS observations, the variation in E_k appears to vary weakly with seasonal changes if at all. But μ_0 and α exhibit the same seasonal pattern. Thus if it is assumed E_k is not seasonal, then it can be taken as constant with respect to time, or with respect to seasonal parameters, e.g. $\partial E_k/\partial\alpha = 0$. And since $\mu_0 = \alpha E_k$, then $\partial\mu_0/\partial\alpha = E_k$. Under this assumption the dependence of net growth on α becomes

$$\frac{\partial\mu}{\partial\alpha} = E_k \left(1 - \mathrm{e}^{-E/E_k}\right) - E_C \tag{3.9}$$

In conditions where $\partial\mu/\partial\alpha > 0$, i.e. where the partial derivative of μ with respect to α is positive, increased α leads to an increase in net growth μ. Yet where $\partial\mu/\partial\alpha < 0$, a reduction in α becomes energetically beneficial, as every positive $\Delta\alpha$ translates into a negative $\Delta\mu$. The threshold light level, E_*, which marks the boundary between these

regimes, is that which makes $\partial\mu/\partial\alpha$ equal to zero,

$$E = E_* \equiv E_k \ln\left(\frac{E_k}{E_k - E_C}\right) \tag{3.10}$$

The Taylor expansion for $E_*(E_C)$ around $E_C = 0$ is:

$$\begin{aligned} E_* &\approx E_*(0) + E_k \frac{\partial}{\partial E_C}\left[\ln\frac{E_k}{E_k - E_C}\right] \cdot E_C + \mathcal{O}(E_C^2) \\ &= 0 + E_k \frac{1}{E_k} E_C + \mathcal{O}(E_C^2) \end{aligned} \tag{3.11}$$

where $\mathcal{O}(E_C^2)$ denotes terms of the second and higher orders. These terms are increasingly vanishingly small for small values of E_C, and can be ignored. The first order approximation (ignoring the errors of higher order) yields

$$E_* \approx E_C \tag{3.12}$$

for small values of E_C. As with the relationship between α and R_M, this result is also to be expected from the near-linearity of the model for small E..

Below the compensation intensity, respiration is greater than growth and can be minimised by decreasing α. It is therefore energetically advantageous to shift from low to high α as the light level experienced by the community increases above E_C.

Figure 3.3 demonstrates this model's behaviour with two hypothetical curves. The values of μ_0 and α for one curve was the average of the open water samples of Figure 3.2, the other using the average from under-ice samples. The curve using open water data, having higher values of maximum growth and a higher initial slope, reaches a higher maximum more quickly, However, this curve also extends much more into the negative below the compensation intensity (arbitrarily chosen to be 20 μE m^{-2} s^{-1}for illustrative purposes here).

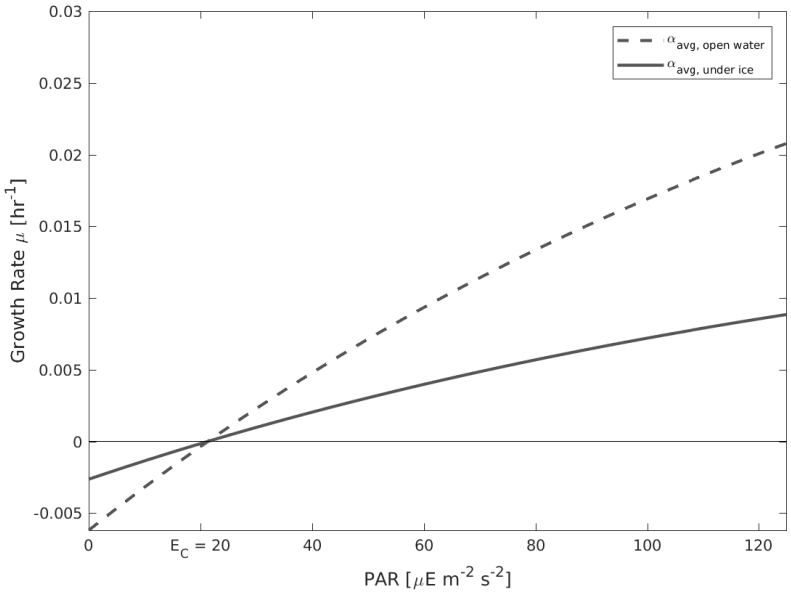

Figure 3.3: Demonstration of the trade-off model. Hypothetical carbon-specific growth curves given by the model given in Equation 3.8 using the mean values of observed α for open water and under-ice samples and the average μ_0 for open-water samples (see Figure 3.2 and Section 3.1). As E_k was assumed to be constant, its value was calculated from the open water values of μ_0 and α, and the result was used to calculate μ_0 for the under ice curve based on Equation 1.5. Above the compensation point (here arbitrarily chosen to be $E_C = 20$ μE m^{-2} s^{-1}), larger α is clearly advantageous, however below this point respiratory losses dominate and a lower α leads to lower loss.

3.3 Threshold Light Level

As demonstrated above and shown in Figs 3.2 and 3.3, the compensation intensity E_C is the threshold below which it is more advantageous to have a decreased α and thereby decrease losses due to respiration. Therefore by estimating E_C and comparing with the observed transition light level, the model can be tested for consistency with the Eastern Bering Sea data. This required establishing the mean PAR experienced by the sampled phytoplankton, a function of mixing depth, turbulence, surface PAR, and ice cover. In the mixed layer, individual cells move up and down from the surface to near darkness, and the average light experienced by one cell is significantly less than the maximum. With insufficient data to establish more realistic estimates, mean PAR was approximated by applying a single correction factor to the surface PAR, such that $E_{mean} = cE_{surf}$. This correction factor c was estimated to be 0.2, based on observations in environments with similar mixed-layer depths (Diehl *et al.*, 2002; Long, 2010). This approximation also matches the biophysical model of Banas *et al.* (2016, cf. Figure 7 in that study), and corresponds to uniform mixing of a 40 m euphotic zone.

The cruise data is re-plotted in Figure 3.4 as a function of this estimated E_{mean} as opposed to E_{surf}. A range for E_C of 5–25 μE m^{-2} s^{-1}was estimated based on the wide ranges of measurements in the literature (cf. Langdon, 1988; Quigg & Beardall, 2003; Siegel *et al.*, 2002). These values may not reflect the reality of Bering Sea phytoplankton, but were a range of measured phytoplankton compensation intensities that encompassed several measurements for multiple species of phytoplankton.

The estimated E_C range as well as the corresponding range of E_* values, lie across the domain between total darkness and spring-bloom light levels. As mentioned in Section 2, the actual transmittance through the ice was not known. Higher transmittance would shift all the under-ice points toward higher PAR in the figure.

The EBS data are thus broadly consistent with the energetic model above, or rather, as consistent as they might be expected to be given the uncertainty surrounding the exact light environment and light history of the sampled plankton patches.

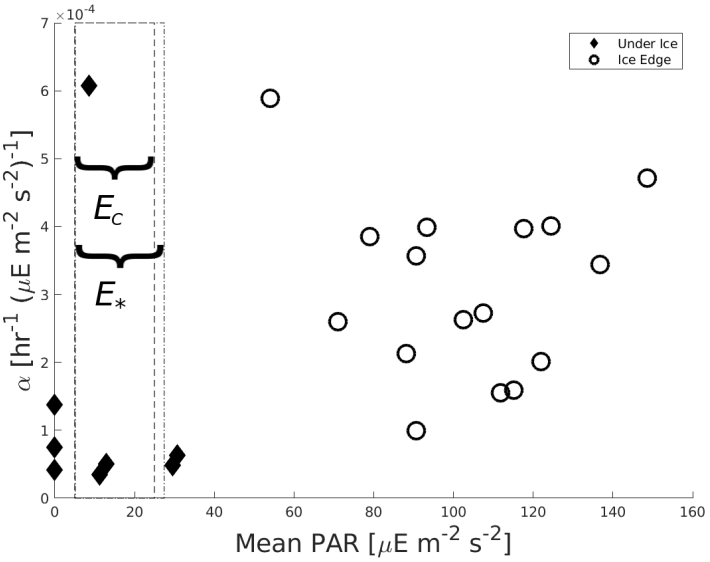

Figure 3.4: Observed α plotted against the approximate mean PAR cells would experience in the mixed layer. See Figure 3.2, middle row, for the plot of α against surface PAR. The rectangular boxes indicate the estimated range of E_C and subsequent range of E_* using Equation 3.11 and the mean values of E_k (see Section 3.1). As was shown in Equation 3.12, E_* deviates only very slightly from E_C, the offset being negligible when $E_k \gg E_C$.

3.4 Discussion

All other things being equal, within the Platt model and related models of growth, higher α means higher rates of photosynthesis and growth. Such a model alone does not predict why over-wintering cells would decrease α. Expressing α in terms of a respiration cost (Equation 3.7) provides such an explanation.

Although the data presented from the 2007-2009 cruises were sampled in different regions at similar times of year, there are good reasons to believe they represent seasonal change. Spatially, the under-ice and open water regions were close, with surface currents exchanging water between them (Stabeno *et al.*, 2016). Therefore it is unlikely that the distances spanned represent substantially different ecosystems or communities. Additionally, prior observations of this seasonality in the EBS (Sambrotto *et al.*, 1986) and elsewhere (see Tables 1 and 2 in the prior chapter) have been more explicitly seasonal in their time scales. The observations of Sambrotto *et al.* (1986) and the modelling experiments of Banas *et al.* (2016) both point to seasonality in this region. As spring blooms tend to begin at the ice edge during the thaw (Sigler *et al.*, 2014), using under-ice versus open-water as proxies for pre- and post-bloom is not unreasonable. Past literature has also considered this (Palmer *et al.*, 2011, 2013).

Taken altogether, the data presented in this chapter reinforce the larger picture of seasonal behaviour, with the photoparameters μ_0 and α being lower in winter under near-total darkness. That the photosynthetically available light in these conditions is below estimates of the compensation intensity lends credibility to the trade-off hypothesis. This has implications for modelling efforts which seek to use light-limitation models of phytoplankton growth across seasonal time scales.

3.4.1 Comparison with Other Growth Functions

Multiple models of P and μ as functions of E have similar efficacy at describing observed relationships (Lederman & Tett, 1981). Similar to the functional form of $\mu(E)$ in Equation 1.4 following the Platt model, the model in Smith (1936) has also been used

for specific growth rates (e.g. in Banas *et al.*, 2016):

$$\mu = \frac{\alpha E}{\sqrt{\alpha^2 E^2 + \mu_0^2}} \tag{3.13}$$

As with Platt, functions of light that follow the above relationship will be referred to as the "Smith model", even though it was originally devised for rates of photosynthesis.

Mathematically, both Platt and Smith both reduce to nearly linear equations at low irradiances and approach asymptotic limits at high irradiances. It is therefore no surprise that when given the same parameters, the equations follow each other closely (see Appendix B for a full discussion, and in particular Figure B.1 for an illustration of this similarity). One important distinction is that the full Platt model of photosynthesis P accounts for photoinhibition at high irradiances through the parameter β, shown in the full form in Equation 1.1 (also fully discussed in Appendix B). The similarity between Smith and Platt means both reproduce the seasonal behaviour of the observed P-E data. For modelling purposes, though there can be small quantitative offsets between them in addition to differences in interpretation, especially in the absence of photoinhibition the two models are both valid approaches and will exhibit the same patterns of behaviour (see, again, Appendix B and the discussion of multiple models in Lederman & Tett, 1981).

3.4.2 Perspectives for Modelling

Quantifying seasonal phytoplankton values, including the photoparameters, remains a challenge. Many difficulties abound for measuring over-wintering phytoplankton. There are technical challenges in sending ships to sample under-ice communities during the polar night, as well as preserving their dark acclimation when samples are brought deckboard. Uncertainties are high when attempting to measure extremely low values of photosynthesis, with simply accounting for the total amount of phytoplankton in a winter sample being a challenge. Large errors in measurements of photosynthetic ability mean much uncertainty about natural variability (McKee *et al.*, 2014; Neeley *et al.*, 2015).

As a result, much remains to be explored here, in finding more accurate measurements of the threshold light level, in the compensation intensity for the different species in the EBS, and the nature of the transition between low and high photoparameters. Despite these uncertainties and open questions, the data presented here further demonstrates the case for seasonality and illustrates the need for further research to target this area.

Modelling studies are, on the one hand, limited by the uncertainties in the parameters. Yet on the other hand, they offer a space to explore possibilities. As Banas *et al.* (2016) discovered the need for a seasonal α to produce an accurate spring bloom, on the basis of the limited data of (Sambrotto *et al.*, 1986), so can the data in this chapter guide modelling investigations. With the evidence presented, the minimal expectation is that a model with higher μ_0 and α in spring, after crossing a threshold E_* close to the compensation intensity E_C, should produce realistic spring bloom behaviour. That the data strongly suggest this seasonality exists and the evidence this chapter has shown for their being a biological justification for it strengthens the expectation that including this seasonality could even improve a model's accuracy. The next chapters will therefore use an NPZD model to explore the ramifications of seasonality in spring bloom dynamics.

Chapter 4

Seasonality in an NPZD Model of the Eastern Bering Sea

In this chapter, an existing NPZD model of the Eastern Bering Sea (EBS) is adapted to test the importance of seasonal light response in the timing of the spring bloom. This was done by changing the photoparameters to be seasonal. In this case, we use the initial slope α and the maximum specific uptake of nitrogen, denoted μ_0. Specifically, and in accordance with the previous chapter, below the threshold light level E_*, the model used lower values for the photoparameters.

Previous use of this model only had seasonality in α, based on data from Sambrotto *et al.* (1986). Incorporating seasonality in μ_0 as well brings the model in line with more recent observations (see Chapter 3), as well as providing a mechanistic basis for the model's behaviour. Further, this allowed for a more comprehensive exploration of model behaviour with respect to varying degrees of seasonality in the photoparameters, and a thorough investigation of the potential parameter space that firmly established the necessity of seasonality.

Using 2009 as a case study, this version of model was verified against observational data, through a parameter analysis that explored the space of possibilities for key parameters including the photoparameters. The spring bloom of 2009 was particularly well documented, with measurements before, during, and after the bloom of nitrate concentration as well as specific uptake rates and biomass for phytoplankton and

zooplankton. The multiple methods of measurement make for a robust, well-defined bloom. This case study, designated the IEB60 test-bed, allowed for a well constrained cost-function in the parameter analysis.

The next sections will describe the structure of the one-dimensional NPZD model. The physics was extracted from a biophysical model by way of tracking particle trajectories. These trajectories provided the physical forcing applied to the one-dimensional model, effectively simulating the flow of the water column along a trajectory. The results of the model runs and parameter analysis found parameter values that best fit observations using versions of the model with and without seasonality. Comparison between these two fits will then show how increasing the strength of the seasonality enhances model accuracy.

4.1 Structure of the Ecosystem Model

An existing NPZD model hind-cast, developed for the EBS (Banas *et al.*, 2016) and using a nitrogen budget, was modified into two versions: a model with seasonality in v_m and α and a model without seasonality (i.e. constant photoparameters throughout the year). The components of the model are diagrammed in Figure 4.1 and outlined in detail below.

This ecosystem model is one-dimensional, but is able to capture advection as a flow-following water column. This flow is simulated by tracking particle trajectories in an existing 3-D physical model, BESTMAS (Bering Ecosystem Study Modelling and Assimilation System) model, described and validated in Zhang *et al.* (2010b).

Physical forcing was extracted from BESTMAS along particle trajectories which follow the 0–35 m depth-average currents and which intersect with the region of interest in time and space. Thus, at every time step, the ecosystem model is fed the physics of the next point in the trajectory. Further details are given in Section 4.2.

The model has a six-compartment nitrogen budget, tracking phytoplankton biomass B, micro-zooplankton biomass Z, small and large detritus D_S and D_L, and the nutrients nitrate (NO_3) and ammonium (NH_4^+). Phytoplankton nitrate uptake rates v is a function of irradiance and concentration of NO_3 and NH_4^+, with loss terms from

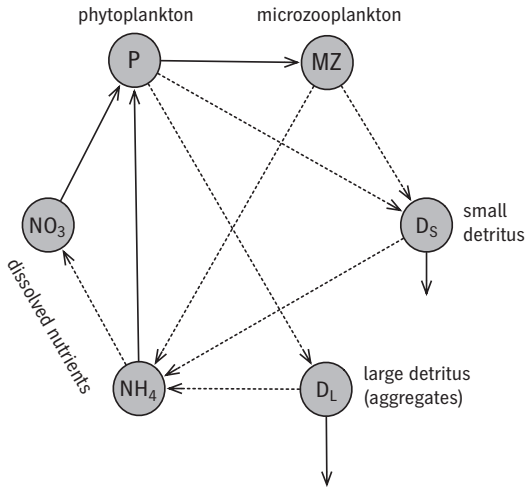

Figure 4.1: Structure of the ecosystem model, reproduced from Figure 4 in Banas *et al.* (2016). Solid arrows denote growth for the compartments being fed into, with the exception of the solid arrows from detritus which are losses from the system. Dotted arrows denote regeneration pathways.

micro-zooplankton ingestion I, mortality m_P and aggregation m_{agg}. The model uses a nitrogen budget as nitrogen is the most limiting nutrient in the EBS, especially as it pertains to spring blooms (Aguilar-Islas *et al.*, 2007; Mathis *et al.*, 2010; Sambrotto *et al.*, 1986; Strom & Fredrickson, 2008).

The model equations governing the evolution of phytoplankton biomass B, zooplankton biomass Z, small detritus D_S, large detritus D_L, ammonium concentration $[\mathrm{NH}_4^+]$, and nitrate $[\mathrm{NO}_3]$, are a system of ODEs.

$$\frac{\mathrm{d}B}{\mathrm{d}t} = q_P\mu(E, \mathrm{NO_3}, \mathrm{NH_4^+})B - q_z I(B)Z - q_R m_P B - q_P m_{agg} B^2 + \text{mixing} \quad (4.1)$$

$$\frac{\mathrm{d}Z}{\mathrm{d}t} = \epsilon q_z I(B)Z - q_z m_z Z^2 + \text{mixing} \quad (4.2)$$

$$\frac{\mathrm{d}D_S}{\mathrm{d}t} = (1 - \epsilon - f_{ex})q_z I(B)Z + q_R m_P B - q_R r_{remin} D_S + \text{sinking} + \text{mixing} \quad (4.3)$$

$$\frac{\mathrm{d}D_L}{\mathrm{d}t} = q_P m_{agg} P^2 - q_R r_{remin} D_L + \text{sinking} + \text{mixing} \quad (4.4)$$

$$\begin{aligned}\frac{\mathrm{d}[\mathrm{NH_4^+}]}{\mathrm{d}t} = &-\frac{\varphi_{\mathrm{NH_4^+}}\mathrm{NH_4^+}}{N_{tot}}\ell q_P \mu_0 B + f_{ex} q_z I(B)Z \\ &+ q_R r_{remin}(D_S + D_L) - q_R r_{nitrate}\mathrm{NH_4^+} + \text{mixing}\end{aligned} \quad (4.5)$$

$$\frac{\mathrm{d}[\mathrm{NO_3}]}{\mathrm{d}t} = -\frac{\mathrm{NO_3}}{N_{tot}}\ell q_P \mu_0 B + q_R r_{nitrate}\mathrm{NH_4^+} + \text{mixing} \quad (4.6)$$

All parameters above are defined with values and sources in Table 4.1. A brief description and summary of the terms and equations follows here, addressing the components of each equation and defining the sources and sinks of each component of the model.

4.1.1 Phytoplankton

Phytoplankton evolution in Equation 4.1 is a nitrogen budget, with an uptake term that combines temperature dependence q_P with the nitrogen uptake rate v. This uptake rate depends on light E and the availability of the nutrients $\mathrm{NO_3}$ an $\mathrm{NH_4^+}$. Specifically, nutrient limitation depends on the effective total nutrient concentration N_{tot}:

$$N_{tot} = \mathrm{NO_3} + \varphi\mathrm{NH_4^+} \quad (4.7)$$

where $\varphi < 1$ represents the reduced preference for ammonium relative to nitrate, and k_{min} is the minimum half-saturation for $\mathrm{NO_3}$. The resulting equation for nutrient

limitation v, following Smith *et al.* (2009), is

$$v(E, N_{tot}) = \frac{N_{tot}}{k_{min} + 2\sqrt{k_{min} N_{tot}} + N_{tot}} v(E) \tag{4.8}$$

where $v(E)$ is the light-limited nitrogen uptake. The model assumes a constant C:N ratio within the phytoplankton, and sets C:N=9 as suggested by data for the Eastern Bering Sea in Sambrotto *et al.* (2016). This entails that any uptake in carbon must be balanced by a proportional uptake in nitrogen. Therefore, $v(E)$ can be derived by dividing photosynthetic carbon fixation by the constant C:N, allowing the model to include a light-limited component in its nitrogen uptake that is also affected by seasonality of photoparameters, and the equation for v becomes:

$$v(E, N_{tot}) = \frac{N_{tot}}{k_{min} + 2\sqrt{k_{min} N_{tot}} + N_{tot}} \cdot \frac{P}{\mathrm{C:N}} \tag{4.9}$$

The Smith (1936) model describes photosynthesis P as a function of irradiance E:

$$P(E) = \frac{\alpha E}{\sqrt{\alpha^2 E^2 + P_m^2}} P_m \tag{4.10}$$

As noted in prior chapters, $P_m = \alpha E_k$, and thus the Smith model can be simplified to the form:

$$P(E) = \frac{E}{\sqrt{E^2 + E_k^2}} P_m \tag{4.11}$$

In the previous chapter, values of E_k changed little between pre-bloom and bloom samples. Therefore this model assumes a constant E_k, with seasonal variation in the Smith model being expressed through changing P_m.

As was discussed in previous chapters (see Sections 1.4 and 3.4.1) the Smith model has a very similar shape to the Platt model without photoinhibition. The differences in parameterisation are very small, especially compared to the proposed differences between winter and spring parameters.

The more significant distinction is the lack of photoinhibition. Part of the reason is before and even partly into the spring bloom, phytoplankton cells in the mixed layer

experience on average less light than the saturating intensity E_k, and are not subject to supra-optimal intensities until later in or even entirely after the bloom peak. The high-irradiance, nitrogen-deplete environment of the post-bloom summer months are expected to exacerbate photoinhibition in phytoplankton, especially diatoms, (Loebl *et al.*, 2010), but are beyond the scope and focus of this study. Further discussion on the effects of photoinhibition are found in Appendix B.

Once again considering the assumption of constant C:N, P_m can be rewritten as a maximum nitrogen uptake v_m multiplied by C:N. Similarly, we can convert between specific growth for both nitrogen and carbon, and so shall use μ to represent specific nitrogen uptake in the model as it is also our means of tracking growth. The full equation for nitrogen uptake μ as a function of light and nutrient concentration can now be written as

$$\mu(E, N_{tot}) = \left(\frac{E}{\sqrt{E^2 + E_k^2}} \right) \left(\frac{N_{tot}}{k_{min} + 2\sqrt{k_{min} N_{tot}} + N_{tot}} \right) \mu_0 \tag{4.12}$$

The amount of light experienced by a cell in the water column was defined with respect to light at the water surface E_0, attenuation by sea-water att_{sw}, and the ratio of vertical diffusivity κ to the time-scale of phytoplankton nutrient uptake μ_0:

$$E_{eff} = E_0 \exp\left(-\text{att}_{sw} \sqrt{\frac{\max\kappa}{\mu_0}} \right) \tag{4.13}$$

The dimensions of κ are length-squared over time.

The saturation irradiance E_k is assumed to be constant, based on data presented in the previous chapter. As such seasonality is defined by the variation in μ_0 and by extension α. Once E_{eff} exceeded the compensation intensity E_C, winter values for μ_0 and α switched to higher summer values. For both parameters, the transition was defined by a hyperbolic tangent function:

$$\mu_0 = \mu_{0,win} + \frac{1}{2} \left(\mu_{0,sum} - \mu_{0,win} \right) \left(1 + \tanh \frac{E_{eff} - E_C}{\Delta E} \right) \tag{4.14}$$

The choice of hyperbolic tangent allowed for a continuous yet narrow transition.

Equation 4.1 also includes a temperature term, q_P, which is a function given by $q_P(T) = Q_{10,P}^{T/10\mathrm{C}}$, where $Q_{10,P}$ is the temperature coefficient (Q_{10}) for phytoplankton. Thus, every 10°C increase in temperature is an exponential increase in q_p. The choice of $Q_{10,P}$ reflects a common value in the modelling literature. It should be noted this study focuses on the transition from winter to spring and the onset of the bloom, which occurs over a narrow temperature range, rarely exceeding 3°C until late spring and late into the bloom (see next section). Within that range, the difference between a Q_{10} of 1.5 (a lower estimate such as found in Sherman *et al.*, 2016) and a Q_{10} of 2 could alter q_P by as much as 10%, though this again would be more of an issue later in the bloom. At the latest stages of the bloom and into summer, the choice of Q_{10} becomes ever more significant.

The combination of temperature, light, and nutrient availability leads to a combined positive term for $\mathrm{d}B/\mathrm{d}t$.

$$\frac{\mathrm{d}B}{\mathrm{d}t} = q_P(T)\left(\frac{E}{\sqrt{E^2 + E_k^2}}\right)\left(\frac{N_{tot}}{k_{min} + 2\sqrt{k_{min}N_{tot}} + N_{tot}}\right)\mu_0 - \text{losses} \tag{4.15}$$

Losses come from grazing by zooplankton through ingestion I (also temperature dependent through q_Z), and a generic mortality term m_P. Mortality due to aggregation and sinking is encompassed by the term m_{agg}.

The general mortality m_p represents general loss terms and therefore accounts for, in part, losses due to respiration. Respiration is typically defined as the production and release of CO_2, and is therefore a loss term for the carbon budget (Falkowski & Raven, 2007). Nitrate uptake would therefore be affected by changes to uptake parameters and an increase in mortality due to respiration, but respiration itself would not be considered a loss term for the nitrogen budget with this definition.

Considering then only loss terms for nitrogen, there are pathways for excretion, primarily as nitrite (NO_2^-, cf. Anderson & Roels, 1981; Lomas & Lipschultz, 2006) but also ammonium (Kamp *et al.*, 2011; Lomas *et al.*, 2000). Estimates of how this excretion affects external nitrogen budgets and nitrate-uptake kinetics vary depending on taxa and environment (Collos, 1982; Glibert *et al.*, 2016; Lomas & Glibert, 2000; Sciandra

& Amara, 1994), making an estimation for a community (whose bloom is dominated by diatoms but pre-bloom is more diverse) difficult in a model. Therefore this model does not attempt to represent this variability in the effect of respiration on nitrogen loss in any detail, opting instead for a crude tuning parameter of phytoplankton mortality, m_P.

4.1.2 Zooplankton

Zooplankton are governed by ingestion I, which is a function of phytoplankton B, but is tempered by grazing efficiency $\epsilon < 1$, excretion $f_{ex} < 1$, and temperature dependence $q_z = Q_{10,Z}^{T/10C}$. As with phytoplankton, the choice of $Q_{10,Z}$ represents an approximate value based on averages from the literature (Hansen *et al.*, 1997), bearing in mind the small temperature range explored within the model's boundaries.

4.1.3 Nutrients, Detritus, and Recycling

Nitrate concentrations were determined as a function of water-column depth H. First the surface and bottom NO_3 concentrations were calculated as a function solely of H:

$$\mathrm{NO}_3^{bottom} = (42\text{mmol m}^{-3})\frac{H^2}{(116\text{m})^2 + H^2} \tag{4.16}$$

$$\mathrm{NO}_3^{surface} = (24\text{mmol m}^{-3})\frac{H^2}{(86\text{m})^2 + H^2} \tag{4.17}$$

Then both were used in setting the initial NO_3 depth profile as follows:

$$\mathrm{NO}_3^{initial}(z, H) = -\frac{z}{H}\mathrm{NO}_3^{bottom} + \left(1 + \frac{z}{H}\right)\mathrm{NO}_3^{surface} \tag{4.18}$$

All three equations were used in the initial study (Banas *et al.*, 2016) as they are presented above. The values 42 and 24 mmol m^{-3} in the equations for top and bottom nitrate were fit by Banas *et al.* to observation data from bottle samples within 10 metres of the bottom and 2 metres of the surface taken in the spring 2009 BEST cruise (Mordy *et al.*, 2012). These equations also result in a decrease in nitrate in surface waters along the inner shelf approaching the coast, consistent with observations of low nitrate

concentrations and low replenishment in the coastal waters (Kachel *et al.*, 2002; Mordy *et al.*, 2017; Stabeno *et al.*, 2010).

The nutrient fields were then evolved according to the ODEs above. Both have loss terms from phytoplankton uptake, moderated by light limitation ℓ (see Equations 4.11 and 4.12). Phytoplankton have a preference for nitrate over ammonium denoted by φ.

Nitrate is regenerated in part from nitrification of ammonium, which in the model is regulated by the term $r_{nitrate}$, with a temperature dependence q_R. Ammonium is regenerated in part by excretion by zooplankton, a fraction of ingestion denoted by f_{ex}. Ammonium is also regenerated by remineralisation r_{remin} of detritus D.

Small detritus derives from the inefficiency of zooplankton ingestion as well as zoo plankton excretion, encapsulated in the term $(1-\epsilon-f_{ex})q_z I(P)Z$. Small detritus also increases from phytoplankton mortality m_P, which has its temperature dependence q_R. Large detritus results from aggregation and sinking of phytoplankton cells, accounted for in the term m_{agg}. Both detritus types have losses due to remineralisation r_{remin} which converts them into ammonium. And both are affected by sinking through their sinking rates w_S and w_L which shifts their positions in the water column.

4.1.4 Mixing

All components are affected by mixing, determined by the one-dimensional diffusion equation with diffusivity κ being a non-constant function of z:

$$\frac{\partial u}{\partial t} = \frac{\partial}{\partial z}\left(\kappa(z)\frac{\partial u}{\partial z}\right) \tag{4.19}$$

where u stands in for any of the components of the model (B, Z, the detritus and nutrients).

Parameter	Symbol	Value	Units	Source
Fixed Parameters				
Phytoplankton C:N ratio		9	mol:mol	Spring '09 observations, (Sambrotto *et al.*, 2016)
Chlorophyll:N ratio		2.2	mg:μM	
Minimum half-saturation for NO_3	k_{min}	0.16	μM N	Collos *et al.* (2005)
Preference for NH_4^+	φ_{NH_4}	2		
Grazing half-saturation	K	1	μM N	
Microzooplankton growth efficiency	ϵ	0.3		Hansen *et al.* (1997)
Fraction of grazing excreted to NH_4^+	f_{ex}	0.35		
Microzooplankton mortality	m_z	1.5	day^{-1}	
Small detritus sinking rate	w_S	3	m dy^{-1}	
Large detritus sinking rate	w_L	100	m dy^{-1}	
Detrital remineralization rate	r_{remin}	0.05	day^{-1}	
Nitrification rate	r_{nitr}	0.03	day^{-1}	Banas *et al.* (2016), cf. Zhang *et al.* (2010a)
Temperature Coefficients (Q_{10}):				
Q_{10} for phytoplankton	$Q_{10,P}$	2		Bissinger *et al.* (2008)
Q_{10} for zooplankton	$Q_{10,Z}$	2.8		Hansen *et al.* (1997)
Q_{10} for bacterial respiration	$Q_{10,R}$	2.8		
Width of $\mu_{0,win} - \mu_{0,sum}$ transition	ΔE	5	W m^{-2}	
Subject to Parameter Analysis in Section 4.3		*Initial Value*		
Maximum N uptake rate, winter & summer	$\mu_{0,win}$ $\mu_{0,sum}$	1.2	dy^{-1}	Zeeman & Jensen (1990)
Initial growth-light slope, winter & summer	α_{win} α_{sum}	0.01 0.16	(W m^{-1})$^{-1}$ dy^{-1}	Banas *et al.* (2016) Sambrotto *et al.* (1986)
Threshhold light level	E_*	30	W m^{-1}	Banas *et al.* (2016)
Phytoplankton mortality	m_P	0.03	dy^{-1}	*ibid.*
Phytoplankton loss via aggregation	m_{agg}	0.009	(μM N)$^{-1}dy^{-1}$	*ibid.*
Light attenuation by seawater	att_{sw}	0.05	m^{-1}	*ibid.*
Light attenuation by phytoplankton	att_P	0.006	$m^{-1}\mu$M N^{-1}	*ibid.*
Max microzooplankton ingestion rate	I_0	2.4	day^{-1}	Sherr *et al.* (2013)
Initial Conditions				
Integrated phytoplankton	B	6	μM N m	prebloom chl, spring 2009, Lomas *et al.* (2012)
Integrated microzooplankton	Z	0.4	μM N m	prebloom C biomass, spring '09, Sherr *et al.* (2013)
Small detritus	D_S			
Large detritus	D_L			
Nitrate	NO_3	Eq. 4.18		
Ammonium	NH_4^+	0		Mordy *et al.* (2012)

Table 4.1: Parameters of the NPZD model. The majority follow Banas *et al.* (2016), with ten parameters subject to analysis described in Section 4.3 in order to test the hypothesis of this chapter: that seasonality of α and μ_0 are effective in ecosystem modelling.

4.2 Particle Tracking and Physical Forcing

4.2.1 IEB Testbed

The tuning of the two model versions was done by randomly varying the model parameters in 50 000 different runs (see Section 4.3). These runs were then compared with observational data taken in spring and summer 2009 in the mid-shelf region of the EBS, referred to here and in the prior paper as the "IEB60" case, the boundaries of which are shown in Figure 4.2.

The IEB60 data resolved an ice-edge spring bloom near 60°N in late April to early May, 2009, from BEST/BSIERP observations (Lomas *et al.*, 2012; Mordy *et al.*, 2012; Sambrotto *et al.*, 2016; Sherr *et al.*, 2013; Stabeno *et al.*, 2012; Stoecker *et al.*, 2013). These included concentrations of NO_3, phytoplankton and micro-zooplankton biomass, specific growth rates determined from dilutions as well as ^{14}C, ^{13}C, and ^{15}N uptake experiments.

In the prior paper, the model already contained seasonality in α that was enabled by an arbitrary critical light level. When the effective light, E_{eff} experienced by a phytoplankton cell in the mixed layer exceeded this critical light level, the model switched from low pre-bloom winter α to a high summer α. This transition was defined by a hyperbolic tangent function. Here this critical light level is replaced by the compensation light intensity E_C. As both the present model, and the prior model it was adapted from, are nitrogen based and not carbon, the maintenance respiration cost (as in Equation 3.8) is not explicitly defined.

4.2.2 Particle Trajectories

As mentioned above, the NPZD model is a one-dimensional Eulerian model which approximates a Lagrangian approach by taking particle trajectories as inputs. This is an approximation as the ecosystem model is constructed in an entirely static, 1-D form, only moving with currents if those inputs represent movement. These trajectories contain the physical forcing including ice cover, surface PAR, and depth profiles of temperature and vertical diffusivity. Thus the one-dimensional water column of the

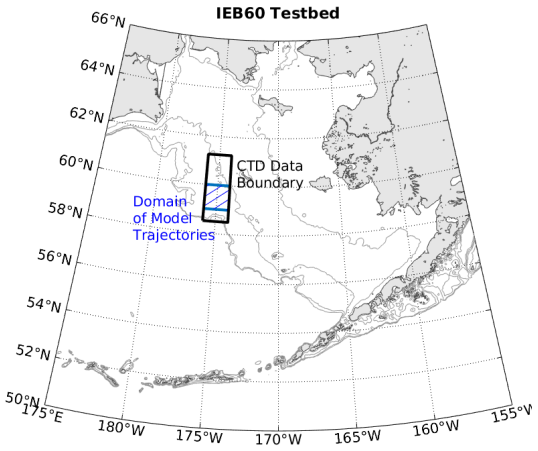

Figure 4.2: Location of the "IEB60" case-study. Black region indicates the boundary of the CTD data used in validation of the model. Blue hatched region indicates domain from which particle trajectories were extracted (see Section 4.2).

ecosystem model follows a specified trajectory. These trajectories were creating by tracking particle paths in the BESTMAS model described and validated in Zhang *et al.* (2010a,b, 2012). BESTMAS models the Northern Hemisphere from 39 °N across the Arctic Ocean. That its physics, especially sea-ice, were validated against data over this whole region made it a useful source of physical forcing for the NPZD model in the EBS, which is highly influenced by its neighbouring regions.

Particles trajectories started on the first of January of 2009, one per horizontal grid cell. Tracking was done in two-dimensions by averaging the velocities over the top 35 metres of the water column, using a time step of one day. The necessary trajectories for this experiment were those which intersected with the study region (see Figure 4.2), all other trajectories were discarded. The trajectories are mapped in Figure 4.3. Their corresponding physical variables are plotted in Figure 4.4, showing ice cover, temperature, surface PAR, and vertical diffusivity over time for each trajectory.

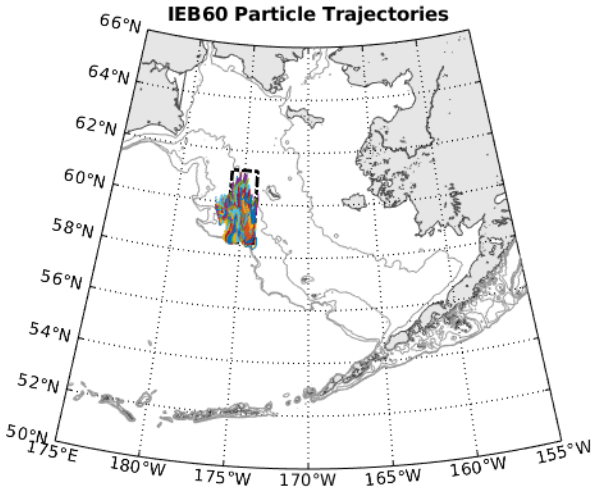

Figure 4.3: Map of particle trajectories, with the CTD data boundary denoted by the black dash-dot rectangle.

4.3 Parameter Analysis

The parameter analysis was conducted with respect to ten parameters (shown in Table 4.2). These parameters were selected on the basis of observational uncertainty (i.e. there was justification for considerable flexibility in their values) and their relevance to the new model (i.e. α and μ_0 would necessarily need re-tuning in a model that argued for their change, as would related terms such as E_C). Four were the photoparameters whose seasonality was in question, μ_0 for winter and summer, and α for winter and summer. The compensation intensity E_C was also an unknown, both its value and its degree of influence on model performance.

In addition to phytoplankton specific uptake rate, the maximum ingestion rate by zooplankton, I_0, was included in the analysis because uncertainty in its value also meant previous fits of this parameter that were based on different values of phytoplankton growth may be incorrect. Similarly, the high degree of uncertainty of the loss terms– phytoplankton mortality m_P and phytoplankton loss via aggregation m_{agg}– meant their values needed re-evaluation as well. Finally, as this study is focused on the role of light limitation, the final two parameters of the analysis were the attenuation factors.

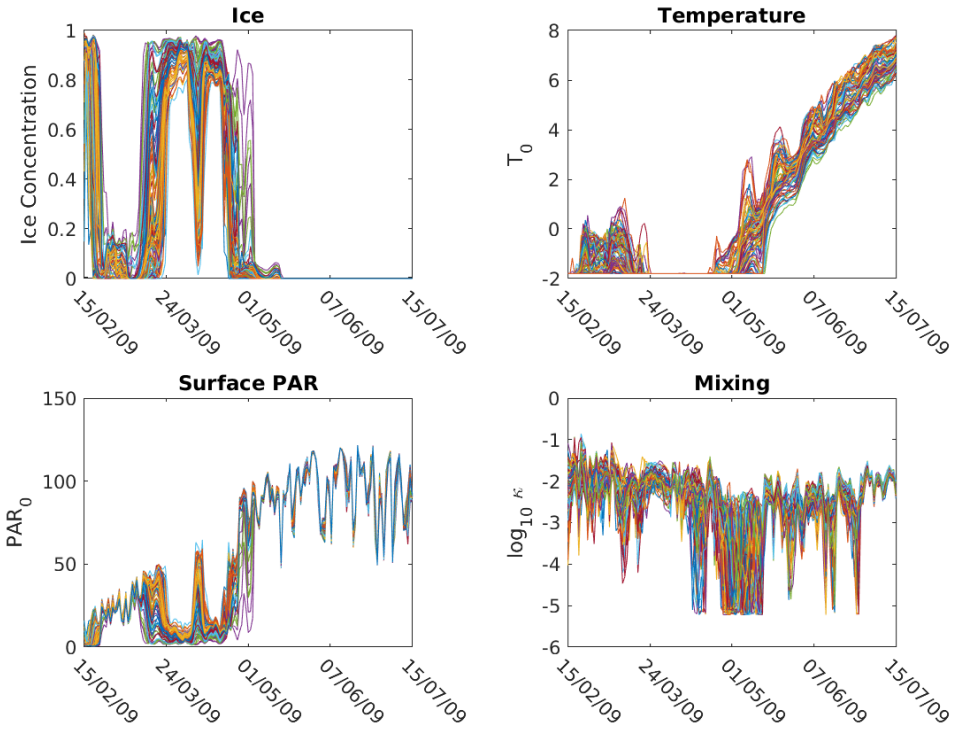

Figure 4.4: Physical variables along each trajectory. At each time step, the physics were extracted from the BESTMAS model at the corresponding points for each trajectory. The NPZD model was then run as a one-dimensional ecosystem model following the paths mapped in 4.3 and experienced the ice concentration, temperature, surface PAR, and vertical diffusivity plotted here.

Attenuation by sea-water att_{sw} and by phytoplankton cells att_P represented two more uncertainties directly related to light limitation.

These parameters were randomly varied over the course of 50 000 model runs. In each run, each of these parameters was assigned a random value from a wide range that encompassed prior observations. This range was a factor of 3 above and below the parameters used in Banas *et al.* (2016). The exception was for E_C, whose range was from 0 to 25 W m^{-2}, a rough estimate based on prior literature (Langdon, 1988; Quigg & Beardall, 2003). Effectively, this was a brute-force approach to searching a broad parameter space for possible good fits. Because it was assumed that E_k was constant, once α_{sum} and $\mu_{0,sum}$ were selected, E_k was fixed. As a result, the tenth parameter, α_{win} was fixed by the selection of $\mu_{0,win}$, as a result of

$$\alpha_{win} = \mu_{0,win}\frac{1}{E_k} = \mu_{0,win}\frac{\alpha_{sum}}{\mu_{0,sum}} \tag{4.20}$$

The results of each run were also compared with the IEB60 data: NO_3 concentrations, phytoplankton and micro-zooplankton biomass (B and Z were converted to g C m^{-2} by assuming constant C:N), f-ratio, and the specific N uptake rate μ and grazing rates I of phytoplankton and micro-zooplankton, respectively.

A cost c was then calculated from the mean-squared error between the model outputs m_i and the observed data points o_i.

$$c = \frac{1}{n}\sum_i \left(\frac{o_i - m_i}{\sigma_i}\right)^2 \tag{4.21}$$

The values of o_i correspond to averages of each metric (e.g. NO_3 concentration) at a specific phase in bloom development. The four phases considered were pre-bloom, early bloom, late bloom, and summer. For each metric, an average was taken of the observational data and the model outputs within each of the four phases, producing four points for each metric representing different periods in time. This averaging was done to eliminate potential sampling bias that might give more weight to one time period over the others. The term σ_i reflected a heuristically determined range of error for each metric, such that the model was not constrained to get as close as possible to

Parameter		Search Bounds	Best Fit Range	Units
Max phyto growth rate (Summer)	$\mu_{0,sum}$	0.6 – 5	2.6 – 3.6	d^{-1}
Max phyto growth rate (Winter)	$\mu_{0,win}$	0.002 – $\mu_{0,sum}$	0.2 – 0.4	
Initial growth-light slope (Sum)	α_{sum}	0.034 – 0.16	0.10 – 0.14	$(W\ m^{-2})^{-1}\ d^{-1}$
Initial growth-light slope (Win)	α_{win}	$\mu_{0,win} \cdot (\alpha_{sum}/\mu_{0,sum})$	0.008 – 0.012	
Compensation intensity	E_C	0 – 25	13 – 17	$W\ m^{-2}$
Max ingestion rate	I_0	1 – 7	1.1 – 1.9	d^{-1}
Phytoplankton mortality	m_P	0.001 – 0.03	0.01 – 0.03	d^{-1}
Phyto loss via aggregation	m_{aggr}	0.003 – 0.015	0.005 – 0.015	$(\mu M\ N)^{-1}\ d^{-1}$
Light attenuation, sea-water	att_{sw}	0.002 – 0.08	0.05 – 0.07	m^{-1}
Light attenuation, phytoplankton	att_P	0.002 – 0.09	0.002 – 0.009	$m^{-1}\ \mu M\ N^{-1}$

Table 4.2: Parameters varied and the ranges of values providing the best fits to observation data. Without seasonality, μ_0 and α were constant. "Search Bounds" indicates the minimum and maximum values of the parameter space, with α_{win} being related to α_{sum} by the same ratio as the two μ_0s, due to the assumption of E_k being constant.

the actual points, but within a wide range.

The parameter combinations which yielded model runs that minimised c for the model without seasonality were compared with those for the model with seasonality. As this was a random sampling without direction, there was no cutoff or target value for c, both the seasonal and nonseasonal models were given 50 000 runs each in the tuning process. The lowest cost results were then compared for their ability to capture key observations such as the timing and magnitude of the phytoplankton bloom and the corresponding rapid decrease in NO_3 concentration.

4.3.1 Measure of Seasonality

The strength of seasonality was quantified by the variable s:

$$s = 1 - \frac{\mu_{0,win}}{\mu_{0,sum}} = 1 - \frac{\alpha_{win}}{\alpha_{sum}} \tag{4.22}$$

The ratio $\mu_{0,win}/\mu_{0,sum}$ is equal to $\alpha_{win}/\alpha_{sum}$ because E_k was taken to be constant. A higher value of s indicates a smaller ratio of winter to summer values, i.e. a greater increase in both μ_0 and α in spring/summer relative to winter. For each of the model

Variable	**Time Period**	**Mean Obs. Value**
NO_3, top 35 metre average [μM N]	10–11 Apr (pre-bloom)	16.5
	26–30 Apr (early bloom)	7.7
	6–7 May (late bloom)	1.9
	26 June – 6 July (summer)	4.3
Integrated phytoplankton P [g C m^{-2}]	10–11 Apr	0.86
	26–30 Apr	34
	6–7 May	47
	26 June – 6 July	2.0
Integrated microzooplankton Z [g C m^{-2}]	10–11 Apr	0.0028
	26–30 Apr	0.066
	6–7 May	0.18
Phytoplankton specific growth rate μ [day^{-1}]	10–11 Apr	0.091
	26–30 Apr	0.38
	6–7 May	0.19
	26 June – 6 July	0.22
Specific grazing rate I [day^{-1}]	10–11 Apr	0
	26–30 Apr	0.15
	6–7 May	0.17
	26 June – 6 July	0.24
f-ratio	26–30 Apr	0.94
	6–7 May	0.71
	26 Jun – 6 July	0.31

Table 4.3: Target values for model runs from IEB60 data, spring to summer 2009 (Cross *et al.*, 2012; Lomas *et al.*, 2012; Mordy *et al.*, 2012; Sambrotto *et al.*, 2016; Sherr *et al.*, 2013; Stoecker *et al.*, 2013).

runs in the parameter analysis, the cost c and seasonality s were recorded. This way, any relationship between c and s could be tracked across the parameter space.

4.4 Results

The best fit model runs with the lowest costs c are show in Figure 4.6, plotted with the observational data. While noticeable errors still remain at specific points, the model run with seasonality performs substantially better.

The IEB60 data show nitrate declining rapidly as phytoplankton biomass and uptake rates increase. It should be noted in July many measurements recorded an increase in NO_3. One source of this error could be a pycnocline shallower than 35 m, with the high concentration mostly being below the pycnocline but increasing the 0–35 m depth average. It may also be the result of the limits of the one-dimensional approach used here, as it does not fully reproduce patchy wind mixing, which may be a source of intermittent resupply of nitrate (Eisner *et al.*, 2016).

Without seasonality, the best fit runs were unable to reproduce the magnitude of the spring bloom in terms of phytoplankton biomass. As can be seen in Figure 4.6, there is a slight increase in phytoplankton biomass around the correct date, but is an order of magnitude below the observed peak. More importantly, even if the magnitude is increased through an increase in α or μ_0, a spurious early bloom becomes increasingly pronounced. When the other observational metrics are ignored and only the error for B is used in the cost function, the magnitude of the bloom can be replicated but also occurs a month or more too early.

With seasonality, however, stronger fits are found. While the lowest cost for the nonseasonal model was $c_{min,nonseasonal} \approx 1.771$, the model with seasonality was able to reduce the minimum cost by over two thirds, with $c_{min,seasonal} \approx 0.496$, and no spurious bloom. Many low cost ($c < 0.7$) fits for the seasonal model still have spurious early blooms, however, and these are shown in Figure 4.6 for completeness.

Caveats for the success of the model include that the highest values of error exist for the micro-zooplankton grazing rates and biomass. The parameter ranges for these fits are shown in Table 4.2, with I_0 being less than half the value used in Banas *et al.*

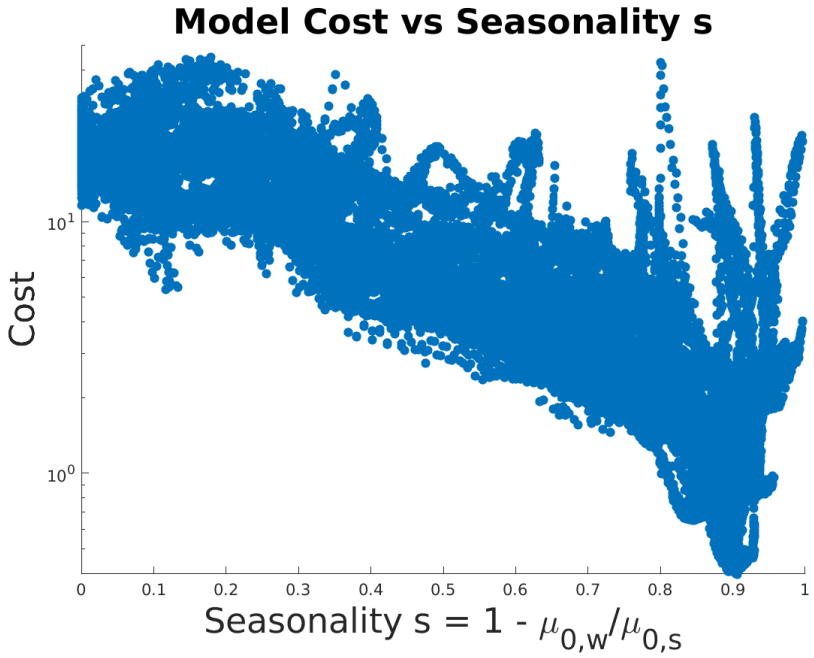

Figure 4.5: Cost function of the seasonal model (Eq. 4.21) versus seasonality s, the measure of seasonality defined above (Eq. 4.22). The full range of costs spanned orders of magnitude from 10^{-1} to 10^4. The ranges for each parameters which had an order of magnitude of 10^{-1} are presented in Table 4.2

(2016) of 3.4 day^{-1} (derived from Sherr *et al.*, 2013). This may be due in part to the original model having higher μ_0 year round, which would then need a higher I_0 to balance phytoplankton in the lead-up to the bloom. E_C remains the most uncertain parameter. As there is limited data for comparison, more investigation would need to be done to help constrain its value.

The relationship between the cost function and seasonality is shown in Figure 4.5. While any given value of s can have a range of costs, a strong constraint is immediately evident. Low cost fits only begin to be found above a seasonality of 0.85, with hundreds of low cost points occurring in the vicinity of $s = 0.9$.

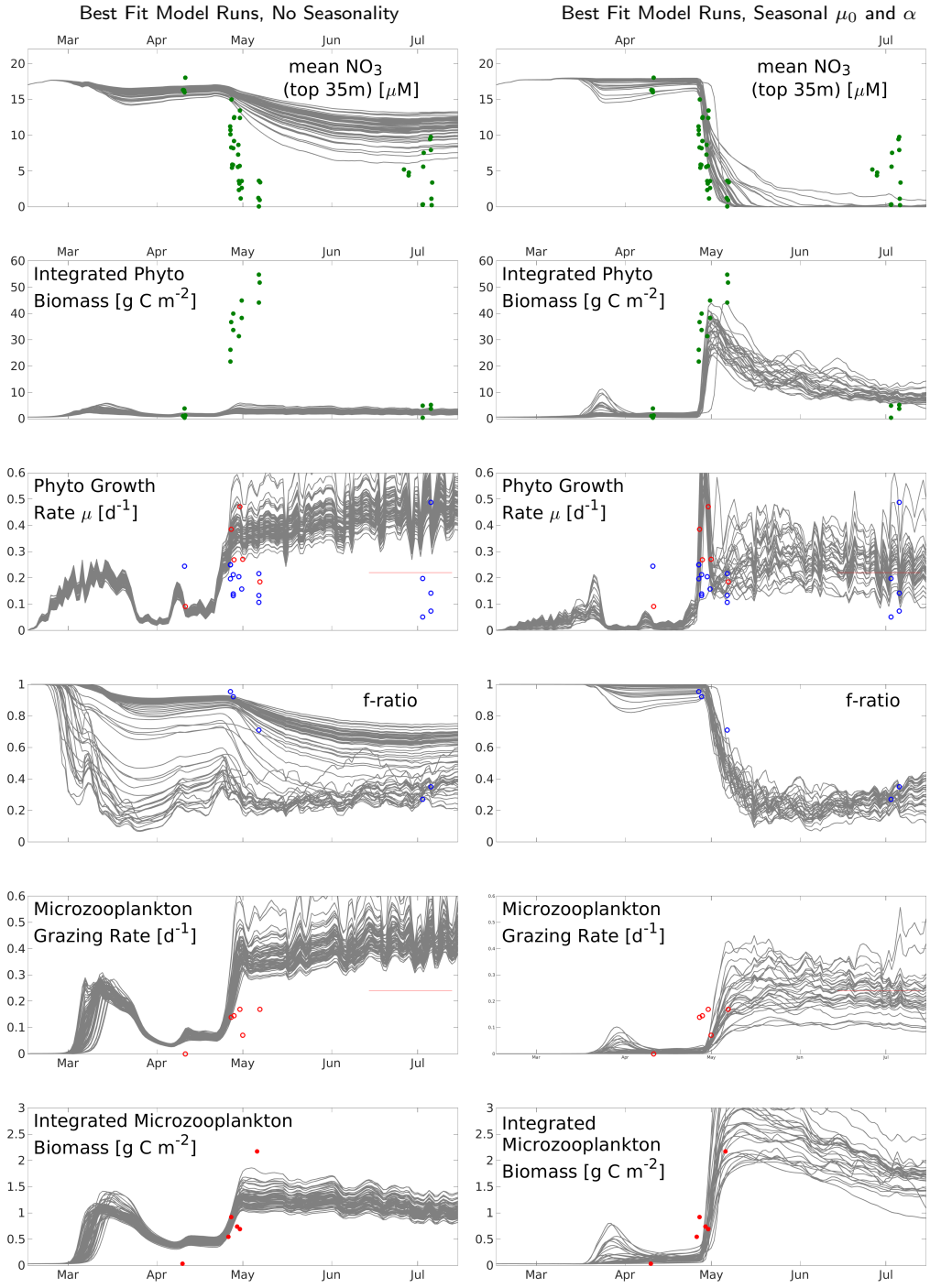

Figure 4.6: The best fitting model results, as determined by the cost function using observational data, for the NPZD model without seasonal photoparameters (left column) and the NPZD model with seasonal α and μ_0.

4.5 Discussion

While Banas *et al.* (2016) fit a transition from low winter α to high summer α, at a threshold light level, in an ad-hoc manner by tuning to observations, this chapter has presented a model that *a priori* includes such behaviour. Equation 3.8 implies the need for seasonality. The nature of the winter to summer transition is yet uncertain, and more data are needed from this range to clarify, however it was still possible to generalise the trend in the model.

The results above strongly suggest seasonality in light response is necessary to fully explain bloom dynamics in the EBS. In Banas *et al.* (2016), seasonality of α was a necessity for the model to accurately reproduce observed data. Here it has been shown through multiple runs of the model and a search through parameter space that an alternative parameterisation which lacks strong seasonality cannot account for the timing, magnitude, and rapid development of the spring bloom.

Questions of interpretation still remain, however. We must discuss the limitations and the advantages of the present model design to fully understand its usefulness for exploring the question of photo-seasonality. Many modelling approaches were introduced by way of examples in Section 1.2.1, and we must first consider comparisons and contrasts with other model designs before we can assess the performance of the one presented here.

4.5.1 Model Complexity: Physics, Nutrient Budgets, and Behaviour

Biogeochemical models are often 3-dimensional, as noted in the examples in Section 1.2.1. This is true for the global models such as MEDUSA as well as regional such as SINMOD. This chapter's model is given its physical forcing from BESTMAS, a 3D regional physical model, but that physics is extracted along trajectories to permit a 1-Dimensional NPZD to follow currents. The ecosystem model is therefore less computationally demanding and can run in minutes or hours, which facilitated the tens of thousands of parameterisations run in this chapter.

As noted in Section 1.2, NPZD models can also be limited by any manner of nu-

trients including nitrogen and phosphorus. This model was a nitrogen budget because of its limiting role in the EBS compared with other nutrients, both macro- and micro- (Aguilar-Islas *et al.*, 2007). Some biogeochemical models (such as that described in Baklouti *et al.*, 2006a,b) also include carbon budgets as part of an broader approach of mechanistic models as discussed in Section 1.2.1. A major distinction is, while carbon is generally not a limiting nutrient in the oceans, explicitly tracking net carbon uptake necessitates accounting for losses due to respiration (Baklouti *et al.*, 2006a; Cullen, 1990; Cullen *et al.*, 1993). Respiration is not explicitly addressed in this model because it is a nitrogen budget, however as noted in the prior chapter we hypothesise that the respiration cost of high α is one factor in the seasonality of photoresponse, and it is known that nitrogen uptake is affects by the metabolic cost of maintenance of photosystems (Li *et al.*, 2015).

While more recent developments are highlighting the advantages of models with variable stoichiometry, it is common for models, even those which have both carbon and nitrogen budgets, to assume a constant C:N (Moloney & Field, 1991). In the case of a model with constant C:N, the maximum uptake rate for one is capped by the limits of the other. Where nitrogen is more limiting, carbon fixation cannot exceed nitrogen uptake, and vice versa. Two recent papers explore models with variable C:N (cf. Anugerahanti *et al.*, 2021; Kerimoglu *et al.*, 2021) suggest that this improves the portability of models, though this can also limit model performance by introducing more room for error.

In the case of the EBS, across the decades the limiting role of nitrogen in controlling the end of the spring bloom is well established (Banas *et al.*, 2016; Sambrotto *et al.*, 1986; Stabeno *et al.*, 2012). A nitrogen budget is therefore a necessity. With a constant C:N, carbon fixation can be approximated from nitrogen uptake. One drawback is the lack of explicit respiration loss in a nitrogen budget. But while Chapter 3's trade-off hypothesis provides a potential causal explanation for the community-level behaviour, the model in this chapter (and the next) is designed to test only the impact of seasonality on the whole community's dynamics. Thus explicit carbon is not needed for this purpose, and the model was kept with only nitrate and ammonium.

It is worth noting when considering nutrient budgets that photoparameters may also be affected by nutrient limitation. In experiments documented by Smith Jr. & Donaldson (2015), nutrient limitation was not relevant until the bloom was fully initiated. The focus of these experiments was on the run-up to the spring bloom and the timing of its onset, all periods wherein the model nutrients were saturated. In other scenarios or models this may not be the case, and could be a confounding factor.

4.5.2 Community Structure

The model used only one class of phytoplankton and one of zooplankton. Mesozooplankton were not included in the model due to the constrained focus on the timing and peak magnitude of the spring bloom. Mesozooplankton in the EBS have been found to primarily prey on microzooplankton, with phytoplankton less than 10% of their prey in ice-edge bloom regions (Campbell *et al.*, 2016), compared to the high grazing rates of microzooplankton (Sherr *et al.*, 2013). While this may have ramifications for microzooplankton population numbers, and may be more significant for phytoplankton grazing over the whole year, for the study at hand these effects were found to be negligible in the model of Banas *et al.* (2016) and hence excluded here.

Many of the studies cited in this thesis not only demonstrate changes in phytoplankton community composition during spring blooms, but also measured α on a community level and not separately by species (see Table 2.2). It is possible that with 2 phytoplankton classes, or more, that for each class smaller variations in α or even none at all are sufficient to provide a good fit to data, if the classes with higher α become dominant in spring.

Yet the literature summarised in Chapter 2 still show individual cells can experience seasonal α, making seasonal light response at a minimum something to consider in model development, even with multiple phytoplankton classes. The pressing implication for model design from this chapter is the sensitivity of the spring bloom to seasonal photoacclimation.

4.5.3 Model Performance

With the caveats and contrasts with other models in mind, the results of this chapter have shown the potential of photoparameter seasonality. Figure 4.6 shows this clearly. As was noted in Section 4.4, setting the photoparameters high enough to match the observed peak magnitude of phytoplankton biomass can't occur too early, essential making the non-seasonal model unviable from the start.

In Section 1.2 we established that model complexity can be measured by more than just geometry, and all forms of complexity carry their own trade-offs. When Kerimoglu *et al.* (2017) noted how uncommon it was for models to include photoacclimation, they suggest that adapting and developing models to improve realism should consider physiology as well as geometry or dimensionality. More recent work has also found improved model performance when photoacclimation is added to a fixed-stoichiometry model (Anugerahanti *et al.*, 2021). The results of this chapter therefore concords with other studies modelling photoacclimation.

While numerous complicated factors have been expounded upon above, and new degrees of freedom increase flexibility generally, the fundamental change of the model from a static light response to one which can in a very short time switch from slow to rapid growth fundamentally enables a rapid bloom. Importantly, while the rapid bloom can be captured with the nonseasonal model, the threshold light level used in the seasonal model allows for a tuning of the timing of the bloom, making it possible to match both timing and magnitude together.

Chapter 5

Inter-annual Variation Between Cold and Warm Years

This chapter presents a case-study in applying the model, as it was developed in the previous chapter with its final parameterisation, to multiple years with large inter-annual differences in the physical environment. The results were then used to examine how the physical changes in the EBS affect the model bloom phenology.

The previous chapter demonstrated the success of the seasonal NPZD model in a specific case study. The IEB60 test-bed represented an exceptionally well documented spring bloom during which many measurements were taken. This year, 2009, was also representative of a cold year, in which low temperatures led to thicker ice the maximum extent of which reached southerly latitudes of the Eastern Bering Sea.

In this chapter, the implications of seasonality within this model will be explored on an inter-annual scale, looking between 2009 as a representative cold year, and 2015 as a representative warm year, with 2014 and 2016 also included as warm years. The impact of including seasonality is quantified and compared with the effect of inter-annual variations in the physical environment.

5.1 Introduction

Chapter 1 laid out the stark impact warming temperatures have had on sea-ice, leading to a decrease in the extent and thickness of ice. While year-to-year variability continues, annual ice cover in the Arctic and sub-Arctic seas continues a downward trajectory over the multi-decadal trend of global warming (Bliss *et al.*, 2019; Kwok, 2018; Stroeve & Notz, 2018), driven by the changing temperatures (Olonscheck *et al.*, 2019).

This has a profound impact on the light regime in the Bering Sea, both through the direct attenuation of light by snow and sea-ice (Kauko *et al.*, 2017) and the influence of ice on stratification and the depth of the mixed layer (Brown & Arrigo, 2013). Prior chapters (specifically the introduction in Chapter 1 and literature review in Chapter 2) have discussed the relevance of mixed layer depth to phytoplankton blooms.

Now, with a model of photoresponse seasonality set out in Chapters 3 and 4, the question remains how well this model can be applied to changing light regimes and physical environments in the test area. While the previous chapter focused on winter to spring 2009, categorised as a "cold year" in the Bering Sea and featuring extensive ice cover, recent years have seen a return of warm conditions, with substantially less ice (Kikuchi *et al.*, 2020; Stabeno *et al.*, 2017).

Figure 5.1 demonstrates the difference in ice cover between 2009 and 2015, using ice cover from the biophysical model BIOMAS (Zhang *et al.*, 2010a). This stark difference is also highlighted in observation data such as in Stabeno *et al.* (2017). The years 2014 through 2016 exhibited higher temperatures and substantially less ice cover than cold years such as 2009 (*ibid*). For an inter-comparison of the model's efficacy across multiple environmental regimes, 2009 and 2015 were chosen. Given the role of ice in limiting light in the IEB60 case study of the prior chapter, the question then arises how the model will fare under the warm year conditions. Less ice would mean more incoming surface light E_0, and an E_{eff} influenced by altered vertical mixing.

It should be noted that the relationship between vertical mixing and phytoplankton growth is complex. Hunt, Jr *et al.* (2002) proposed that sea-ice's effects on mixing is a significant control on inter-annual variability in spring blooms, via what they named

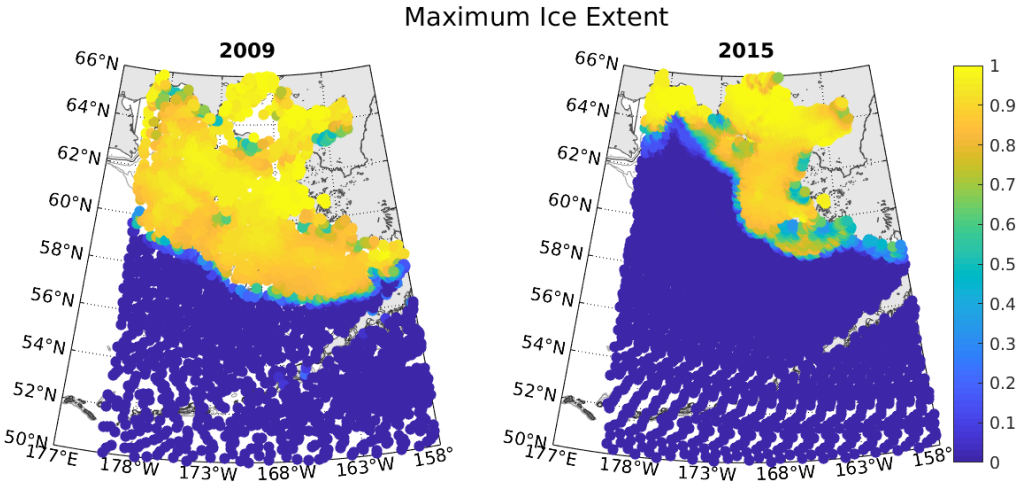

Figure 5.1: Map of ice concentrations at points in the biophysical BIOMAS model for 2009 and 2015, on the day of greatest ice extent by total area covered. The BIOMAS model is described in Zhang *et al.* (2010a), and is plotted here as its outputs will provide the physical forcing in this chapter's model runs, and thus provide a clear picture of the environment the NPZD model will be operating in. These model data compare well with observations in warm years (Stabeno *et al.*, 2017).

the Oscillating Control Hypothesis (OCH). The OCH posits that ice cover protects the water column from being mixed by winter storms, allowing for early stratification and, in accordance with the critical depth hypothesis of Sverdrup (1953), setting the conditions for a bloom once the ice retreated. Conversely, the authors hypothesised that in a year without ice cover, the resultant winter mixing would delay a bloom as compared to a cold year, as stratification would come later in the year. Note also that Hunt, Jr *et al.* (2002) acknowledge other factors are involved, and available observational data are not inherently clear cut, as is also shown in discussions of inter-annual bloom dynamics in Stabeno *et al.* (2001).

Thus, this case-study in applying the model to different (physically and temporally) years has to contend with the rather large array of potentially relevant variable, interactions, and systems, and the paucity of data for them. Assessing the reasonableness or validity of results takes these issues into consideration.

5.2 Data & Methods

5.2.1 Cruise Data for Warm Years

Similar to the data presented in Chapter 3, data were obtained from research cruises undertaken by the USCGC *Healy* in 2014, 2015, and 2016. The cruises followed the 70-metre isobath in late spring, and took samples from multiple depths at each sampling site, as described in Lomas *et al.* (2020). The map in Figure 5.2 shows the location of sampling sites in 2015 along with the location of key moorings and the 70-metre isobath.

Measurements were made of nitrate and chlorophyll-*a* concentrations. Samples were also incubated to measure carbon and nitrogen uptake rates. The 2015 depth-integrated values for nitrate concentration, carbon uptake rates, chlorophyll-*a* concentration, and nitrate uptake rates are presented in Figure 5.3.

These cruises were designed around mooring recovery and the data cover a handful of days for each year. The minimal number of data points, and the lack of any visible directional trend, makes it difficult to draw any conclusions about the spring bloom in this year.

Using fluorometry data from the moorings M2 and M4 on the 70m isobath in the Bering Sea, Stabeno *et al.* (2017) show that M2 experienced a clear chlorophyll peak in the latter half of May 2015, with M4 having multiple peaks from late April to early June 2015 (cf. Figure 5 in the paper). Mooring data also show a mid-May peak in 2014 at M4, and a wide peak beginning mid-April and continuing at high levels into April for M2 in 2016. Thus we can infer from Stabeno *et al.* (2017) that the cruise data in Figure 5.3 are insufficient to capture the latter half of the bloom or the post-bloom phase, if they even properly represent the peak at all.

Sigler *et al.* (2014) provide data on spring bloom maxima for multiple years between 1995 and 2011, across the Bering Sea encompassing moorings M2, M4, M5, and M8. These were compared with the dates of ice retreat at different locations. For years with early ice retreat, the bloom maximum could be as late as June at M2 and M4.

Thus from a historical perspective, it is unclear where in the bloom development

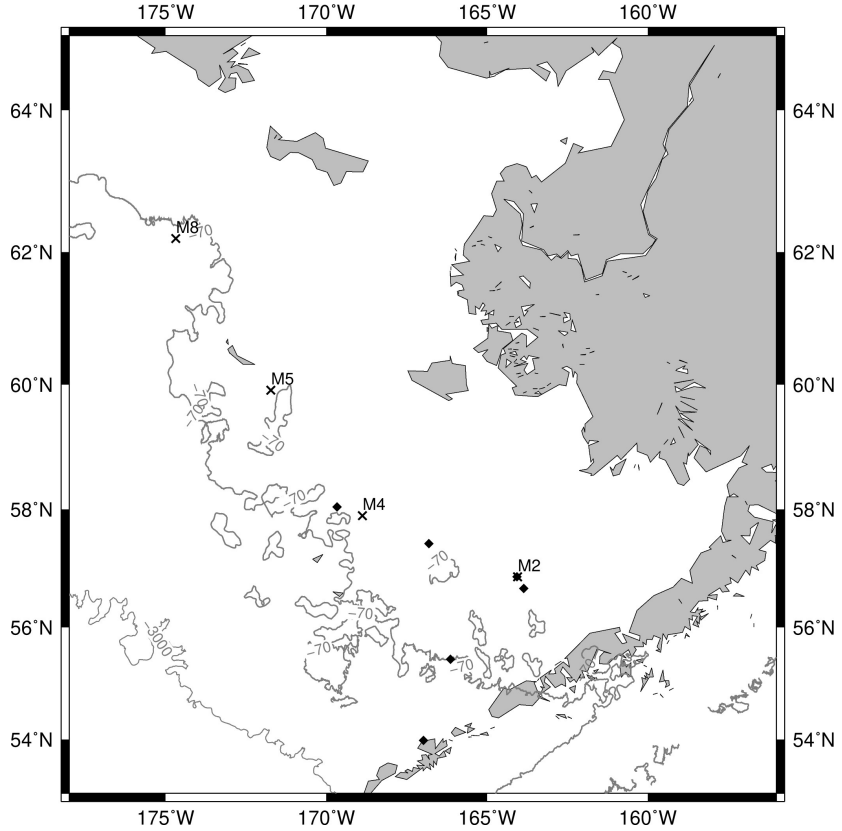

Figure 5.2: Map of sampling sites of 2015 cruise data, indicated by solid diamonds. At each site, samples were taken across multiple depths, the vertically integrated data present in Figure 5.3. Moorings indicated by crosses. Mooring data provide a reference for bloom dynamics in prior years (Sigler *et al.*, 2014) and 2015 in particular (Stabeno *et al.*, 2017), see text for details.

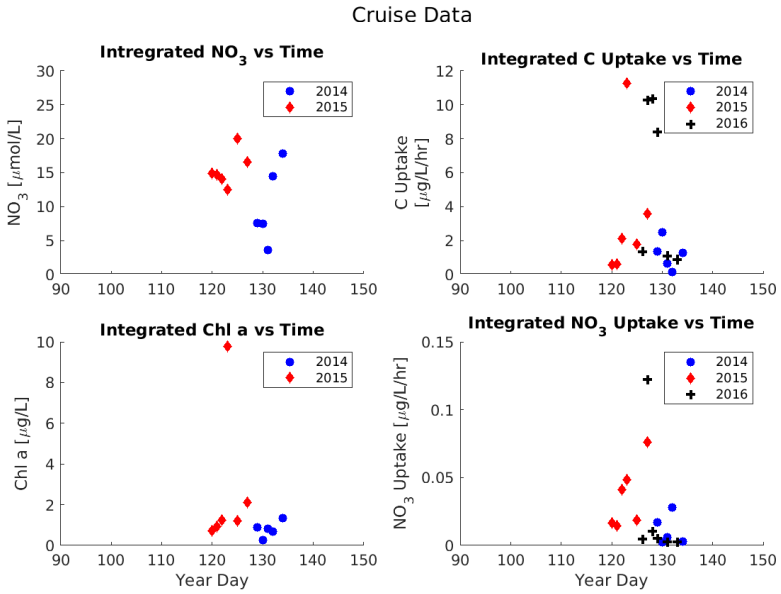

Figure 5.3: Depth-integrated data calculated from measurements taken during cruises of the USGCG *Healy* in the Eastern Bering Sea in late spring of 2014, 2015, and 2016. Each spring cruise took place at roughly similar times of year.

the cruise data might lie, and they cannot be used as test data. Accordingly, bloom phenology is studied for its sensitivity to seasonality and inter-annual variation in physical conditions. Ranges for potential bloom timings, based on location and ice extent, derived from literature are used to aide analysis (Brown & Arrigo, 2013; Sigler *et al.*, 2014; Stabeno *et al.*, 2017).

5.2.2 Physical Forcing for NPZD Runs in Warm Years

As with the IEB60 case, physical forcing was taken from an existing 3D model, which coupled a sea-ice model, an ocean circulation model, and a biological model. The particle tracking method was the same as described in the prior chapter, section 4.2. For this chapter, particles were tracked in outputs from the BIOMAS model, details of which can be found in (Zhang *et al.*, 2010a).

Particle trajectories were extracted along the 70 metre isobath of the EBS, a representative region for the middle shelf and along which are several mooring stations. The extraction was limited to trajectories which began anywhere between 60° N and 80°

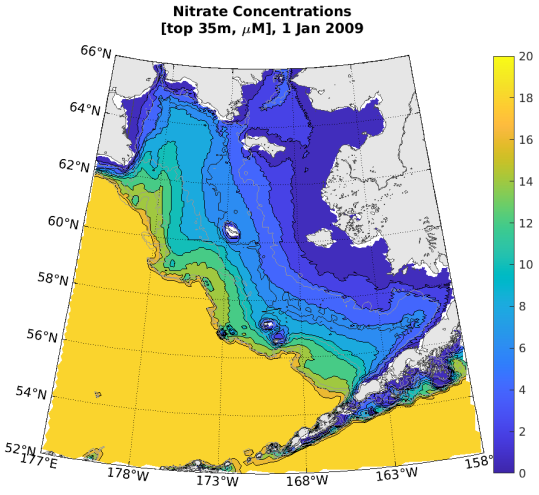

Figure 5.4: Map of initial NO_3 in the top 35 metres. For all years, $[NO_3]$ was determined by Equations 4.16, 4.17 and 4.18.

N, at locations with maximum depths between 60 and 80 metres. Given the prevailing currents in the region, these trajectories predominantly follow the 70 metre isobath in its northwest direction around the coast of Alaska.

As in the previous chapter, physical forcing was derived by extracting the physics at each point in time and two-dimensional space along a trajectory in the BIOMAS model. These were values of maximum depth H, temperature T, surface light E_0, vertical diffusivity κ, and ice concentration.

5.2.3 NPZD Runs for Warm Years

Using the trajectories, the NPZD model was initially run for the years 2009 and 2015. The parameter values used were those determined from the previous chapter's optimisation. This meant that these initial runs exhibited seasonality in their photoparameters μ_0 and α, where low winter values transition to high spring values after the effective light E_{eff} exceeds a threshold E_*.

The 2009 IEB60 case-study was a particularly well studied bloom, with multiple measurement methods of more than 6 variables recorded before, during, and after the bloom. Such data are difficult to obtain in the best of circumstances, and the blooms of

2014-16 were not so well resolved, and much of the time series data on variables such as nutrient and chlorophyll concentrations were limited to the moorings (see Section 5.2.1). Lacking enough data in nitrate, phytoplankton, and zooplankton, the warm year runs could not be reliably compared against data. Instead, the model was studied for its response to changing physical conditions, to better understand the role of seasonality in modulating inter-annual variation.

Initial nitrate profiles were calculated using the same functions as in the prior chapter, described in Equations 4.16,4.17, and 4.18. As before, the model assumes no carry-over of nitrate from the previous autumn, effectively resetting the nitrate each winter. This was a necessary assumption lacking validated data for inter-annual nitrate variation in the particular years studied here. A map of initial nitrate distribution in the top 35 metres of the water column is shown in Figure 5.4. The discretisation of the NO_3 field arises in part because NO_3 profiles are functions of z and H. The model grid is taken from BIOMAS, which has discrete intervals for the water depth H. The low, near-zero nitrate concentrations on the inner shelf, close to the coast, are consistent with observation data for this region (cf. Kachel *et al.*, 2002; Stabeno *et al.*, 2010).

As described in the previous chapter, within the model E_{eff} is explicitly defined as a function of vertical diffusivity κ, attenuation by seawater att_{sw}, surface PAR E_0, and the growth rate μ_0:

$$E_{eff} = E_0 \exp\left(-\text{att}_{sw}\sqrt{\frac{\max(\kappa)}{\mu_0}}\right) \tag{5.1}$$

One result of the Chapter 4 was the sensitivity of bloom timing to the strength of seasonality in the photoparameters μ_0 (maximum growth rate) and α (initial slope of the light response curve, a proxy for photosynthetic efficiency). That chapter defined seasonality s as

$$s = 1 - \frac{\mu_{0,win}}{\mu_{0,sum}} = 1 - \frac{\alpha_{win}}{\alpha_{sum}} \tag{5.2}$$

That is, where there is no seasonality and winter values equal summer, then seasonality s is equal to 0, with the strongest possible seasonality being 1, where winter values are zero. The effect of changing seasonality was studied by fixing all parameter except $\mu_{0,win}$ and α_{win}. Degrees of seasonality were applied to $\mu_{0,sum}$ to calculate

$\mu_{0,win}$, and both terms were used along with α_{sum} to calculate α_{win}, in accordance with Equation 4.14 and the assumption that E_k is constant. The timing of the bloom was calculated for the same region around the 70 metre isobath. For each trajectory, the bloom start was considered to be the date at cumulative phytoplankton biomass up to that point was equal to 15% of the sum total. This metric is used in such past work as Greve *et al.* (2005) and Brody *et al.* (2013).

This experiment in varying s, while keeping other parameters fixed, was repeated for 2014 and 2016 as well, to ensure any trends in 2015 are consistent with other warm years. The earliest date of initiation for any trajectory within the specified region was taken as the beginning of the bloom for the whole region.

5.3 Results

5.3.1 Trajectories and Physical Forcing

The warm temperatures of 2015 contributed to a smaller area covered by ice at the maximum extent, only reaching as far south as 58 °N, and an earlier thaw. In addition, 2015 also saw the formation of the ice much later in the winter season. In 2009, ice had already formed at the most northerly latitudes in early December, while in 2015 ice formation began in January. Figure 5.5 shows the average ice concentration at each latitude in the study region from the beginning of the year into mid-summer. The cold of 2009 allowed for ice to extend further south, barring a brief ice retreat in late February and early March which was discussed in the previous section.

The forcing fields are shown in Figures 5.6 and 5.7, along with a map of the trajectories in the EBS. Trajectories all begin in the immediate vicinity of the 70m isobath. In both years trajectories head in many directions with a general trends to follow the 70m isobath northward. In 2009 trajectories don't reach north of 64°N, while several paths extend much further north in 2015. However, the large majority of 2015 trajectories remain in the same region. Regarding ice cover, only in the most northerly trajectories does ice persist as long into 2015 as in 2009. Most 2015 trajectories begin, if not remain entirely, further south than the southernmost extent of ice. However those trajectories

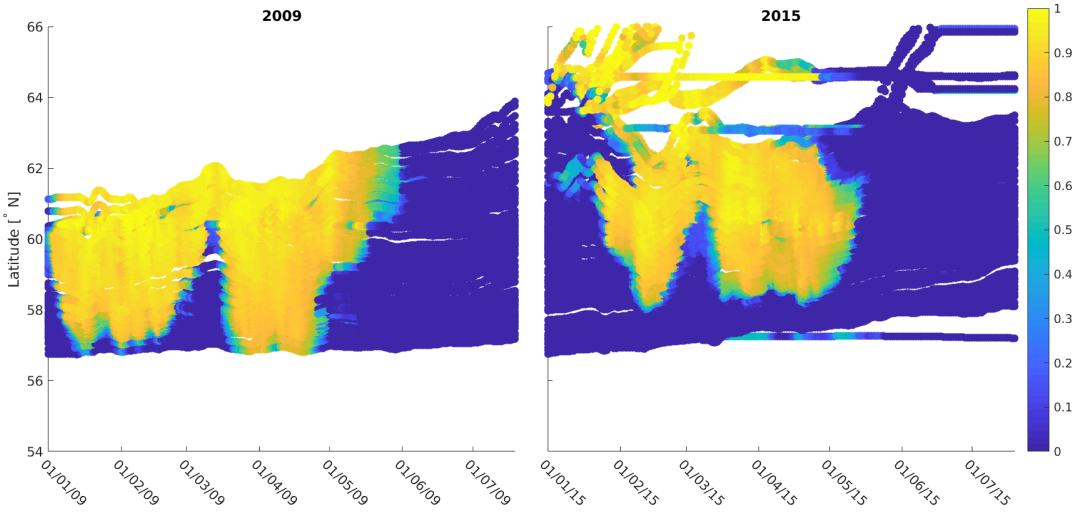

Figure 5.5: Scatter plot of trajectory points by latitude and time, coloured by ice concentration. In 2009, trajectories even south of 58°N experience thick ice cover. In 2015 ice not only forms later in the year and never extends as far south. Both years experience a brief retreat in ice in their most southerly regions in early March.

which continue north toward the Bering Strait experience ice cover late in the year.

Trajectories in both 2015 and 2009 generally begin with higher temperatures then move northward with currents to colder regions. In 2015 trajectories that begin in open water may move toward an ice covered region, but some do not and remain at higher temperatures. All trajectories have a lower bound nearly -2° C, being the freezing point of sea water. All trajectories' temperatures increase as they continue into spring.

Surface light, PAR_0, increases steadily across most trajectories in 2015 as there is no ice attenuation. Those that do flow under ice can be seen in the plots as having a delayed increase in light. In 2009 changes in ice cover cause some variation, but as ice retreats in both years PAR_0 increases.

Greater mixing is evident in the early months of 2015 as shown in the plots of κ in Figure 5.7. By late April in both years there is a reduction in κ which can be taken as evidence of stratification. Therefore we see that stratification occurs in both years around the same time. Early in the year, more trajectories in 2009 experience low values of κ. Conversely, in 2015, κ stays high into late April, when most trajectories experience a decline in this factor.

Figure 5.7 also plots the effective PAR E_{eff} at each point in the trajectories. Effective PAR is a function of the physics (ice, mixing, and incoming surface light). A jump in effective PAR in 2009 corresponds to ice retreat and stratification, although a steeper increase among several 2015 trajectories can also be seen to correspond with stratification.

5.3.2 Model Outputs

Figure 5.8 shows the results for nitrate, phytoplankton biomass, and phytoplankton carbon-specific growth rates along each trajectory in both years. As in the previous chapter, the nitrogen budget model was converted into carbon assuming a constant C:N. Nitrate concentrations are generally lower in 2015, and have a wider distribution. Most 2009 trajectories being with nitrate between 6 and 12 μM, with just one trajectory quickly rising to nearly 14. But in 2015 trajectory starting points have nitrate between 2 and just over 10 μM. As trajectories were selected based on whether they cross the 70-metre isobath, despite having the same initial field of nitrate concentrations (see Figure 5.4), the differences in currents resulted in different trajectory starting points in both years and thus rather different nitrate conditions.

The onset of the bloom is consistent with the model's light threshold, as the increase in phytoplankton biomass in Figure 5.8 follows an increase in effective PAR, which can be seen in Figure 5.7. In 2009, this increase in PAR corresponds to ice retreat. In 2015, the southernmost trajectories are absent ice and so light-limitation is primarily driven by mixing. Consequently, bloom timing in 2015 corresponds to the decrease in mixing.

In 2015, the southernmost trajectories reach optimal conditions for a bloom slightly earlier in the year, resulting in a wider spread of bloom peaks as the bloom moves northward. Out of 143 trajectories, more than half (83) experience blooms after mid-May. Less than one tenth (9) occur in mid to late June, well after the latest for 2009. A substantial fraction (39 trajectories) experience earlier blooms than the earliest blooms in 2009. Overall, bloom initiation spans from early May to the start of June for 2009, and from mid-April to late June for 2015. For both years, the majority of blooms begin in mid to late May. Thus while for the whole region, the spring bloom begins earlier

in 2015, much of the bloom occurs around the same year-day as in 2009.

The bottom row of Figure 5.8 shows the phytoplankton growth rates. While a handful of 2015 trajectories experience very high rates of growth by comparison to 2009, nearly reaching the maximum growth rate μ_0, the majority stay within the same range, below 1 day^{-1}. Much like with the integrated biomass, growth rates in 2015 are more spread out over time, while in 2009 have a sharp increase and peak immediately following ice retreat.

Figure 5.9 uses an example trajectory from 2015 to illustrate the transition to spring conditions using the threshold light model. Blooms begin when the effective light increases above the threshold light level, with the bloom peak occurring on the order of days after the transition.

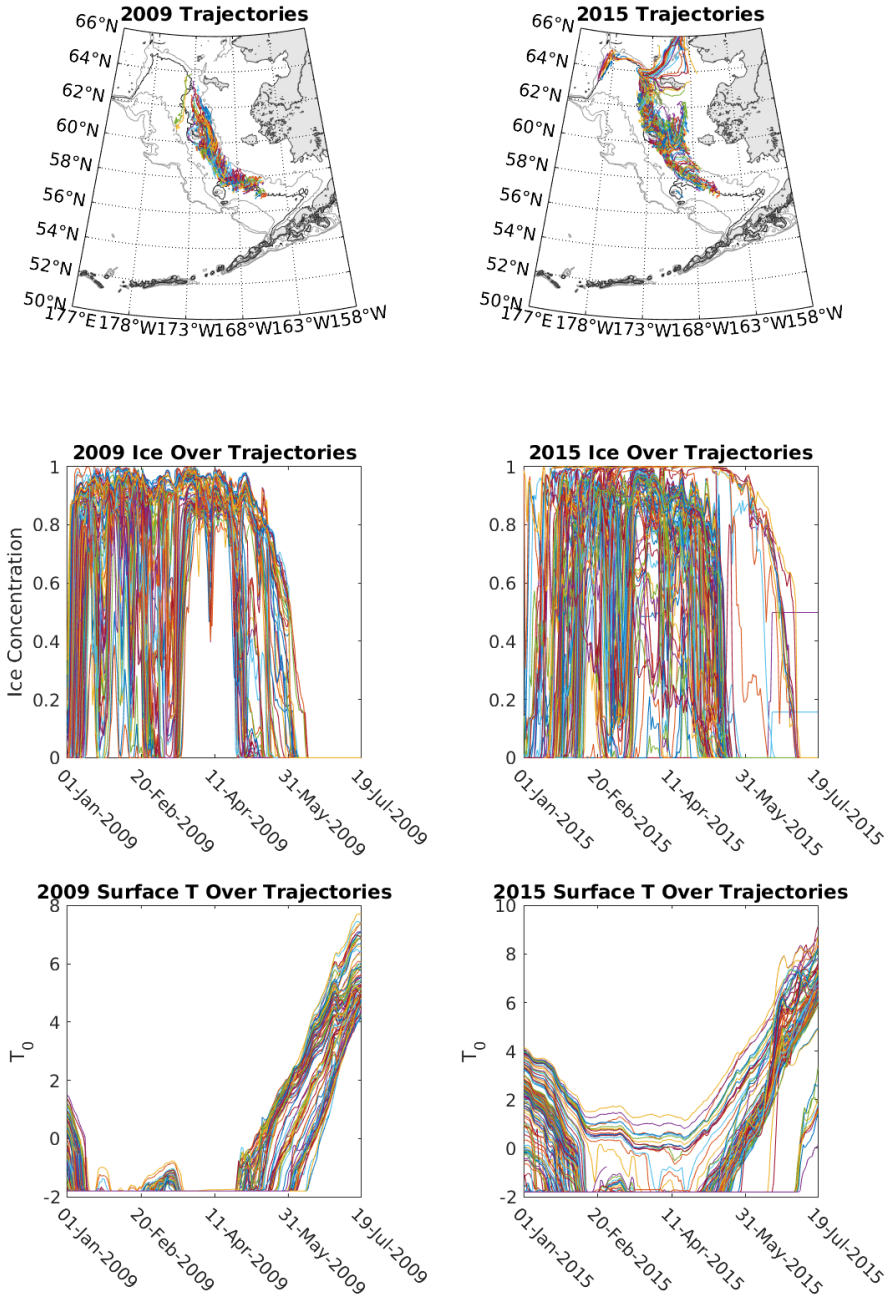

Figure 5.6: Particle trajectories for 2009 (left) and 2015 (right). Top row: Map of trajectories in the EBS. Middle row: Ice concentration over the trajectories. Bottom row: Surface temperature T_0 across trajectories.

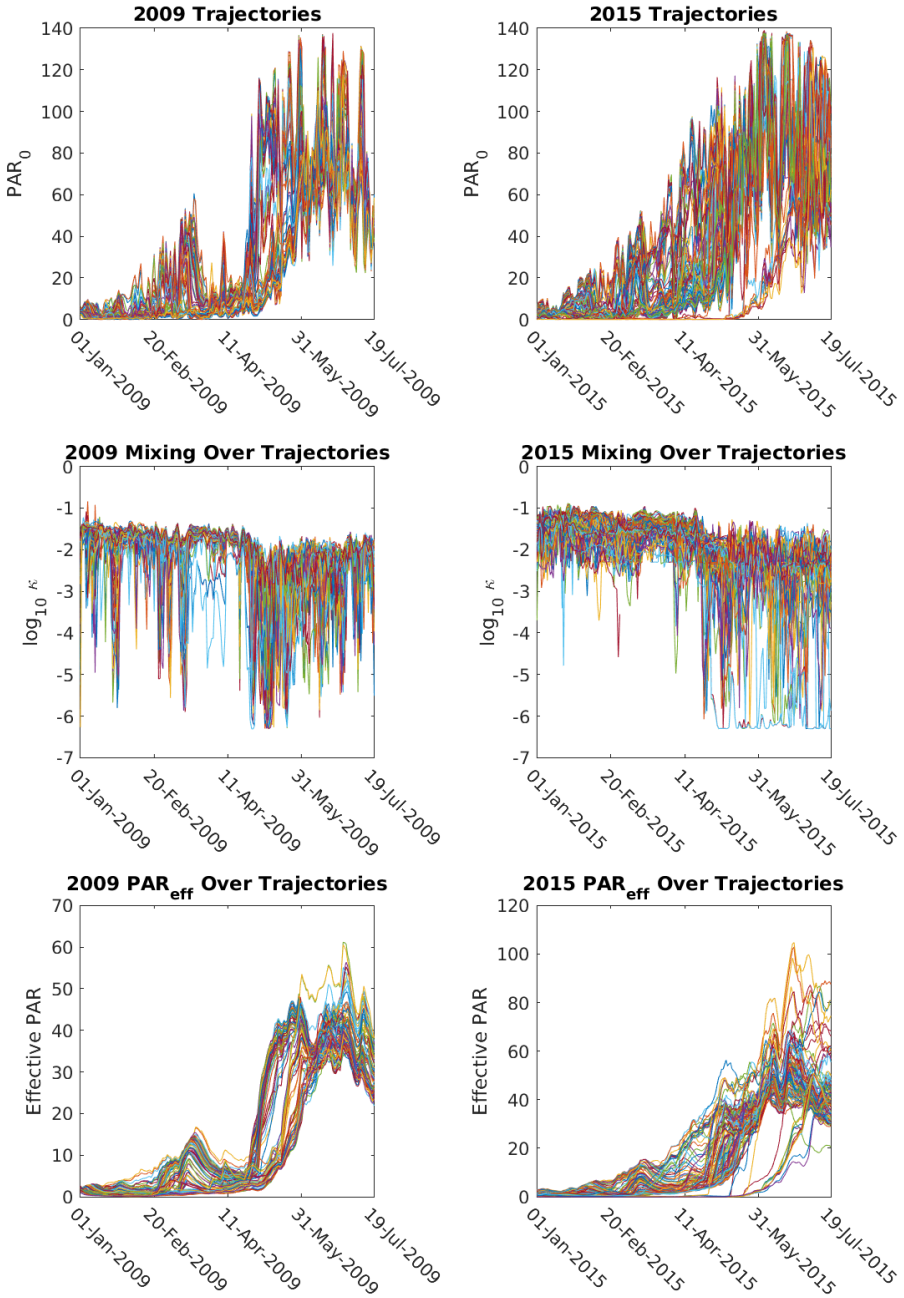

Figure 5.7: Physical forcing along the extracted trajectories. Top row: Surface PAR. Middle row: $\log_{10}$ of average vertical diffusivity κ. Bottom row: Effective PAR experienced by a cell mixed through the water column.

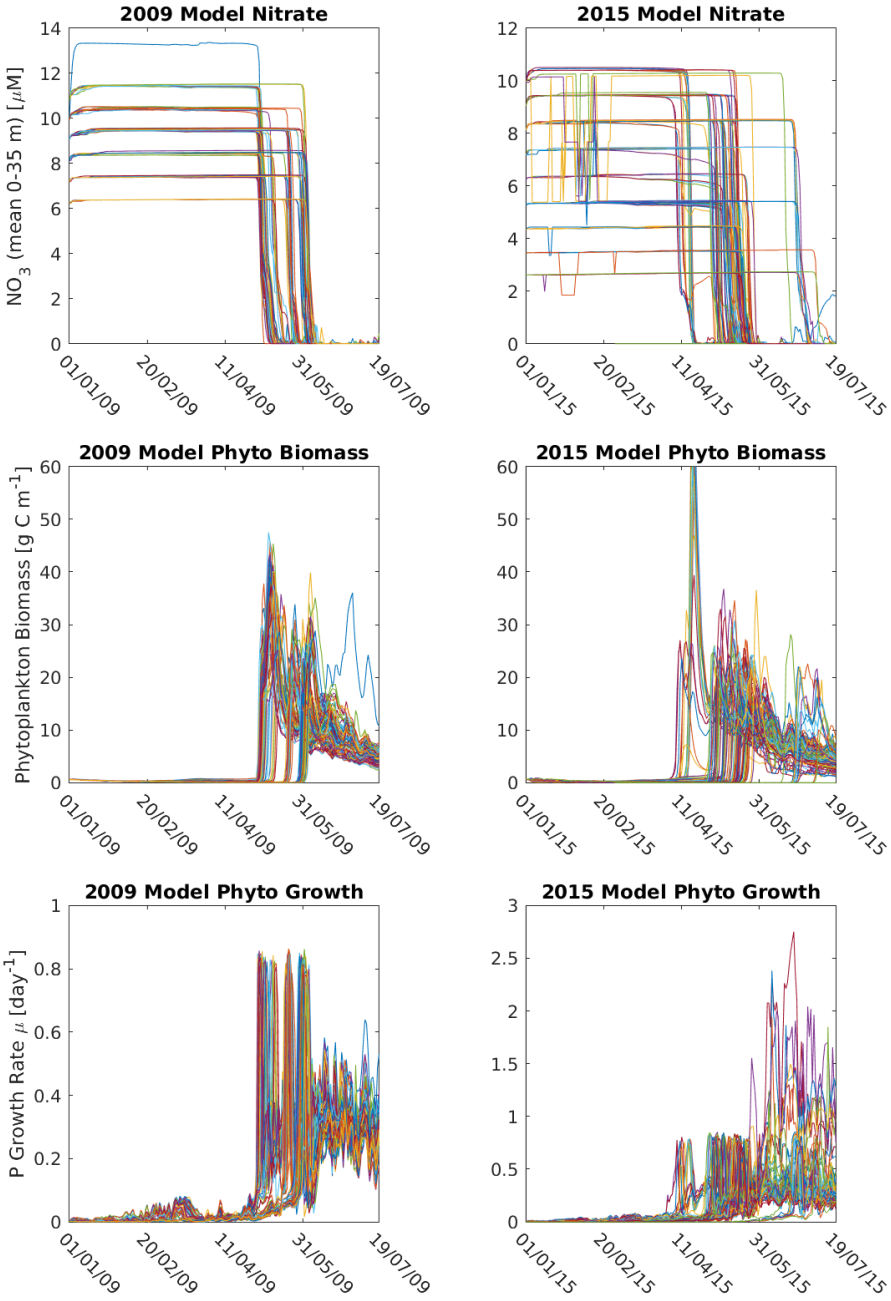

Figure 5.8: Model runs for 2009 and 2015 trajectories along the 70m isobath: Top row: Nitrate in the top 35 m. Middle row: Phytoplankton biomass. Bottom row: Phytoplankton specific growth rate.

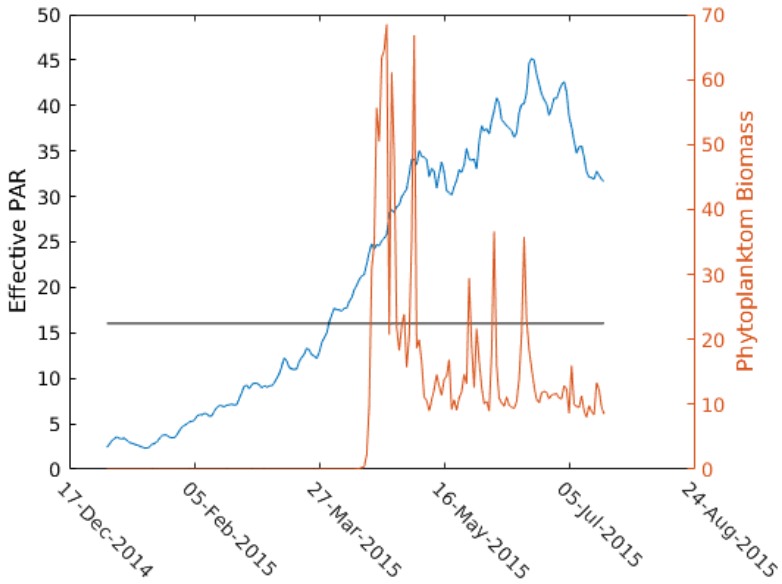

Figure 5.9: Illustration of the threshold light level model using one trajectory from the 2015 model run. The left y-axis shows effective PAR, the blue curve being the model output and the horizontal line being the threshold light level E_*. The right y-axis show phytoplankton biomass, plotted in the orange curve. The intersection between E_{eff} and E_* occurs as biomass begins to increase, with the peak of the bloom days after.

5.3.3 Seasonality and Bloom Phenology

Spring bloom start dates for each trajectory were determined as the day at which cumulative phytoplankton biomass was 15% of the total across the time space (cf. Ferreira *et al.*, 2014). Dates for bloom maxima were also calculated for each trajectory. These were calculated for model runs with varying strengths of seasonality. The seasonality s (see Equation 4.22) was varied between no seasonality ($s = 0$) and maximum seasonality ($s = 1$) by varying $\mu_{0,win}$ between 0 and $\mu_{0,sum}$. Using the assumption of a constant E_k from Chapter 3, winter α was the same fraction of its summer counter-part as $\mu_{0,win}$ was of $\mu_{0,sum}$.

In Figure 5.10, the start date of the model spring blooms are plotted against seasonality, including model runs for 2009, 2014, 2015, and 2016. Figure 5.10a takes the earliest bloom initiation out of all trajectories, while Figure 5.10b averages all trajectories' starting dates. Figure 5.11 plots the average dates for bloom maxima against seasonality. Also included are the approximate dates for the maximum at the mooring M4 in 2014 and 2015 shown in Figure 5b of Stabeno *et al.* (2017), as well as average dates from years with early and late ice retreats shown in Table 1 of Brown & Arrigo (2013).

These results align well with those shown in the previous chapter for the cold year (2009), where it was shown that incorporation of seasonality was necessary to avoid spurious formation of early blooms. Here we see evidence that the high mixing of the early months in the warm years (see again Figure 5.7) is also insufficient to delay a bloom without a seasonal factor. More concisely, without seasonality, either winter photoparameters values are high enough to initiate a bloom on the minimal light received at the start of the year; or summer values are too low to initiate a bloom at all later in the year.

Increasing seasonality from 0 to 1 delayed the average bloom initiation date by 63 days for 2009, 71 days for 2014, 72 days for 2015, and 68 days for 2016. Start dates at maximum seasonality were later than those at minimum seasonality by 35 days for 2009, 39 days for 2014, 38 days for 2015, and 28 days for 2016. Inter-annual variation, at maximum seasonality, accounted for at most 20 days difference for the state date

between 2009 and a warm year (the largest difference being with 2016), and 21 days difference for the date of the maximum (comparing 2009 with both 2014 and 2016).

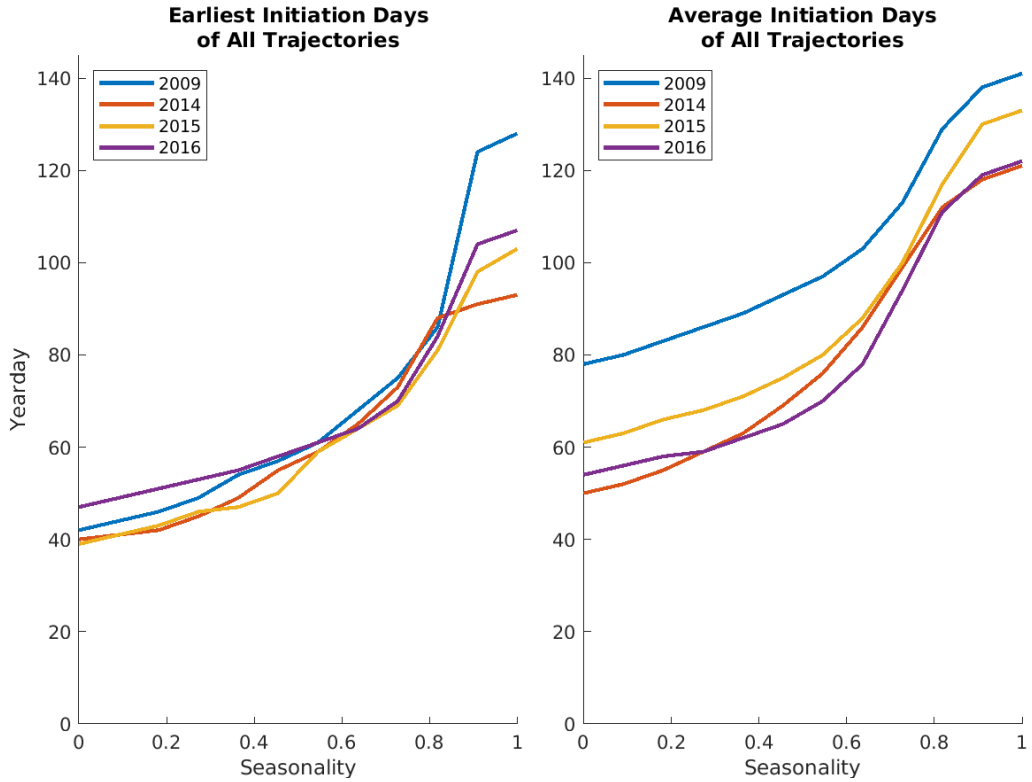

Figure 5.10: Timing of the spring bloom by year-day plotted against the seasonality s. Start date of the spring bloom was determined as the day at which cumulative phytoplankton biomass was 15% of the total across the whole time span. Seasonality was varied by varying $\mu_{0,win}$ between 0 and $\mu_{0,sum}$, which α_{win} being recalculated assuming constant E_k. Other parameters were the same for each run.
Left: The earliest single-trajectory bloom initiation date for each year and value of s.
Right: The average across all trajectories of bloom initiation dates for each s.

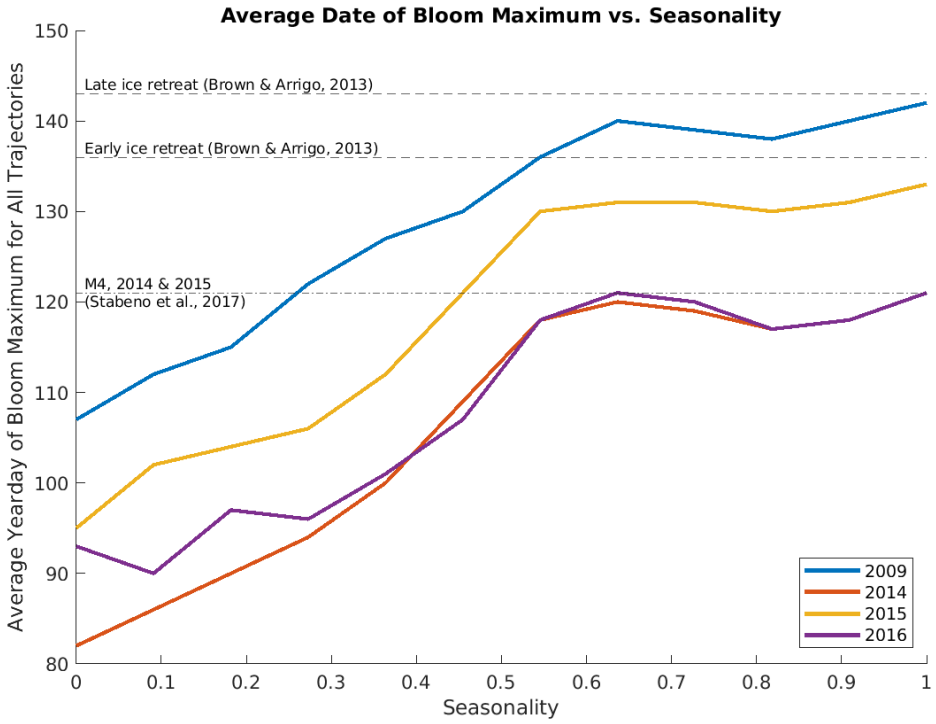

Figure 5.11: Timing of the spring bloom maximum by year-day plotted against the seasonality s. The dates of each trajectory's maximum were averaged for one overall point per year. Seasonality was varied by varying $\mu_{0,win}$ between 0 and $\mu_{0,sum}$, which α_{win} being recalculated assuming constant E_k. Other parameters were the same for each run. The dash-dot line is an approximation of the maximum for 2014 and 2015 at M4 shown in Figure 5b in Stabeno *et al.* (2017). The two dash-dash lines are averages for years with early and late ice retreats from Brown & Arrigo (2013), taken from Table 1 in that paper, specifically "Region 2", a comparable geographic partition of the study region.

5.4 Discussion

5.4.1 Physical Controls of Bloom Timing

Sea-ice has the potential to be an important control on the timing of the spring bloom in the EBS. Later melts can aid earlier blooms, as without sea-ice the sea is exposed to winter storms, which can drive the mixed layer deeper than the critical depth (Sverdrup, 1953), thus delaying the bloom until stratification increases. This mechanism is the previously mentioned OCH, or Oscillating Control Hypothesis (Hunt, Jr *et al.*, 2002).

Ice directly attenuates incoming light, the light which passes through to reach the water column being PAR_0. Ice also influences vertical mixing by shielding the water column from wind. The effective light experienced by phytoplankton is then a function of the amount of mixing throughout the water column and the surface PAR.

Surface light and mixing are themselves functions of more than ice cover, however it is through these factors that ice impacts effective light. As a direct impact, ice attenuates incoming light before it reaches the water surface. Indirectly, ice is one control on vertical mixing.

As Hunt, Jr *et al.* (2002) acknowledge, sea-ice may shield the water column from winter storms, but the strength of winter storms and how late they persist in the year is also variable. When also considering how changes to currents outside the region can impact inflow and outflow of nutrients and plankton, and the authors specify that the OCH is not a guarantee, but rather an expectation under specific assumptions. This has also been acknowledged in other literature. In Sigler *et al.* (2014), the negative correlation between ice retreat and spring bloom time in the southeastern Bering Sea is shown to be weaker than the OCH may suggest. Brown & Arrigo (2013) and Stabeno *et al.* (2010) report wind-driven mixing can decrease for periods in winter. And Ladd *et al.* (2018) adds an additional complexity in the impact of mixing on nutrient distributions on the inner shelf. While this study has focused on the middle shelf, on a larger scale the timing of blooms on the inner shelf can impact the rest of the EBS.

Many confounding factors arise from a more highly resolved picture of the EBS

ecosystem. Also noted in Brown & Arrigo (2013) is variation with latitude. The authors divided the eastern Bering Sea into four regions from north to south, with regions 3 and 4 being centred on the moorings M4 and M2, respectively. For the most southerly regions, late ice retreat corresponded to earlier blooms, in line with the OCH, but in the northern regions where ice persists later into the year, the earlier ice retreat corresponded with an earlier bloom on average. Returning to impact of the physics on light, seasonal light response continues to have a strong influence even relative to inter-annual variation, as discussed next.

5.4.2 Effects of Seasonality & Inter-annual Variation

The differences in bloom timings between the non-seasonal and high-seasonality runs were greater than the difference from inter-annual variation. Bloom initiation varied more than three times as much due to increasing seasonality as from inter-annual variation. And the date of the maximum of the bloom had larger variation from seasonality than inter-annual differences as well, though not as strong. That the bloom peak didn't vary as much with seasonality as initiation may be related to the fact that at lower seasonalities, bloom peaks were wider, and trajectories could have multiple peaks. As a result, initiation would be registered as being much earlier while taking many days to reach the overall maximum.

Looking at the variations in physical conditions between warm and cold years helps elucidate the linkage between the cell-level perspective of photoacclimation discussed in Chapter 3 and the annual and inter-annual ecological perspectives of this chapter and Chapter 4. The extreme light limitation that necessitated seasonal photoacclimation discussed in Chapter 3 becomes relevant on the ecosystem level when the system experiences large scale ice cover, vertical mixing, and the dark winters of high-latitudes. While the incoming light above ice will not experience significant inter-annual variation, warming temperatures will lead to more change in mixing and ice cover. As the above has shown, both factors need to be considered when predicting changes to phytoplankton blooms.

For example, the OCH predicts the reduced ice cover in a warm year would delay

the onset of the spring bloom. Yet this is only as a result of how ice can protect the water column from deep mixing in winter. This coupling of mixing and light is the same mechanism used in the NPZD model here. As such, the results from the NPZD model don't disagree with the OCH in terms of its ecological mechanisms, but these results could reflect what happens when winter mixing is weak. The phytoplankton in the model respond to the effective light, which regulates the timing of the bloom. Therefore estimates of mixing, ice, and surface PAR can be used to predict the timing of a spring bloom through the calculation of E_{eff}.

Ice cover is as an appealing proxy for spring bloom timing as it is one of the easiest physical factors to measure. However, ice alone is not the most reliable proxy. The model did not produce delayed blooms in the warm year because in spite of the lack of ice protection, winter mixing was weak and stratification appeared early. Note as well the geographic dependence. As mentioned above, in Brown & Arrigo (2013) the predictable pattern of the OCH is detected at the lower latitudes of the EBS, around moorings M2 and M4. Further north, later ice retreat is associated with a slightly later bloom than for earlier ice retreat. The average latitudes for all trajectories was approximately 60°N, with many trajectories running north toward mooring M8 (at 62.194°N) and beyond.

Stabeno *et al.* (2017) presents chlorophyll time series for 2014 and 2015 at M4, and 2015 and 2016 at M2. An estimate of M4 bloom initiation (based on Figure 5b in that paper) is plotted with the model runs in Figure 5.11, as M4 (located at 57.895°) is closer to the average trajectory locations. The start date of the blooms could not be estimated from this paper as the data were not presented, and only the maximum date could be roughly approximated from the plot. However this provides for some comparison. This intersects with 2015 at $s > 0.4$ and roughly matches the 2014 and 2016 model runs above $s = 0.6$. Stabeno *et al.* (2017) also note in figure 5d and the text that 2016 had an anomalously early bloom at M2, beginning in mid to late April, which is slightly earlier than the model predicts.

5.4.3 Implications for Modelling

Seasonality in photoparameters can have a strong control over model blooms, with seasonality alone able to account for weeks of difference in bloom timing. While inter-annual variation can account for substantial variation on its own, this analysis suggests seasonality can be even more influential and thus merits consideration in modelling studies.

Within the limited scope of this study, many factors were controlled that might, in a real ecosystem, dominate the system. For example, on an ecological level, the average α and μ_0 for a whole community glosses over the inter-species differences. A change in the composition of a community can account for a change in average α.

Oh a physical level, there remain open questions that need to be addressed in a model, if not explicitly accounted for in the equations then excluded with justification. In Sigler *et al.* (2014), the negative correlation between ice retreat and spring bloom time in the southeastern Bering Sea is shown to be weaker than the OCH may suggest. And this is because, as discussed in Brown & Arrigo (2013) and Stabeno *et al.* (2010) wind-driven mixing can decrease for periods in winter. Here, the physical forcing is derived from a model that incorporates surface winds. The variability of winter winds, their influence on the variability of mixing, and thus their influence on bloom phenology, is important to understanding the results in the regional context. While there is a correlation between temperature, winter storms, surface winds, and ice, the relations between each are complex and additionally all are influenced by other factors. As a result, a simplified prediction of spring bloom dynamics using ice retreat as a proxy, but not accounting for factors such as winds, will not necessarily yield accurate results.

The implication for modelling spring blooms is therefore strict scrutiny toward factors regulating E_{eff}, and to acknowledge vertical mixing is not simply coupled to ice cover. By following this approach it becomes possible to understand how the timing of blooms in the northeastern Barents sea can deviate from the predictions of the OCH. Revisiting the question of how an NPZD model with seasonal light response behaves in a warm year, the results presented here (summarised in Figs. 5.8–5.11) suggest that seasonality is not only as important for warm year bloom phenology as in a cold

year, but that seasonality can have as much an impact as physical variation in the environment.

Looking to a warming future, whether or not to account for seasonality in an ecosystem model will need to consider all of the above, including the caveats. Yet it is safe to say that seasonal variation in photoresponse, whether at the intra-cellular or community level, has the potential to act as a significant regulator of bloom development even in the face of large inter-annual changes. Knowing from previous chapters that plastic photoresponse exists at both levels, and seeing in this chapter how that translates into bloom phenology, phytoplankton models in similar conditions would do well to address this mechanism.

Chapter 6

Conclusion

Numerical ecosystem models expand our conceptual understanding of ecosystems by following assumptions and hypotheses, codified in mathematical equations, to their natural conclusions. Models are never exact analogues to reality (see again Section 1.2), nor do we always want them to be. Validating a model requires asking specific questions, and the problems in a model (such as its outputs not matching observations, or matching observations but using contradictory or impossible physics) can point to knowledge gaps or re-affirm expectations. That is the space in which this thesis has explored the dynamics of a regional NPZD model. Establishing the numerically significant change in model performance with seasonal photoacclimation furthers the case for seasonality and dynamic parameterisation, while also providing more insights into our understanding of the modelled ecosystem.

In a previous study of small region within the EBS (the IEB60 test-bed of Banas *et al.*, 2016, see also Chapter 4), it was established that seasonality in α needed to be accounted for to reproduce observed data. This thesis has provided evidence that this seasonality can be seen in the data gathered from Bering Sea communities (as well as other high-latitude environments, cf. Table 2.2). That this model performs well when considering seasonality in both α and nitrogen-specific uptake rates and cannot accurately reflect the data without seasonality (Chapters 4 & 5) fits well with the observation of seasonality shown in the data (Chapter 3). While many ecosystem models do not account for seasonality in these parameters, this study has provided

evidence that such seasonality may well be essential for accuracy of bloom timing and magnitude. This study has also provided a simple mechanistic explanation and a means of implementing seasonality with minimal alterations to the model, further justifying its inclusion in model experiments not simply as a hack or a cover for unresolved issues but as an actual biological process that needs to be accounted for (or, if left out, justified).

Questions of interpretation still remain, however, both in terms of 1) the physiological interpretation of the seasonal variation in photoparameters; and 2) how intra-cellular and inter-species variation in photoparameters should be coordinated within models. Many of the studies cited in this thesis not only demonstrate changes in community composition during spring blooms, but also measured α on a community level and not separately by species (see Chapter 2). Finer questions can also be asked about how seasonal photoacclimation fits into the pre-existing understanding of the EBS, especially in regards to the Oscillating Control Hypothesis, as discussed in Section 5.4.

On top of that, we can look for lessons with modelling methods generally, and formulate new hypotheses regarding phytoplankton ecology based on the model results. Therefore we can group conclusions for this thesis as being within the realm of modelling, within the realm of ecology, and the intersection of the two. Of course, the strongest conclusions pertain to the narrow focus of the above models: of seasonal phytoplankton photoacclimation and how to model highly seasonal marine ecosystems. But it is worth considering how these conclusions relate to research fields beyond the narrow.

Thus we must look back at the implications this thesis has for the physiological and ecological bases for photosynthetic seasonality, the implications these would have for model design generally, and then what we can learn about the Eastern Bering Sea. Finally, this thesis will conclude with a note on the limitations across all these categories, and what future research in the high latitudes should consider.

6.1 The Role of Photoacclimation in Seasonality

Chapters 2 and 3 make the case for a biological basis in seasonality at least at a community level if not the level of individual cells. For a cell, there are many factors

which can lead to a decrease in α. In the case of over-wintering in polar ecosystems, the need for efficiency in low light regimes must be balanced with the respiratory costs of maintaining photosynthetic apparati. The association of α with R_M in Langdon (1988) and Siegel *et al.* (2002) was derived from a fit to experimental data, yet the physical underpinning of this relationship can be seen in Equation 1.6, expressing α as a function of chlorophyll-specific absorption cross-section $\bar{a}^*$ and maximum quantum yield ϕ_{max}.

Chlorophyll-specific absorption cross-section $\bar{a}^*$ is a measure of the amount of PAR absorbed by chlorophyll-a, normalised to the amount of chlorophyll-a. Increases in chlorophyll-a arranged in a thin layer or shell increase the amount of surface area to absorb light and therefore cause an increase in $\bar{a}^*$. Excessive pigment depletion can lower the absorption cross section, thereby reducing α (Dubinsky & Stambler, 2009). However, in a three-dimensional cell, chlorophyll can self-shade. This self-shading is known as the "package effect", and it causes an effective decrease in absorption cross section while increasing the total amount of chlorophyll-a, causing a decrease in $\bar{a}^*$ (Rochet *et al.*, 1986). Thus either an increase or decrease in chlorophyll can cause a decrease in $\bar{a}^*$ and therefore α, generally speaking. Both phenomena have been observed in polar phytoplankton (Jochem, 1999).

Another layer of complexity is added by the diversity of pigments. While $\bar{a}^*$ may decrease as a result of decreased chlorophyll, an increase in other pigments mean the cell may still darken and the overall absorption remain the same or even increase (Matsuoka *et al.*, 2011, 2009). In that sense, $\bar{a}^*$ is not always a proxy for α, and the whole photosystem must be considered, a helpful parameter being ϕ_{max}, a function of absorption cross sections of Photosystem II and the Photosynthetic Unit as shown in Equation 1.7.

Thus the maintenance respiration cost associated with α could be the effect of any of several of the molecular mechanisms of photosynthesis: the amount of chlorophyll-a, or the amount of reaction centres or other pigments in the antennae. Chlorophyll concentration needn't necessarily decrease for α to decrease either, as the package effect yields a reduction in $\bar{a}^*$. Many diatoms are known to increase their pigments and darken as

light decreases (Dubinsky & Stambler, 2009). Moreover, adding to the complexity is the fact that antennae and reaction centres can be regulated independently (Falkowski & Raven, 2007). Decreasing reaction centres increases the "size" of the PSU by decreasing the amount of evolved O_2 per amount of chlorophyll, effectively increasing σ_{PSU} and therefore decreasing ϕ_{max} while saving respiration costs. Morgan-Kiss *et al.* (2016) describe possible processes of down-regulating this activity in freshwater Antarctic communities.

The implication of these multiple regulatory processes is that the hypotheses of this thesis– that over-wintering phytoplankton communities at high latitudes have lower values of μ_0 and α, at least in part to reduce maintenance respiration costs– may be too simple to fully explain the high degree of variation that is noted in the literature on a purely mechanistic basis. Yet despite both uncertainty as well as known variability in cellular-level mechanistic controls, there does appear to be a large scale trend that can be modelled as a community seasonality in the photoparameters. That this improves model performance points to community-wide ecological implications for seasonal photoparameters.

6.2 Ecology of α and Model Design

As mentioned in the literature review (Chapter 2), there does not appear to be a consistent hypothesis regarding the taxonomic scope of the strategy of reduced light responses over winter. Nevertheless, community composition is an important question to explore in this regard. If Matsuoka *et al.* (2011) are correct (see brief summary in Section 2.3), then the above models of dynamic community-level photoacclimation in the EBS may be more accurately seen as the result of the increase in the proportion of large-celled diatoms. The NPZD model used in this thesis is a 1-P model, in that there is only one type of phytoplankton with a single set of parameters (whether those parameters are constant or not, there is only one value per parameter at each time). It is, therefore, a model of the whole community.

Considering further the possibility that the better fitting of the seasonal model is

more to do with extra degrees of freedom, the model used here is also a 1-P case. It is possible that with 2 phytoplankton classes, or more, that for each class smaller variations in α or even none at all are sufficient to provide a good fit to data, if the classes with higher α become dominant in spring. Yet the literature review (Chapter 2) still shows individual cell lines can experience seasonal α and maximum photosynthesis P_m and specific growth rates μ_0. While every model, regardless of how many classes of phytoplankton are included, necessarily aggregates and conglomerates a myriad of different species into each phytoplankton class, the impact of cell-level acclimation on community-wide photoparameters may need consideration.

While the rapid nature of the bloom's onset can be captured with the nonseasonal version of the model, the threshold light level used in the seasonal model allows for accurately timing the bloom, making it significantly easier to match both timing and magnitude together. Because the model is using a threshold light level to determine the switch from one regime to another, there is an implicit assumption in the text of the thesis, the model code, and even the naming of variables that this is the crux of the issue of photoacclimation. Yet the mathematics remains the same even with the interpretation that greater α represents an increase in the proportion of taxa with high α in the community. A 2-P-class model would add equations to make this interpretation explicit.

A non-seasonal model with multiple phytoplankton classes would still need a mechanism for preventing those classes with inherently higher α and μ_0 from blooming too early. The work of this study suggests the threshold light level is an effective tool and the literature review suggests a biological basis. We might therefore conclude that models with more phytoplankton categories find themselves in need of the same solution to the problem.

In Section 1.2.1 other approaches were presented. Trait-based approaches with adaptive dynamics vary traits according to a fitness function. And while this is ostensibly done for the purposes of capturing evolutionary processes (cf. Abrams *et al.*, 1993; Merico *et al.*, 2009), in which mutations across generations are filtered through natural selection based on some relative fitness, the equations do not themselves entail

adaptation. Variation in a trait between generations (or simply time-steps, depending on the model set up) can also be interpreted as acclimation. This poses an interesting possibility for seasonal photoacclimation, be it occurring at the cellular or community level. Without more information, there is much left unknown about the upper and lower limits of α and the shape of the function between winter and summer values, or whether it is even continuous. The model here assumes a sharp transition because a two-domain framework could be demonstrated in observation, further assumptions were beyond the scope of this thesis. Nevertheless, much like more complex models with more compartments could hold value for future projects with seasonality, so too might an adaptive dynamical approach.

6.3 Between First Principles Models and Observations of the EBS

The pressing implication for model design from this study is the sensitivity of the spring bloom to seasonality of light response. While numerous complicating factors have been expounded upon above, and new degrees of freedom increase flexibility generally, the fundamental change of the model from a static light response to one which can in a very short time switch from slow to rapid growth fundamentally enables a rapid bloom.

Exploring the model further led to a comparison of its output in a cold year, 2009, and three warm, 2015–2016, as shown in Chapter 5. As noted, the data available for the warm years was not comparable to that for 2009, in which the spring bloom was well defined across phytoplankton, zooplankton, and nitrate measurements. Data which were available included approximate bloom timings at multiple locations in the Bering Sea for multiple years (Brown & Arrigo, 2013; Stabeno *et al.*, 2017) The experiments subsequently conducted explored the theoretical landscape of the model and tested the sensitivity of bloom timing to the strength of seasonality.

One question was whether the model would replicate the OCH (Oscillating Control Hypothesis, see Hunt, Jr *et al.*, 2002), i.e. whether ice cover would make for a good predictor of spring bloom timing, and whether the agreement between the cell-level

and ecosystem-scales would hold. The result was the model developing a bloom in 2015 around the same year-day as 2009 in spite of the earlier retreat of ice.

Looking back to the physical trajectories, it became clear why this was. Vertical mixing decreased rapidly in 2015 just before the bloom began. This enabled an increase in E_{eff}. Which triggered a spring bloom, consistent with the light-limited perspective of the model and prior theories such as Sverdrup's critical depth (Sverdrup, 1953). Light limitation was upheld in spite of the counter-intuitive bloom timing in 2015. While it has been noted that mixing can control nutrients as well as light, especially in the shallower coastal areas (Brown & Arrigo, 2013; Ladd *et al.*, 2018), on average over the EBS in spring nutrient limitation is not as strong a control. The physics of the light environment is therefore crucial to underpinning an accurate model of spring bloom dynamics in this region.

6.4 Future Perspectives for a Warming Arctic

Even as ice retreats further north, the southeastern Bering Sea will continue to be a highly seasonal environment. This northward ice retreat will cause strong seasonality in the ice cover of regions that previously experienced stable, consistent ice cover. Seasonality in phytoplankton behaviour and parameterisation is therefore important for accurate models and will continue to be so. Arguments can be made for including these processes from the start, such as in the mechanistic model of (Baklouti *et al.*, 2006a), or adding photoacclimation to existing models (Anugerahanti *et al.*, 2021; Banas *et al.*, 2016, and this study) but regardless the conclusion seems strong that it is a necessary consideration at some stage.

While the changing climate will have far wider impacts across high latitudes, this project has made the case for the necessity of studying and understanding light response as a means of understanding ecology in the EBS and similar regions. Melting ice means a changing light environment, the impacts of which still have much to be studied. Little is known about how phytoplankton over-winter in high-latitudes, on account of the difficulty of sampling, compounded with the difficulty of detecting cells in such low concentrations, compounded even further by the difficulty and high errors

in measurements of such low values of irradiance and photosynthesis. Yet as ice retreat increases light availability, the ability of phytoplankton to adapt and bounce back from winter depletion will be dependent on their over-wintering strategies. It is therefore important to try to better understand phytoplankton behaviour in such light-limited regimes, to be in the best position for predicting impending community changes.

Finally, while this project looked only at a 1-phytoplankton model, and has demonstrated the prevalence of photoacclimation within cells, future work with two or more phytoplankton classes may provide even more insight into the changing Arctic. While photoacclimation is known to occur, it is also known that different species have different photoparameters, and therefore changes in community composition can also account for ecosystem-wide changes in α.

What is certain, in a dynamic and rapidly changing environment, is that phytoplankton seasonality can have a strong effect on the dynamics of the whole ecosystem. While uncertainties in photoparameters, especially during winter, may have led to a gap in understanding of this process, going forward it appears ever more important to account for this behaviour as a fundamental process of high latitude phytoplankton behaviour.

Appendix A

Correction

Shortly before submission, a bug was discovered in the NPZD model code, in which microzooplankton grazing rate was not calculated properly. Instead of using net grazing rate (accounting for inefficiency in uptake and losses from excretion), gross grazing was used for the change in microzooplankton biomass at each time step.

The model calculated fluxes at every time step, then added the change over that time step to the associated variables. Microzooplankton had a source term in grazing, and a sink term in mortality m_{zoo}. Grazing ought to be limited by its efficiency ϵ (losses due to this term being a source for small detritus), and the excretion rate (which adds to NH_4^+).

The gross grazing flux $F_{grazing}$ was first calculated before the detrital and ammonium fluxes were determined by

$$F_{eg} = (1 - \epsilon - f_{ex}) \cdot F_{grazing} \tag{A.1}$$

$$F_{ex} = f_{ex} \cdot F_{grazing} \tag{A.2}$$

The detrital flux F_{eg} was then added as a source term to the small detritus, and the ammonium flux F_{ex} added to NH_4^+. However, the change to microzooplankton biomass was only calculated as a result of losses from m_{zoo} and gains from $F_{grazing}$, without accounting for F_{eg} and F_{ex}.

As a result, the model was not mass-balanced, and microzooplankton had incor-

rectly high biomasses. While in the uncorrected model, microzooplankton biomass rose above 3 g C m^{-2}, trajectories in the corrected model peaked between 1 and 1.5 g C m^{-2}.

Phytoplankton growth was therefore more restricted than it ought to have been due to the greater presence of zooplankton. The error therefore impacted bloom dynamics.

When the IEB60 case was run with the corrected fluxes, bloom timing was not affected, however bloom duration was substantially longer, with the peak extended by several days. The decline in phytoplankton biomass was also slower. In the uncorrected versions, most trajectories went from above 40 to below 25 g C m^{-2} by the start of June. This decline could take up to two and a half weeks longer in the corrected version.

For the inter-annual comparison, the effect of the bug on timing was calculated for each year, for the different degrees of seasonality. For the highest two seasonalities (0.9 and 1), blooming timing was off by 1 day for the warm years and zero days for 2009. For seasonalities between zero and 0.6 most year has error in blooming timing between 5 to 16 days. At the higher end, between s =0.6 and 0.8, there was more variance, with 2009 have one to two week errors, but the warm years 2014 and 2016 swiftly moving down to less than 6 day offsets.

Appendix B

Photoinhibition and Different Models of P-E Curves

As mentioned in Sections 1.4 and 3.4, there exist multiple models of P and μ as functions of irradiance. In Chapter 1 the complete Platt Model is shown to include a photoinhibition parameter, and the NPZD model of Chapters 4 and 5 used the Smith model, which also does not include photoinhibition. Figure B.1 demonstrates how the Platt model without photoinhibition compares with the Smith model using the same photoparameters. Both functions were developed to describe data that exhibit similar behaviour and are thus very similar, though differences do exist both in interpretation and quantitative results (Lederman & Tett, 1981).

This section will use data from the cruise discussed in Chapter 3 to discuss the differences between these models and the impact of photoinhibition. These differences are both quantitative and qualitative, and should be born in mind when interpreting values of photoparameters.

In Chapter 3, photoparameters were presented that had been derived from fitting the Platt model to data of carbon (and nitrogen) uptake versus irradiance. These data points were measured in vertical profiles in the mixed layer. The photoparameters discussed in Sections 3.1-3.3 and shown in Figure 3.2 were taken from these fits. These fits also included the photoinhibition parameter β. Photoinhibition is a reduction in photosynthetic rates at irradiances above the saturation point. It is both a function of

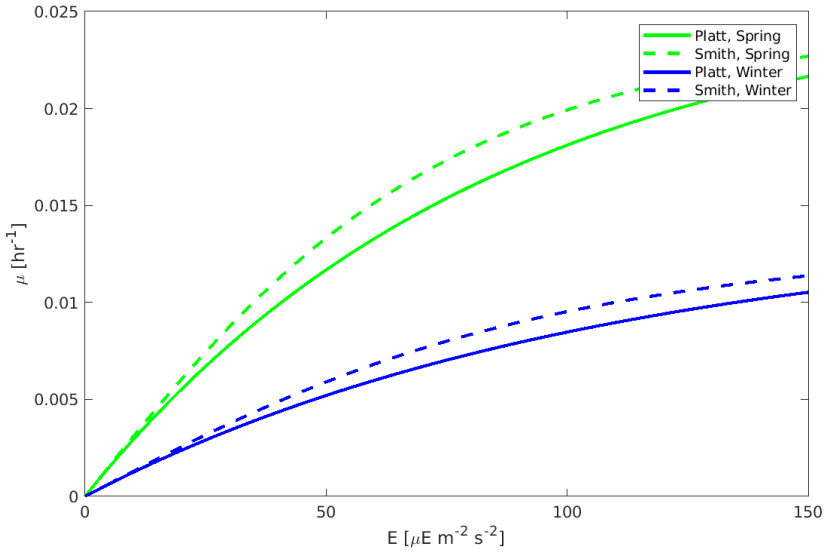

Figure B.1: Comparison of the Platt *et al.* (1980) model without photoinhibition (solid lines) with the Smith (1936) model (dashed lines) using the same photoparameters, the averages of the spring and winter values from the data in Section 3.1.

the intensity and the duration of exposure, and increasing irradiance leads to ever more decreased photosynthesis. As with α and other aspects of photosynthesis discussed in Chapter 1, there are many chemical changes that can induce photoinhibition (Falkowski & Raven, 2007). Figure B.2 shows the distribution of β with respect to surface PAR for the same casts as used in Chapter 3.

Full vertical profiles were available for 9 different casts made on the same cruises from spring 2008 and 2009 that were used in the prior sections. These profiles are not the same as those used for the calculation of the photoparameters presented in Chapter 3, as those were unavailable, therefore a direct comparison cannot be made between those values and the ones here. Additionally, the profiles used here only represent under-ice locations, where phytoplankton are expected to be in their over-wintering state. Each profile included the irradiance and uptake rates of nitrogen and carbon at each depth. As detailed in (Sambrotto *et al.*, 2015), these were obtained through 24-hour on-deck incubations.

For each available profile, three fits were made to both carbon and nitrogen uptake

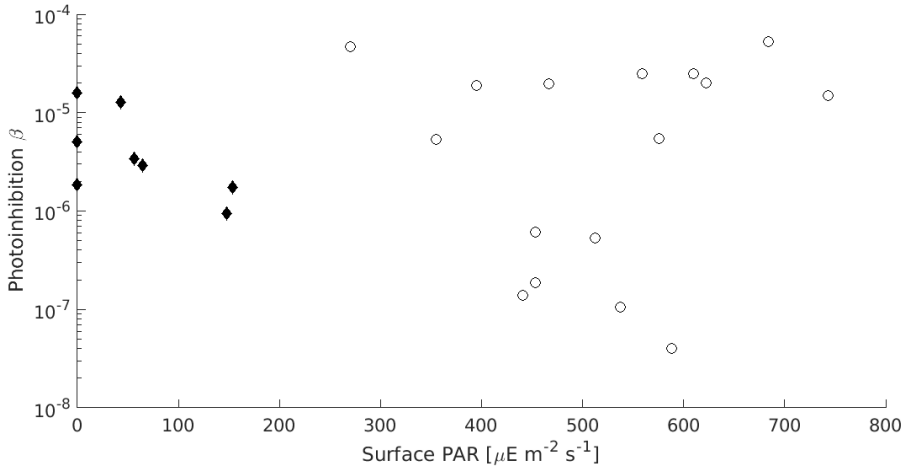

Figure B.2: The photoinhibition parameter vs surface PAR. Open circles are data from open-water sampling sites, closed diamonds are data from sites that were at least partially ice-covered at the time of sampling. Surface PAR was approximated using the estimation of sea-ice attenuation in the Equation 3.1 applied to the irradiance measurements from the ship deck.

data. One following the full form of Platt, including photoinhibition, one following Platt without photoinhibition (equivalent to β being set to 0), and one of Smith. Figure B.3 shows these fits against the carbon uptake rate data. Figure B.6 in the appendices shows the fits against the nitrogen uptake rates.

Figure B.4 shows how the best fit values of α and μ_0 change when the fit is redone including photoinhibition. That is to say, starting with fits without photoinhibition, the plots show how much the parameters will change when photoinhibition is included, with the x-axis being the value of the β fit.

Best-fit values of α decrease when redone with photoinhibition, except where photoinhibition was weak or not present (cf. Figure B.3). This suggests a fit without photoinhibition, such as with the Smith model, would over-estimated α. Best-fit values of μ_0 increased when redone with photoinhibition (again except where photoinhibition was weak or not present). Thus, a model such as Smith's would generally, in the presence of photoinhibition that it cannot capture, under-estimates μ_0.

Referring again to Figure B.2, while the variance of β is higher for open water samples, only six open water points are substantially lower than the cluster of β values

for partially ice covered locations. Were all data to have been fit with a model without photoinhibition, the majority of points both under ice and open water would be affected to roughly the same degree, with only those six open-water points being less affected by removal of β.

For the six open water points with β orders of magnitude smaller than the rest, the effect would be weaker. The over-estimation of α and under-estimation of μ_0 would be less pronounced for these points. For these points specifically, seasonality may appear less pronounced in the α data. These points in particular have lower μ_0 and α values for open water, and so their distance from the under ice μ_0 values would decrease.

The same effects can be seen when redone with the data of nitrogen uptake, shown in Figures B.7 and B.8.

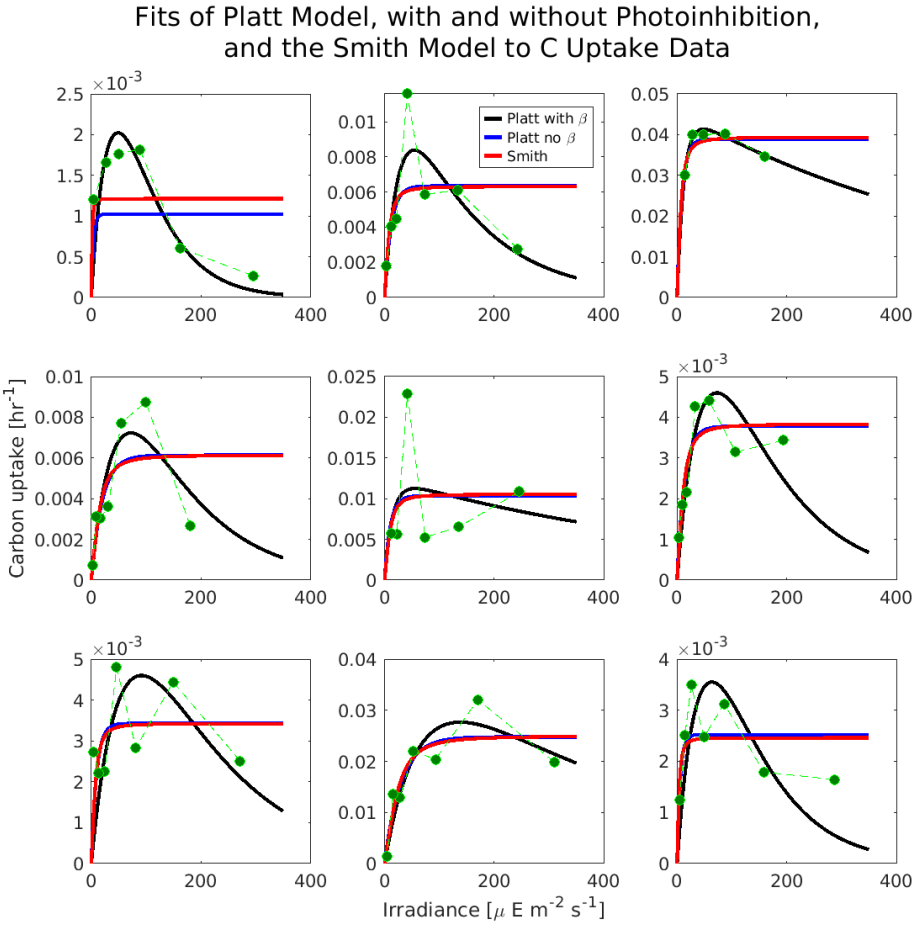

Figure B.3: Refits of cruise data using multiple models: The Platt *et al.* (1982) model with and without photoinhibition (indicated by the photoparameter β, and the Smith (1936) model.

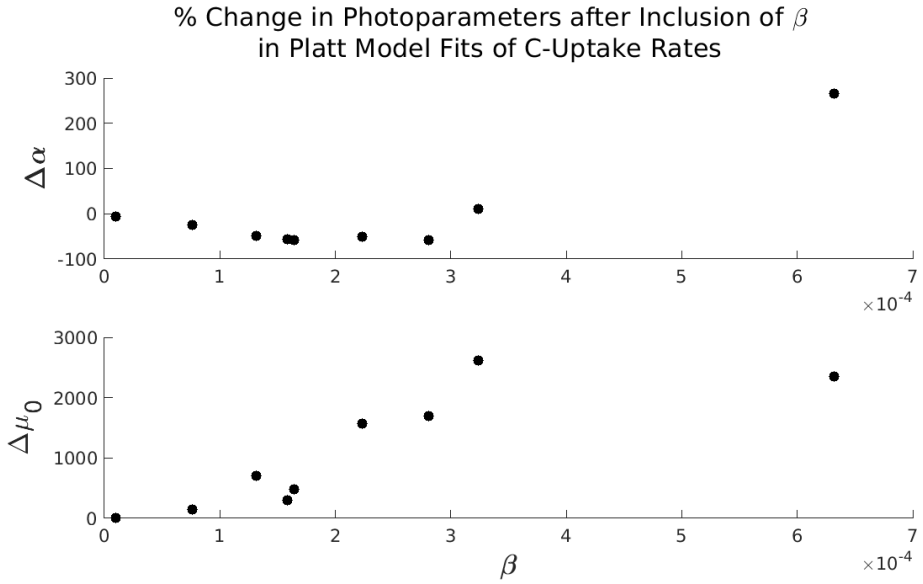

Figure B.4: A comparison of α and μ_0 values between the Platt model fits without photoinhibition and the fits with. The y-axis represents the magnitude and direction of change in a parameter when refit with photoinhibition, while the x-axis represents the best fit value of β for that sample. Thus, we see that including photoinhibition results in smaller α fits, though no change more than 50%, and higher μ_0 ranging up to 15x greater when fit with photoinhibition.

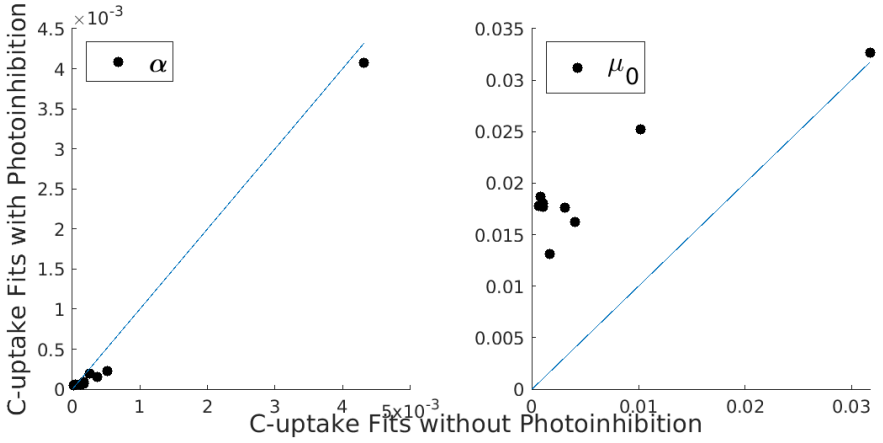

Figure B.5: Comparison of the fit values of μ_0 and α using Platt with photoinhibition versus the same parameters fit without photoinhibition. The dashed line marks the 1:1, indicating the values of μ_0 are higher for fits with photoinhibition that without, and the values of α are lower.

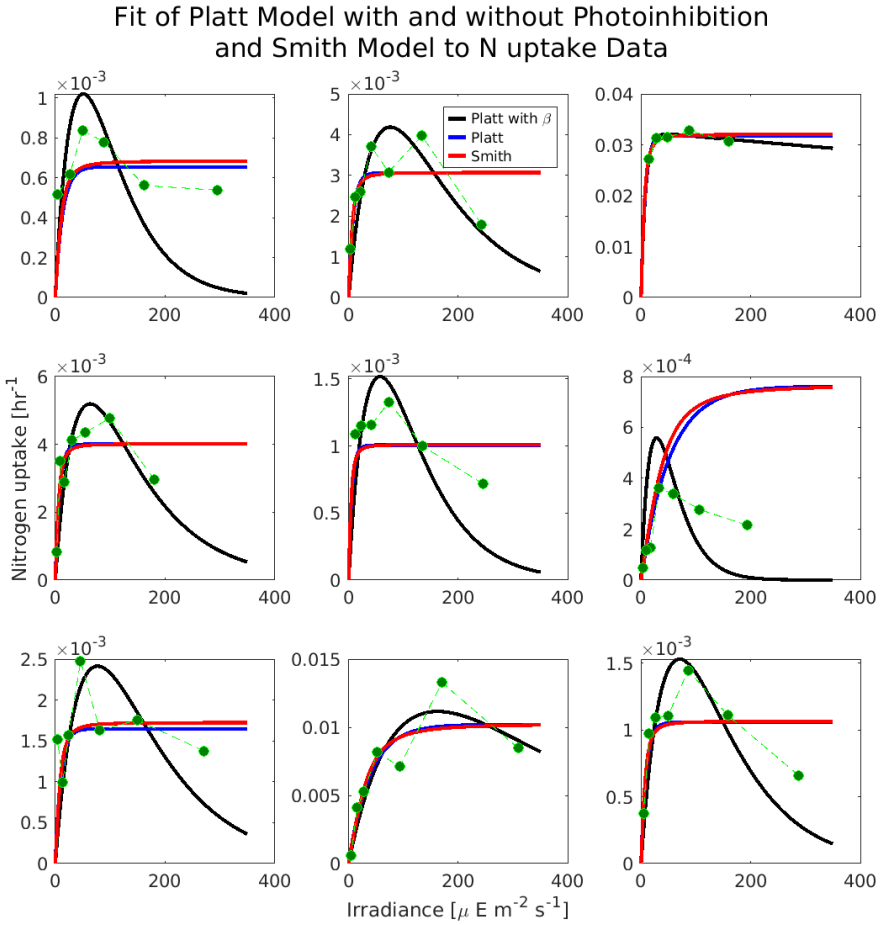

Figure B.6: Refits of cruise data using multiple models: The Platt *et al.* (1982) model with and without photoinhibition (indicated by the photoparameter β, and the Smith (1936) model.

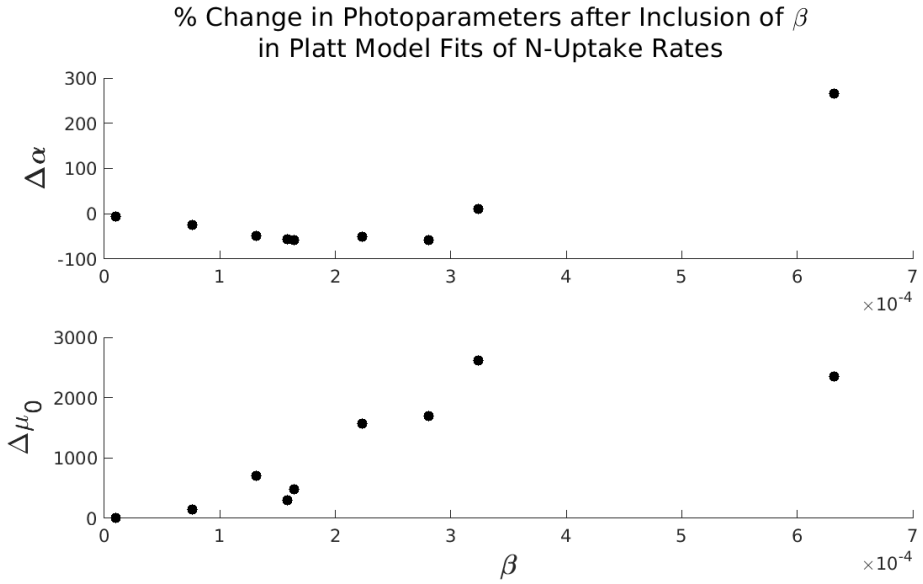

Figure B.7: A comparison of α and μ_0 values between the Platt model fits without photoinhibition and the fits with. The y-axis represents the magnitude and direction of change in a parameter when refit with photoinhibition, while the x-axis represents the best fit value of β for that sample. Thus, we see that including photoinhibition results in smaller α fits, though no change more than 50%, and higher μ_0 ranging up to 15x greater when fit with photoinhibition.

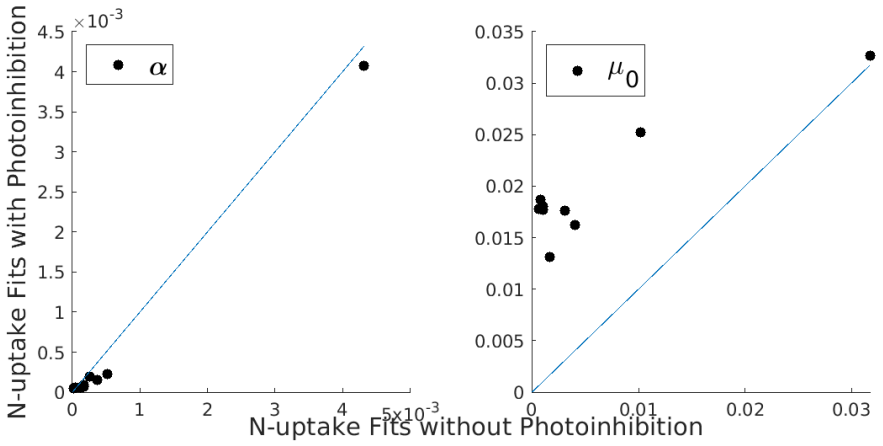

Figure B.8: Comparison of the fit values of μ_0 and α using Platt with photoinhibition versus the same parameters fit without photoinhibition. The dashed line marks the 1:1, indicating the values of μ_0 are higher for fits with photoinhibition that without, and the values of α are lower.

Bibliography

Abrams, Peter A, Matsuda, Hiroyuki, & Harada, Yasushi. 1993. Evolutionarily unstable fitness maxima and stable fitness minima of continuous traits. *Evolutionary Ecology*, **7**(5), 465–487.

Aguilar-Islas, A M, Hurst, M P, Buck, K N, Sohst, B, Smith, G J, Lohan, M C, & Bruland, K W. 2007. Micro-and macronutrients in the southeastern Bering Sea: Insight into iron-replete and iron-depleted regimes. *Progress in Oceanography*, **73**(2), 99–126.

Anderson, SM, & Roels, OA. 1981. Effects of light intensity on nitrate and nitrite uptake and excretion by Chaetoceros curvisetus. *Marine biology*, **62**(4), 257–261.

Anugerahanti, Prima, Kerimoglu, Onur, & Smith, S Lan. 2021. Enhancing Ocean Biogeochemical Models with Phytoplankton Variable Composition. *Frontiers in Marine Science*, **8**, 944.

Assmy, P, Fernández-Méndez, M, Duarte, P, Meyer, A, Randelhoff, A, Olsen, C J Mundy L M, Kauko, H M, Bailey, A, Chierici, M, Cohen, L, Doulgeris, A P, Ehn, J K, Fransson, A, Gerland, S, Hop, H, Hudson, S R, Hughes, N, Itkin, P, Johnsen, G, King, J A, Koch, B P, Koenig, Z, Kwasniewski, S, Laney, S R, Nicolaus, M, Pavlov, A K, Polashenski, C M, Provost, C, Rösel, A, Sandbu, M, Spreen, G, Smedsrud, L H, Sundfjord, A, Taskjelle, T, Tatarek, A, Wiktor, J, Wagner, P M, Wold, A, Steen, H, & Granskog, M A. 2017. Leads in Arctic pack ice enable early phytoplankton blooms below snow-covered sea ice. *Sci Rep*, **7**(40850).

Baklouti, M, Diaz, F, Pinazo, C, & Faure, Vand Quéguiner, B. 2006a. Investigation

of mechanistic formulations depicting phytoplankton dynamics for models of marine pelagic ecosystems and description of a new model. *Progress in Oceanography*, **71**(1), 1–33.

Baklouti, Melika, Faure, Vincent, Pawlowski, Lionel, & Sciandra, Antoine. 2006b. Investigation and sensitivity analysis of a mechanistic phytoplankton model implemented in a new modular numerical tool (Eco3M) dedicated to biogeochemical modelling. *Progress in Oceanography*, **71**(1), 34–58.

Ban, Akiko, Aikawa, Shimpei, Hattori, Hiroshi, Sasaki, Hiroshi, Sampei, Makoto, Kudoh, Sakae, Fukuchi, Mitsuo, Satoh, Kazuhiko, & Kashino, Yasuhiro. 2006. Comparative analysis of photosynthetic properties in ice algae and phytoplankton inhabiting Franklin Bay, the Canadian Arctic, with those in mesophilic diatoms during CASES 03-04. *Polar Bioscience*, **19**, 11–28.

Banas, Neil S, Zhang, Jinlun, Campbell, Robert G, Sambrotto, Raymond N, Lomas, Michael W, Sherr, Evelyn, Sherr, Barry, Ashjian, Carin, Stoecker, Diane, & Lessard, Evelyn J. 2016. Spring plankton dynamics in the Eastern Bering Sea, 1971–2050: Mechanisms of interannual variability diagnosed with a numerical model. *Journal of Geophysical Research: Oceans*, **121**(2), 1476–1501.

Bissinger, Jan E, Montagnes, David JS, harples, Jonathan, & Atkinson, David. 2008. Predicting marine phytoplankton maximum growth rates from temperature: Improving on the Eppley curve using quantile regression. *Limnology and Oceanography*, **53**(2), 487–493.

Bliss, Angela C, Steele, Michael, Peng, Ge, Meier, Walter N, & Dickinson, Suzanne. 2019. Regional variability of Arctic sea ice seasonal change climate indicators from a passive microwave climate data record. *Environmental Research Letters*, **14**(4), 045003.

Brody, S R, Lozier, M S, & Dunne, J P. 2013. A comparison of methods to determine phytoplankton bloom initiation. *Journal of Geophysical Research: Oceans*, **118**, 2345–2357.

Brown, Z W, & Arrigo, K R. 2013. Sea ice impacts on spring bloom dynamics and net primary production in the Eastern Bering Sea. *Journal of Geophysical Research: Oceans*, **118**, 43–62.

Brunelle, Corinne B, Larouche, Pierre, & Gosselin, Michel. 2012. Variability of phytoplankton light absorption in Canadian Arctic seas. *Journal of Geophysical Research*, **117**(C9), 1–17.

Campbell, Robert G, Ashjian, Carin J, Sherr, Evelyn B, Sherr, Barry F, Lomas, Michael W, Ross, Celia, Alatalo, Philip, Gelfman, Celia, & Van Keuren, Donna. 2016. Mesozooplankton grazing during spring sea-ice conditions in the eastern Bering Sea. *Deep Sea Research Part II: Topical Studies in Oceanography*, **134**, 157–172.

Carroll, Sean M. 2019. Beyond Falsifiability: Normal Science in a Multiverse. *Chap. 16 of:* Dawid, R., Dardashti, R., & Thébault, K. (eds), *Epistemology of Fundamental Physics: Why Trust a Theory?* Cambridge University Press.

Cartwright, Nancy, Shomar, Towfic, & Suárez, Mauricio. 1995. The tool box of science: Tools for the building of models with a superconductivity example. *Poznan Studies in the Philosophy of the Sciences and the Humanities*, **44**.

Claustre, Hervé, Bricaud, Annick, Babin, Marcel, & Bruyant, Flavienne. 2002. Diel variations in *Prochlorococcus* optical properties. *Limnology and Oceanography*, **47**(6), 1637–1647.

Coachman, L K. 1986. Circulation, water masses, and fluxes on the southeastern Bering Sea shelf. *Continental Shelf Research*, **5**, 23–108.

Collos, Yves. 1982. Transient situations in nitrate assimilation by marine diatoms. 2. Changes in nitrate and nitrite following a nitrate perturbation. *Limnol. Oceanogr*, **27**(3), 528–535.

Collos, Yves, Vaquer, André, & Souchu, Philippe. 2005. Acclimation of nitrate uptake by phytoplankton to high substrate levels 1. *Journal of Phycology*, **41**(3), 466–478.

Cosper, E. 1982. Influence of light intensity on diel variations in rates of growth, respiration and organic release of a marine diatom: comparison of diurnally constant and fluctuating light. *Journal of Plankton Research*, **4**(3), 705–724.

Coyle, K O, Eisner, L B, Mueter, F J, Pinchuk, A I, Janout, M A, Cieciel, K D, Farley, E V, & Andrews, A G. 2011. Climate change in the southeastern Bering Sea: Impacts on pollock stocks and implications for the oscilalting control hypothesis. *Fisheries Oceanography*, **20**(2), 139–156.

Cross, J N, Mathis, J T, & Bates, N R. 2012. Hydrographic controls on net community production and total organic carbon distributions in the eastern Bering Sea. *Deep-Sea Research II*, **65-70**(C), 98–109.

Cullen, John J. 1990. On models of growth and photosynthesis in phytoplankton. *Deep-Sea Research*, **37**(4), 667–683.

Cullen, John J, Geider, RJ, Ishizaka, J, Kiefer, DA, Marra, J, Sakshaug, E, & Raven, JA. 1993. Towards a general description of phytoplankton growth for biogeochemical models. *Pages 153–176 of: Towards a model of ocean biogeochemical processes*. Springer.

Diehl, Sebastian, Berger, Stella, Ptacnik, Robert, & Wild, Angelika. 2002. Phytoplankton, light, and nutrients in a gradient of mixing depths: field experiments. *Ecology*, **83**(2), 399–411.

Dubinsky, Zvy, & Stambler, Noga. 2009. Photoacclimation processes in phytoplankton: mechanisms, consequences, and applications. *Aquatic Microbial Ecology*, **56**, 163–176.

Duffy-Anderson, J T, Stabeno, P J, Siddon, E C, Andrews, A G, Cooper, D W, Eisner, L B, Farley, E V, Harpold, C E, Heintz, R A, Kimmel, D G, Sewall, F F, Spear, A H, & Yasumishii, E C. 2017. Return of warm conditions in the southeastern Bering Sea: Phytoplankton - Fish. *PloS one*, **12**(6), e0178955.

Eisner, L B. 2018. The Bering Sea: Current status and recent trends. *PICES Press*, **26**(1), 29–36.

Eisner, L B. 2019. The Bering Sea: Current status and recent trends. *PICES Press*, **27**(1), 33–39.

Eisner, L B, Gann, J C, Ladd, C, Ciecciel, K, & Mordy, C W. 2016. Late summer/early fall phytoplankton biomass (chlorophyll a) in the eastern Bering Sea: spatial and temporal variations and factors affecting chlorophyll a concentrations. *Deep-Sea Research II*, **134**, 100–114.

Falkowski, Paul G, & Raven, John A. 2007. *Aquatic Photosynthesis*. Second edn. Princeton University Press.

Ferreira, A Sofia, Visser, Andre W, MacKenzie, Brian R, & Payne, Mark R. 2014. Accuracy and precision in the calculation of phenology metrics. *Journal of Geophysical Research: Oceans*, **119**(12), 8438–8453.

Fujiki, Tetsuichi, & Taguchi, Satoru. 2002. Variability in chlorophyll *a* specific absorption coefficient in marine phytoplankton as a function of cell size and irradiance. *Journal of Plankton Research*, **24**(9), 859–874.

Geider, Richard J. 1992. Respiration: taxation without representation? *Pages 333–360 of: Primary productivity and biogeochemical cycles in the sea*. Springer.

Geider, Richard J, & Osborne, Bruce A. 1989. Respiration and microalgal growth: a review of the quantitative relationship between dark respiration and growth. *New phytologist*, **112**(3), 327–341.

Geider, Richard J, Osbonie, Bruce A, & Raven, John A. 1986. Growth, Photosynthesis and Maintenance Metabolic Cost in the Diatom Phaeodactylum Tricornutum at Very Low Light Levels 1. *Journal of Phycology*, **22**(1), 39–48.

Gentleman, Wendy. 2002. A chronology of plankton dynamics in silico: how computer models have been used to study marine ecosystems. *Hydrobiologia*, **480**(1), 69–85.

Gentleman, Wendy, Leising, Andrew, Frost, Bruce, Strom, Suzanne, & Murray, James. 2003. Functional responses for zooplankton feeding on multiple resources: a review

of assumptions and biological dynamics. *Deep Sea Research Part II: Topical Studies in Oceanography*, **50**(22-26), 2847–2875.

Gibson, C E. 1985. Growth Rate, Maintenance Energy and Pigmentation of Planktonic Cyanophyta During One-hour Light:Dark Cycles. *British Phycological Journal*, **20**(2), 155–161.

Glibert, Patricia M, Wilkerson, Frances P, Dugdale, Richard C, Raven, John A, Dupont, Christopher L, Leavitt, Peter R, Parker, Alexander E, Burkholder, JoAnn M, & Kana, Todd M. 2016. Pluses and minuses of ammonium and nitrate uptake and assimilation by phytoplankton and implications for productivity and community composition, with emphasis on nitrogen-enriched conditions. *Limnology and Oceanography*, **61**(1), 165–197.

Goodman, Nelson. 1968. *Languages of Art: An Approach to a Theory of Symbols*. The Bobbs-Merrill Company, Inc.

Gray, R W. 1931. The colour of the Greenland Sea and the migrations of the Greenland whale and narwhal. *The Geographical Journal*, **78**, 284–290.

Greve, W, Prinage, S, Zidowitz, H, Nast, J, & Reiners, F. 2005. On the phenology of North Sea ichthyoplankton. *ICES Journal of Marine Science*, **62**, 1216–1223.

Griffies, Stephen M. 2004. *Fundamentals of Ocean Climate Models*. Princeton University Press.

Hansen, Per Juel, Bjørnsen, Peter Koefoed, & Hansen, Benni Winding. 1997. Zooplankton grazing and growth: Scaling within the 2–2000μm body size range. *Limnology and oceanography*, **42**(4), 687–704.

Heinle, Anna, & Slawig, Thomas. 2013a. Impact of parameter choice on the dynamics of NPZD type ecosystem models. *Ecological modelling*, **267**, 93–101.

Heinle, Anna, & Slawig, Thomas. 2013b. Internal dynamics of NPZD type ecosystem models. *Ecological modelling*, **254**, 33–42.

Henson, Stephanie A, Robinson, Ian, Allen, John T, & Waniek, Joanna J. 2006. Effect of meteorological conditions on interannual variability in timing and magnitude of the spring bloom in the Irminger Basin, North Atlantic. *Deep Sea Research Part I: Oceanographic Research Papers*, **53**(10), 1601–1615.

Honjo, S. 1990. Particle Fluxes and Modern Sedimentation in the Polar Oceans. *Pages 687–739 of:* Smith, Jr., W O (ed), *Polar Oceanography, Part B: Chemistry, Biology, and Geology.* Academic Press, Inc.

Huisman, J, Sharples, J, Stroom, J M, Visser, P M, Kardinaal, W E A, Verspagen, J M H, & Sommeije, B. 2004. Changes in Turbulent Mixing Shift Competition for Light between Phytoplankton Species. *Ecology*, **85**(1), 2960–2960.

Hunt, Jr, G L, Stabeno, P, Walters, G, Sinclar, E, Brodeur, R D, Napp, J M, & Bond, N A. 2002. Climate change and control of the southeastern Bering Sea pelagic system. *Deep-Sea Research II*, **49**, 5821–5953.

Hunt, Jr, G L, Renner, M, Kuletz, K J, Salo, S, Eisner, L, Ressler, P H, Ladd, C, & Santora, J A. 2018. Timing of sea-ice retreat affects the distribution of seabirds and their prey in the southeastern Bering Sea. *Marine Ecology Progress Series*, **593**, 209–230.

Ikeya, Tohru, Kashino, Yasuhiro, Kudoh, Sakae, Imura, Satoshi, Watanabe, Kentaro, & Fukuchi, Mitsuo. 2000. Acclimation of photosynthetic properties in psychrophilic diatom isolates under different light intensities. *Polar Bioscience*, **13**, 43–54.

Jassby, Alan D, & Platt, Trevor. 1976. Mathematical formulation of the relationship between photosynthesis and light for phytoplankton. *Limnology and oceanography*, **21**(4), 540–547.

Jiang, Weimin, Cornelisen, Chris, Knight, Ben, & Gibbs, Mark. 2015. A pattern-oriented model for assessing effects of weather and freshwater discharge on black coral (Antipathes fiordensis) distribution in a fjord. *Ecological Modelling*, **304**, 59–68.

Jochem, Frank J. 1999. Dark survival strategies in marine phytoplankton assessed by cytometric measurement of metabolic activity with fluorescein diacetate. *Marine Biology*, **135**, 721–728.

Kachel, NB, Hunt Jr, GL, Salo, SA, Schumacher, JD, Stabeno, PJ, & Whitledge, TE. 2002. Characteristics and variability of the inner front of the southeastern Bering Sea. *Deep Sea Research Part II: Topical Studies in Oceanography*, **49**(26), 5889–5909.

Kamp, Anja, de Beer, Dirk, Nitsch, Jana L, Lavik, Gaute, & Stief, Peter. 2011. Diatoms respire nitrate to survive dark and anoxic conditions. *Proceedings of the National Academy of Sciences*, **108**(14), 5649–5654.

Kauko, H M, Taskjelle, T, Assmy, P, Pavlov, A K, Mundy, C J, Duarte, P, Fernández-Méndez, M, Olsen, L M, Hudson, S R, Johnsen, G, Elliott, A, Wang, F, & Granskog, M A. 2017. Windows in Arctic sea ice: Light transmission and ice algae in a refrozen lead. *Journal of Geophysical Research: Biogeosciences*, **122**(6), 1486–1505.

Kerimoglu, Onur, Hofmeister, Richard, Maerz, Joeran, & Wenzel Wirtz, K. 2017. A novel acclimative biogeochemical model and its implementation to the southern North Sea. *Biogeosciences Discussions*, 33.

Kerimoglu, Onur, Anugerahanti, Prima, & Smith, Sherwood Lan. 2021. FABM-NflexPD 1.0: assessing an instantaneous acclimation approach for modeling phytoplankton growth. *Geoscientific Model Development*, **14**(10), 6025–6047.

Kikuchi, Gennosuke, Abe, Hiroto, Hirawake, Toru, & Sampei, Makoto. 2020. Distinctive spring phytoplankton bloom in the Bering Strait in 2018: A year of historically minimum sea ice extent. *Deep Sea Research Part II: Topical Studies in Oceanography*, **181**, 104905.

Kinder, T H, & Schumacher, J D. 1981a. Circulation over the continental shelf of the southeastern Bering Sea. *Pages 53–75 of:* Hood, D W, & Calder, J A (eds), *The Eastern Bering Sea Shelf: Oceanography and Resources*, vol. 1. Seattle, Washington: NOAA Office of Marine Pollution Assessment, distributed by the University of Washington Press.

Kinder, T H, & Schumacher, J D. 1981b. Hydrographic structure over the continental shelf of the southeastern Bering Sea. *Pages 31–52 of:* Hood, D W, & Calder, J A (eds), *The Eastern Bering Sea Shelf: Oceanography and Resources*, vol. 1. Seattle, Washington: NOAA Office of Marine Pollution Assessment, distributed by the University of Washington Press.

Kortum, Gerhard. 2009. Victor Hensen in der Geschichte der Meeresforschung. *Schriften des Naturwissenschaftlichen Vereins für Schleswig-Holstein*, **71**, 3–25.

Kwok, Ron. 2018. Arctic sea ice thickness, volume, and multiyear ice coverage: losses and coupled variability (1958–2018). *Environmental Research Letters*, **13**(10), 105005.

Ladd, C, Eisner, L B, Salo, S A, Mordy, C W, & Iglesias-Rodriguez, M D. 2018. Spatial and Temporal Variability of Coccolithophore blooms in the Eastern Bering Sea. *Journal of Geosphysical Research: Oceans*, **123**, 9119–9136.

Langdon, Christopher. 1988. On the causes of interspecific differences in the growth-irradiance relationship for phytoplankton. II. A general review. *Journal of Plankton Research*, **10**(6), 1291–1312.

Lederman, TC, & Tett, P. 1981. Problems in modelling the photosynthesis-light relationship for phytoplankton. *Botanica Marina*, **XXIV**, 125–134.

Li, Gang, Brown, Christopher M, Jeans, Jennifer A, Donaher, Natalie A, McCarthy, Avery, & Campbell, Douglas A. 2015. The nitrogen costs of photosynthesis in a diatom under current and future p CO 2. *New Phytologist*, **205**(2), 533–543.

Litchman, Elena. 2000. Growth rates of phytoplankton under fluctuating light. *Freshwater Biology*, **44**, 223–235.

Litchman, Elena, Ohman, Mark D, & Kiørboe, Thomas. 2013. Trait-based approaches to zooplankton communities. *Journal of plankton research*, **35**(3), 473–484.

Loebl, Martina, Cockshutt, Amanda M, Campbell, Douglas A, & Finkel, Zoe V. 2010.

Physiological basis for high resistance to photoinhibition under nitrogen depletion in Emiliania huxleyi. *Limnology and Oceanography*, **55**(5), 2150–2160.

Lomas, M W, Moran, S B, Casey, J R, Bell, D W, Tiahlo, M, Whitefield, J, Kelly, R P, Mathis, J T, & Cokelet, E D. 2012. Spatial and seasonal variability of primary production on the Eastern Bering Sea shelf. *Deep-Sea Research II*, **65–70**, 126–140.

Lomas, Michael W, & Glibert, Patricia M. 2000. Comparisons of nitrate uptake, storage, and reduction in marine diatoms and flagellates. *Journal of Phycology*, **36**(5), 903–913.

Lomas, Michael W, & Lipschultz, Fredric. 2006. Forming the primary nitrite maximum: nitrifiers or phytoplankton? *Limnology and Oceanography*, **51**(5), 2453–2467.

Lomas, Michael W, Rumbley, Christina J, & Glibert, Patricia M. 2000. Ammonium release by nitrogen sufficient diatoms in response to rapid increases in irradiance. *Journal of Plankton Research*, **22**(12), 2351–2366.

Lomas, Michael W, Eisner, Lisa B, Gann, Jeanette, Baer, Steven E, Mordy, Calvin W, & Stabeno, Phyllis J. 2020. Time-series of direct primary production and phytoplankton biomass in the southeastern Bering Sea: responses to cold and warm stanzas. *Marine Ecology Progress Series*, **642**, 39–54.

Long, Matthew C. 2010. *Upper Ocean Physical and Ecological Dynamics in the Ross Sea, Antarctica.* Ph.D. thesis, Stanford University.

Madec, Gurvan, Bourdallé-Badie, Romain, Chanut, Jérôme, Clementi, Emanuela, Coward, Andrew, Ethé, Christian, Iovino, Doroteaciro, Lea, Dan, Lévy, Claire, Lovato, Tomas, Martin, Nicolas, Masson, Sébastien, Mocavero, Silvia, Rousset, Clément, Storkey, Dave, Vancoppenolle, Martin, Müeller, Simon, Nurser, George, Bell, Mike, & Samson, Guillaume. 2019 (Oct.). *NEMO ocean engine.*

Marra, John. 1978. Phytoplankton photosynthetic response to vertical movement in mixed layer. *Marine Biology*, **46**, 203–208.

Mathis, JT, Cross, JN, Bates, NR, Bradley Moran, S, Lomas, MW, Mordy, CW, & Stabeno, PJ. 2010. Seasonal distribution of dissolved inorganic carbon and net community production on the Bering Sea shelf. *Biogeosciences*, **7**(5), 1769–1787.

Matsuoka, A, Hill, V, Yannick, H, Babin, M, & A Bricaud, A. 2011. Seasonal variability in the light absorption parameters of western Arctic waters: Parameterization of the individual components of absorption for ocean color applications. *Journal of Geophysical Research: Oceans*, **116**.

Matsuoka, Atsushi, Larouche, Pierre, Poulin, Michel, Vincent, Warwick, & Hattori, Hiroshi. 2009. Phytoplankton community adaptation to changing light levels in the southern Beaufort Sea, Canadian Arctic. *Estuarine, Coastal and Shelf Science*, **82**, 537–546.

McKee, D, Röttgers, R, Neukermans, G, Calzado, V S, Trees, C, Ampolo-Rella, M, Neil, C, & Cunningham, A. 2014. Impact of measurement uncertainties on determination of chlorophyll-specific absorption coefficient for marine phytoplankton. *Journal of Geophysical Research: Oceans*, **119**(12), 9013–9025.

Merico, Agostino, Bruggeman, Jorn, & Wirtz, Kai. 2009. A trait-based approach for downscaling complexity in plankton ecosystem models. *Ecological Modelling*, **220**(21), 3001–3010.

Merico, Agostino, Brandt, Gunnar, Smith, S Lan, & Oliver, Marcel. 2014. Sustaining diversity in trait-based models of phytoplankton communities. *Frontiers in Ecology and Evolution*, **2**, 59.

Moloney, Colleen L, & Field, John G. 1991. Modelling carbon and nitrogen flows in a microbial plankton community. *Pages 443–474 of: Protozoa and their role in marine processes*. Springer.

Moore, C M, Suggett, D J, Hickman, A E, Kim, YN, Tweddle, J F, Sharples, J, Geider, R J, & Holligan, P M. 2006. Phytoplankton photoacclimation and photoadaptation in response to environmental gradients in a sea shelf. *Limnology and Oceanography*, **51**(2), 936–949.

Mordy, C W, Stabeno, P J, Cokelet, E D, Ladd, C, Menzia, F A, Proctor, P, & Wisegarver, E. 2012. Net community producn on the middle shelf of the eastern Bering Sea. *Deep-Sea Research II*, **65–70**, 110–125.

Mordy, C W, Devol, A, Eisner, L B, Kachel, N, Ladd, C, Lomas, M W, Proctor, P, Sambrotto, R N, Shull, D H, Stabeno, P J, & Wisegarver, E. 2017. Nutrient and phytoplankton dynamics on the inner shelf of the eastern Bering Sea. *Journal of Geophysical Research: Oceans*, **122**, 2422–2440.

Morgan-Kiss, R M, Lizotte, M P, Kong, W, & Priscu, J C. 2016. Photoadaptation to the polar night by phytoplankton in a permanently ice-covered Antarctic lake. *Limnology and Oceanography*, **61**, 3–13.

Murray, AG, & Parslow, JS. 1999. The analysis of alternative formulations in a simple model of a coastal ecosystem. *Ecological Modelling*, **119**(2-3), 149–166.

Neale, Patrick J, & Richerson, Peter J. 1987. Photoinhibition and the diurnal variation of phytoplankton photosynthesis—I. Development of a photosynthesis—irradiance model from studies of in situ responses. *Journal of Plankton Research*, **9**(1), 167–193.

Neeley, A R, Freeman, S A, & Harris, L A. 2015. Multi-method approach to quantify uncertainties in the measurements of light absorption by particles. *Optics express*, **23**(24), 31043–31058.

Nickelsen, K. 2015. The Maximum Quantum Yield Controversy (1937–1955). *In: Explaining Photosynthesis. History, Philosophy and Theory of the Life Sciences*, vol. 8. Dordrecht: Springer.

Nickelsen, K, & Govindjee. 2011. *The Maximum Quantum Yield Controversy: Otto Warburg and the "Midwest-Gang"*. Bern Studies in the History and Philosophy of Science.

Nicklisch, Andreas. 1998. Growth and light absorption of some planktonic cyanobacte-

ria, diatoms, and Chlorophyceae under simulated natural light fluctuations. *Journal of Plankton Research*, **20**(1), 105–119.

Obata, Mitsuko, & Taguchi, Satoru. 2009. Photoadaptation of an ice algal community in thin sea ice, Saroma-Ko Lagoon, Hokkaido, Japan. *Polar Biology*, **32**, 1127–1135.

Odenbaugh, Jay. 2008. Models. *Chap. 27 of:* Sarkar, Sahotra, & Plutynski, Anya (eds), *A Companion to the Philosophy of Biology.* Blackwell Publishing.

Okazaki, Y, Takahashi, K, Asahi, H, Katsuki, K, Hori, J, Yasuda, H, Sagawa, Y, & Tokuyama, H. 2005. Productivity changes in the Bering Sea during the late Quaternary. *Deep Sea Research Part II: Topical Studies in Oceanography*, **52**(16-18), 2150–2162.

Olonscheck, Dirk, Mauritsen, Thorsten, & Notz, Dirk. 2019. Arctic sea-ice variability is primarily driven by atmospheric temperature fluctuations. *Nature Geoscience*, **12**(6), 430–434.

Palmer, M, Arrigo, K R, Mundy, C J, Ehn, J K, Gosselin, M, Barber, D G, Martin, J, Alou, E, Roy, S, & Tremblay, J-E. 2011. Spatial and temporal variation of photosynthetic parameters in natural phytoplankton assemblages in the Beaufort Sea, Canadian Arctic. *Polar Biology*, **34**, 1915–1928.

Palmer, Molly A, van Dijken, Get L, Mitchell, B Greg, Seegers, Brian J, Lowry, Kate E, Mills, Matthew M, & Arrigo, Kevin R. 2013. Light and nutrient control of photosynthesis in natural phytoplankton populations from the Chukchi and Beaufort seas, Arctic Ocean. *Limnology and Oceanography*, **58**(6), 2185–2205.

Peacock, Kent A. 2008. Ecosystems. *Chap. 19 of:* Sarkar, Sahotra, & Plutynski, Anya (eds), *A Companion to the Philosophy of Biology.* Blackwell Publishing.

Peters, E. 1996. Prolonged darkness and diatom mortality II: Marine temperate species. *Journal of Experimental Marine Biology and Ecology*, **207**, 43–57.

Peters, E, & Thomas, D N. 1996. Prolonged darkness and diatom mortality I: Marine Antarctic species. *Journal of Experimental Marine Biology and Ecology*, **207**, 25–41.

Platt, T, & Jassby, A D. 1976. The relationship between photosynthesis and light for natural assemblages of coastal marine phytoplankton. *Journal of Phycology*, **12**, 421–430.

Platt, T, Gallegos, C L, & Harrison, W G. 1980. Photoinhibition of photosynthesis in natural assemblages of marine phytoplankton. *Journal of Marine Research*, **38**, 687–701.

Platt, T, Harrison, W G, Irwin, B, & Horne, E P. 1982. Photosynthesis and photoadaptation of marine phytoplankton in the Arctic. *Deep Sea Research*, **29**(10A), 1159–1170.

Powles, Stephen B. 1984. Photoinhibition of photosynthesis induced by visible light. *Annual review of plant physiology*, **35**(1), 15–44.

Quigg, Antonietta, & Beardall, John. 2003. Protein turnover in relation to maintenance metabolism at low photon flux in two marine microalgae. *Plant, Cell and Environment*, **26**, 693–703.

Riley, Gordon A, & Von Arx, Ruth. 1949. Theoretical analysis of seasonal changes in the phytoplankton of Husan Harbor, Korea. *Journal of Marine Research*, **8**(1), 60–72.

Rochet, Martine, Legendre, Louis, & Demers, Serge. 1986. Photosynthetic and pigment responses of sea-ice microalgae to changes in light intensity and quality. *Journal of Experimental Marine Biology and Ecology*, **101**, 211–226.

Sagoff, Mark. 2003. The plaza and the pendulum: Two concepts of ecological science. *Biology and Philosophy*, **18**(4), 529–552.

Sakshaug, E, & Slagstad, D. 1991. Light and productivity of phytoplankton in polar marine ecosystems: a physiological view. *Polar Research*, **10**(1), 69–86.

Sambrotto, R N. 2001. Nitrogen production in the northern Arabian Sea during the Spring Intermonsoon and Southwest Monsoon seasons. *Deep-Sea Research II*, **48**, 1173–1198.

Sambrotto, R N, Niebauer, H J, Goering, J J, & Iverson, R L. 1986. Relationships among vertical mixing, nitrate uptake, and phytoplankton growth during the spring bloom in the southeast Bering Sea middle shelf. *Continental Shelf Research*, **5**(1/2), 161–198.

Sambrotto, R N, Mordy, C, Zeeman, S I, Stabeno, P J, & Macklin, S A. 2008. Physical forcing and nutrient conditions associated with patterns of Chl a and phytoplankton productivity in the southeastern Bering Sea during summer. *Deep-Sea Research II*, **55**, 1745–1760.

Sambrotto, R N, Burdloff, D, & McKee, K. 2015. Spatial and year-to-year patterns in new and primary productivity in sea ice melt regions of the eastern Bering Sea. *Deep-Sea Research II*.

Sambrotto, R N, Burdloff, D, & McKee, K. 2016. Spatial and year-to-year patterns in new and primary productivity in sea ice melt regions of the eastern Bering Sea. *Deep-Sea Research II*, **134**, 86–99.

Sciandra, Antoine, & Amara, Rachid. 1994. Effects of nitrogen limitation on growth and nitrite excretion rates of the dinoflagellate *Prorocentrum minimum*. *Marine Ecology Progress Series*, **105**, 301–309.

Sherman, Elliot, Moore, J Keith, Primeau, Francois, & Tanouye, David. 2016. Temperature influence on phytoplankton community growth rates. *Global Biogeochemical Cycles*, **30**(4), 550–559.

Sherr, E B, Sherr, B F, & Ross, C. 2013. Microzooplankton gazing impact in the Bering Sea during spring sea ice conditions. *Deep Sea Research II*, **94**, 57–67.

Siegel, DA, Doney, SC, & Yoder, JA. 2002. The North Atlantic spring phytoplankton bloom and Sverdrup's critical depth hypothesis. *science*, **296**(5568), 730–733.

Sigler, M F, Stabeno, P J, Eisner, L B, Napp, J M, & Mueter, F J. 2014. Spring and fall phytoplankton blooms in a productive subarctic ecosystem, the eastern Bering Sea, durng 1995-2011. *Deep-Sea Research II*.

Slagstad, Dag, & McClimans, Thomas A. 2005. Modeling the ecosystem dynamics of the Barents Sea including the marginal ice zone: I. Physical and chemical oceanography. *Journal of Marine Systems*, **58**(1-2), 1–18.

Smetacek, V, & Passow, U. 1990. Spring bloom initiation and Sverdrup's critical-depth model. *Limnology and oceanography*, **35**(1), 228–234.

Smetacek, Victor. 1999. Revolution in the ocean. *Nature*, **401**(6754), 647–647.

Smith, E L. 1936. Photosynthesis in relation to light and carbon dioxide. *Proceedings of the Natural Academy of Sciences*, **22**, 504–511.

Smith, S Lan, Yamanaka, Yasuhiro, Pahlow, Markus, & Oschlies, Andreas. 2009. Optimal uptake kinetics: physiological acclimation explains the pattern of nitrate uptake by phytoplankton in the ocean. *Marine Ecology Progress Series*, **384**, 1–12.

Smith Jr., W O, & Donaldson, K. 2015. Photosynthesis-irradiance responses in the Ross Sea, Antarctica: a meta-analysis. *Biogeosciences*, **12**(11), 3567–3577.

Stabeno, P, Napp, J, Mordy, C, & Whitledge, T. 2010. Factors influencing physical structure and lower trophic levels of the eastern Bering Sea shelf in 2005: Sea ice, tides and winds. *Progress in Oceanography*, **85**(3–4), 180–196.

Stabeno, P J, Farley, Jr, E V, Kachel, N B, Moore, S, Mordy, C W, Napp, J M, Overland, J E, Pinchuk, A I, & Sigler, M F. 2012. A comparison of the physics of the northern and southern shelvesof the eastern Bering Sea and some implications for the ecosystem. *Deep Sea Research II*, **65–70**, 14–30.

Stabeno, P J, Danielson, S L, Kachel, D G, Kachel, N B, & Mordy, C W. 2016. Currents and transport on the Eastern Bering Sea shelf: An integration of over 20 years of data. *Deep Sea Research Part II: Topical Studies in Oceanography*, **134**, 13–29.

Stabeno, P J, Duffy-Anderson, J T, Eisner, L B, Farley, E V, Heintz, R A, & Mordy, C W. 2017. Return of warm conditions in the southeastern Bering Sea: Physics to fluorescence. *PloS one*, **12**(9), e0185464.

Stabeno, Ph J, Bond, NA, Kachel, NB, Salo, SA, & Schumacher, JD. 2001. On the temporal variability of the physical environment over the south-eastern Bering Sea. *Fisheries Oceanography*, **10**(1), 81–98.

Steeman Nielsen, E, & Hansen, V Kr. 1959. Light Adaptation in Marine Phytoplankton Populations and Its Interrelation with Temperature. *Physiologia Plantarum*, **12**, 353–370.

Steemann Nielsen, E. 1937. The annual amount of organic matter produced by the phytoplankton in the Sound off Helsingør. *MeddelelserfraKommissionen for DanmarksFiskeriogHavundersogelser. Ser. Plankton*, 1–37.

Stoecker, D K, Weigel, A, & Goes, J I. 2013. Microzooplankton grazing in the Eastern Bering Sea in summer. *Deep Sea Res. II*, **109**, 145–156.

Stroeve, Julienne, & Notz, Dirk. 2018. Changing state of Arctic sea ice across all seasons. *Environmental Research Letters*, **13**(10), 103001.

Strom, Suzanne L, & Fredrickson, Kerri A. 2008. Intense stratification leads to phytoplankton nutrient limitation and reduced microzooplankton grazing in the southeastern Bering Sea. *Deep Sea Research Part II: Topical Studies in Oceanography*, **55**(16-17), 1761–1774.

Strzepek, R F, & Harrison, P J. 2004. Photosynthetic architecture differs in coastal and oceanic diatoms. *Nature Letters*, **431**(7 Oct), 689–692.

Sverdrup, H U. 1953. On the conditions for the vernal blooming of phytoplankton. *Journal du Conseil International pour l'Exploration de la Mer*, **18**, 287–295.

Takahashi, K, Fujitani, N, Yanada, M, & Maita, Y. 2000. Long-term biogenic particle fluxes in the Bering Sea and the central subarctic Pacific Ocean,1990–1995. *Deep-Sea Research Part I*, **47**, 1723–1759.

Takahashi, K, Fujitani, N, & Yanada, M. 2002. Long term monitoring of particle fluxes in the Bering Sea and the central subarctic Pacific Ocean, 1990–2000. *Progress in Oceanography*, **55**(1-2), 95–112.

Taniguchi, A. 1999. Differences in the structure of the lower trophic levels of pelagic ecosystems in the eastern and western subarctic Pacific. *Progress in Oceanography*, **43**(2-4), 289–315.

Tett, Paul, & Wilson, Hilary. 2000. From biogeochemical to ecological models of marine microplankton. *Journal of Marine Systems*, **25**(3-4), 431–446.

Thimijan, R W, & Heins, R D. 1983. Photometric, radiometric, and quantum light units of measure: a review of procedures for interconversion. *HortScience*, **18**(6), 818–822.

Tsunogai, S, Kusakabe, M, Iizumi, H, Koike, I, & Hattori, A. 1979. Hydrographic features of the deep water of the Bering Sea– the sea of silica. *Deep Sea Research Part A. Oceanographic Research Papers*, **26**(6), 641–659.

van Hilst, Christina M, & Smith, Jr, Walker O. 2002. Photosynthesis/irradiance relationships in the Ross Sea, Antarctica and their control by phytoplankton assemblage composition and environmental factors. *Marine Ecology Progress Series*, **226**, 1–12.

Wassmann, Paul, Slagstad, Dag, Riser, Christian Wexels, & Reigstad, Marit. 2006. Modelling the ecosystem dynamics of the Barents Sea including the marginal ice zone: II. Carbon flux and interannual variability. *Journal of Marine Systems*, **59**(1-2), 1–24.

Wu, Z, Song, L, & Li, R. 2008. Different tolerances and responses to low temperature and darkness between waterbloom forming cyanobacterium *Microcystis* and a green alga *Scenedesmus*. *Hydrobiologia*, **596**, 47–55.

Wulff, A, Roleda, M Y, Zacher, K, & Wiencke, C. 2008. Exposure to sudden light burst after prolonged darkness– a case study on benthic diatoms in Antarctica. *Diatom Research*, **23**(2), 519–532.

Yool, A, Popova, EE, & Anderson, TR. 2011. Medusa-1.0: a new intermediate complexity plankton ecosystem model for the global domain. *Geoscientific Model Development*, **4**(2), 381–417.

Yool, A, Popova, EE, & Anderson, TR. 2013. MEDUSA-2.0: an intermediate complexity biogeochemical model of the marine carbon cycle for climate change and ocean acidification studies. *Geoscientific Model Development*, **6**(5), 1767–1811.

Zeeman, Stephan I, & Jensen, Paul R. 1990. Photoresponses of phytoplankton in the Bering Sea. *Results of the Second Joint US-USSR Bering Sea Expedition, Summer 1984*, 87–96.

Zhang, J, Spitz, Y H, Steele, M, Ashjian, C, Campbell, R, Berline, L, & Matrai, P. 2010a. Modeling the impact of declining sea ice on the Arctic marine planktonic ecosystem. *Journal of Geophysical Research*, **115**(C10015).

Zhang, J, Woodgate, R, & Moritz, R. 2010b. Sea ice response to atmospheric and oceanic forcing in the Bering Sea. *Journal of Physical Oceanography*, **40**(8), 1729–1247.

Zhang, J, Woodgate, R, & Mangiameli, S. 2012. Towards seasonal prediction of the distribution and extent of cold bottom waters on the Bering Sea shelf. *Deep Sea Research Part II: Tropical Studies in Oceanography*, **65**, 58–71.

Zhang, Jinlun, Ashjian, Carin, Campbell, Robert, Hill, Victoria, Spitz, Yvette H, & Steele, Michael. 2014. The great 2012 Arctic Ocean summer cyclone enhanced biological productivity on the shelves. *Journal of Geophysical Research: Oceans*, **119**(1), 297–312.

Zhang, Jinlun, Ashjian, Carin, Campbell, Robert, Spitz, Yvette H, Steele, Michael, & Hill, Victoria. 2015. The influence of sea ice and snow cover and nutrient availability on the formation of massive under-ice phytoplankton blooms in the Chukchi Sea. *Deep Sea Research Part II: Topical Studies in Oceanography*, **118**, 122–135.